UiT
THE ARCTIC UNIVERSITY OF NORWAY

FACULTY OF SCIENCE AND TECHNOLOGY

Department of Geosciences

3-D seismic interpretation of the Samson Dome in the framework of the tectonostratigraphic and fluid migration development of the Western Barents Sea

Daria Martiuk

EOM-3901 Master thesis in Energy, Climate and Environment
June, 2017

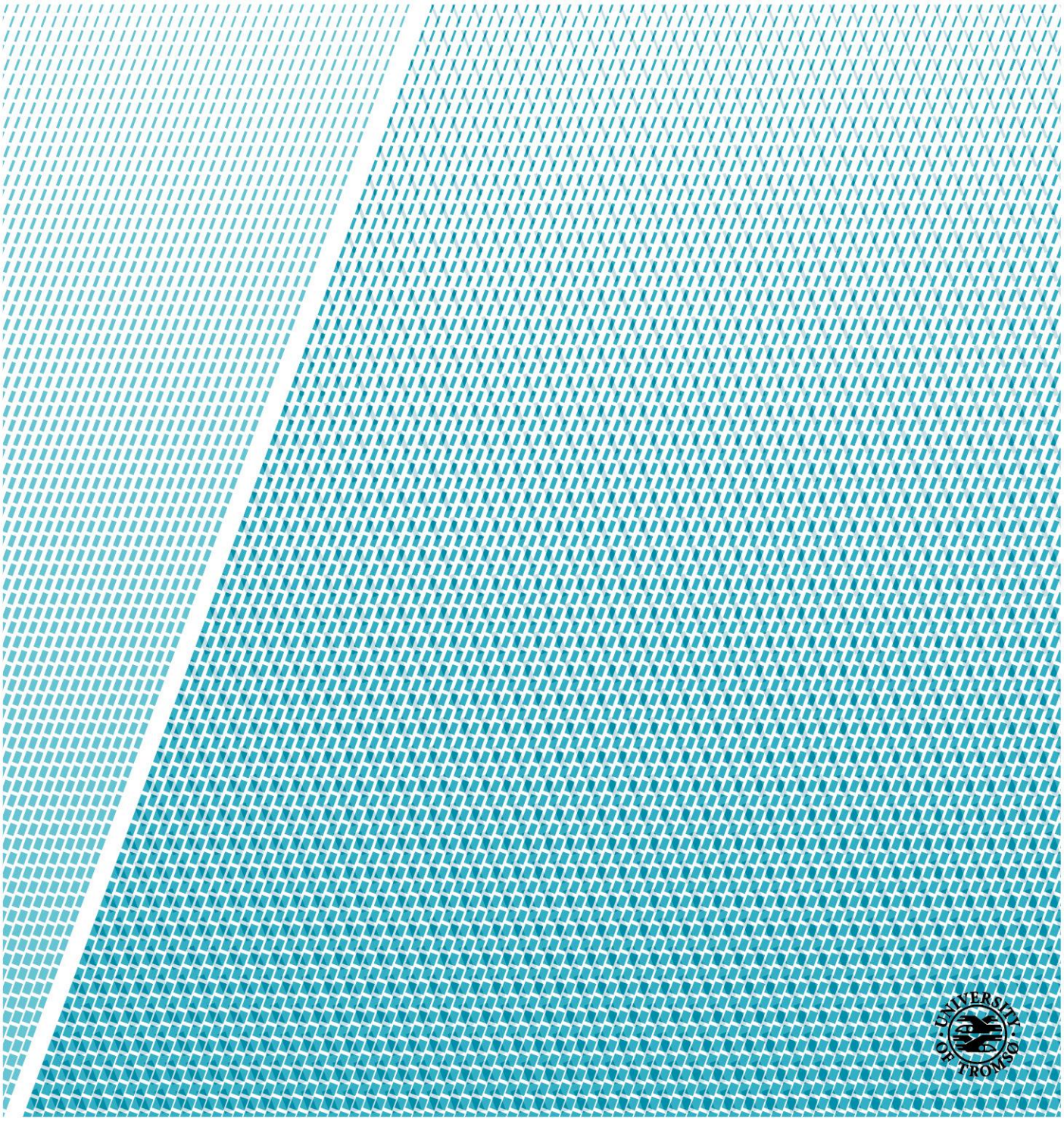

UiT / THE ARCTIC UNIVERSITY OF NORWAY

3-D seismic interpretation of the Samson Dome in the framework of the tectonostratigraphic and fluid migration development of the Western Barents Sea

FACULTY OF SCIENCE AND TECHNOLOGY

Department of Geosciences

Daria Martiuk

EOM-3901 Master thesis in Energy, Climate and Environment

June 2017

Abstract

Three-dimensional (3-D) seismic interpretations of data from the Samson Dome show direct connection between the local geological evolution of the area and the regional tectonic and stratigraphic development of the western Barents Sea. Rifting events, halokinetic movements, uplift and glacial processes influenced the area of the Samson Dome. The Samson Dome structure, located in the south-western part of the Ottar Basin, represents a structural high on the Upper Paleozoic depocentre of the Bjarmeland Platform. Salt volumes beneath the Samson Dome are in a range of 500 to 600 km^3. Many hydrocarbon indicators such as high amplitude anomalies, bright spots, zones of chaotic reflections, phase reversal reflections have been observed in the area adjacent to the salt dome. Presence of potentially significant shallow gas accumulations in the area make the Samson Dome the largest fluid-flow feature in the eastern part of western Barents Sea covering approximately 150 km^2. Here, three fault types exist in the study area, where Type 1 faults represent crestal faults, Type 2 comprises elongated sub-parallel faults, and Type 3 includes polygonal faults surrounding the dome structure. These faults act as potential fluid leakage pathways for hydrocarbons observed in shallow strata of the Samson Dome. My Master thesis comprises: analysis of the stratigraphy of the Samson Dome and mappings of acoustic anomalies and faults in the area with the aim to propose a tectonostratigraphic and fluid-flow model for the area in connection with the overall geological evolution of the western Barents Sea.

Acknowledgements

I would like to express my gratitude to my principal supervisor Professor Jürgen Mienert and co-supervisor Postdoctoral researcher Sunil Vadakkepuliyambatta for their help, advices, support and inspiration. Without your guidance this master thesis would not be possible. I was very glad to get an opportunity to work on this topic for my master thesis, during which I learned a lot and got an important experience of working with Petrel software.

I would like to thank all my friends and fellow students, especially Andrei Roman, Elisabeth K. Røynestad, Daria Shvets, Katerina Savinkova, Petter Andersen, and Per Inge Lindi for their support and advices not only during the writing of this master thesis, but also during all the 5 years of my studies.

Last but not least, I express my deepest gratitude to whole my family both in Russia and Norway for their greatest support, motivation and love.

Daria Martiuk,

Tromsø, Mai 2017

Table of Contents

1. Introduction and fundamental theory

1.1 Objectives

The tectonic development of the Barents Sea fault system influences both fluid migration pathways and shallow gas accumulations. The tectonostratigraphic development varies over time, and the high number of basins, platforms and domes reflect the complex development of the area. Previous studies in the western Barents Sea have suggested that fluid flow exists in many areas and therefore is widespread and abundant (e.g. Faleide et al., 2015, Knies et al., 2009, Henriksen et al., Chand et al., 2008). Many structural features in western Barents Sea are associated with hydrocarbon fluid-flow. These structural features include basins, highs, platforms, as well as salt structures and accumulations (e.g. Vadakkepuliyambatta et al., 2013). It appears that a characteristic pattern of fluid accumulations shows up acoustically as high amplitude anomalies in seismic records. They have been associated with faults and related tectonostratigraphic developments (Faleide et al., 2015, Knies et al., 2009, Henriksen et al., Chand et al., 2008).

My master thesis consists of theoretical and practical parts. The theoretical framework comprises discussion of fluid migration, its mechanisms and indicators of hydrocarbon migration. The description of geology of the study area includes the theoretical part and is made by the compilation of updated and relevant literature, particularly literature focusing on the western Barents Sea. The practical part represents seismic interpretation of the 3D seismic cube BG1002 in Petrel E&P Software Platform 2015 and wellbore data from the well 7224/7-1.

The aim of this master thesis is to study and describe local tectonostratigraphic and fluid migration development of the Samson Dome within the overall geological evolution of the region (Figure 1-1). It is conducted by seismic interpretation of the 3D seismic cube BG1002 in Petrel E&P Software Platform 2015. The interpretation should allow deciphering important tectonic phases and their influence on fluid migrations and shallow gas accumulations. The objectives are twofold. First, to apply the Petrel E&P Software Platform 2015 for mapping geological formations, structures and acoustic high amplitude anomalies. Second, to develop a stratigraphy for the cube using borehole information, identify major individual faults and fault networks using seismic attributes and automatic fault detection, determine the

tectonostratigraphy including fault system development. For this, I map acoustic anomalies and their stratigraphic position in space, and propose a conceptual model for the fluid flow, gas accumulation and tectonic development.

Figure 1-1. *Location of the Barents Sea. Modified from Mattos et al., 2016.*

1.2. Fluid flow in the subsurface

There are many types of fluids present in the subsurface: hydrocarbons, mud, water, brine, etc. It is important to understand principles of their migration in order to analyze possesses that are going on in the subsurface, interpret seafloor and underground structures and features, study marine biological processes and composition of the oceans, and identify potential geohazards (Judd, Hovland, 2007). In this paper, the theoretical part is primarily focusing on fluid migration of hydrocarbons.

1.2.1. Hydrocarbon fluid migration

Hydrocarbon fluid migration is a process of movement of hydrocarbons within the subsurface due to excess pore-fluid pressure. Such processes as sediment loading, uplift, erosion, dissociation of a gas hydrate, polygonal faulting, generation of hydrocarbons and their seepage from source rock and reservoir may cause fluid migration (Løseth et al., 2009).

Hydrocarbon migration can be subdivided into three phases, primary, secondary, and tertiary migration (Figure 1-2):

Primary migration implies transport of newly generated hydrocarbons from the source rock into the adjacent reservoir rock. Once hydrocarbon are expelled from the source rock, they may form tiny oil globules or gas bubbles within the coarse-grained carrier beds. Since more hydrocarbons migrate to the carrier rocks, these globules and bubbles grow and are influenced by buoyancy forces. If buoyancy forces exceed capillary forces that prevent migration, upward secondary migration of hydrocarbons occur. Secondary migration occurs during long time and long distances through permeable rocks, fractures and faults. Thus, secondary hydrocarbon migration is the movement of hydrocarbons after expulsion from a source rock through carrier and reservoir rocks or fault and fracture systems into the trap (Jahn and Graham, 1998). During next hundreds of years and even longer, fluids that abandoned the reservoir proceed to move. This movement is referred as tertiary migration (Minescu et al., 2010).

Tertiary migration represents movement of hydrocarbons from one trap to another or to a surface by seeping primarily due to the gravitational forces of water influx. This type of migration occurs in all the petroleum reservoirs, and may induce reduction of hydrocarbon volumes and changes in fluid character. The main concept of tertiary migration is based on

the tendency of all natural systems to reach equilibrium. After the end of two first migration phases, fluids are chaotically distributed and pressures are not in equilibrium in the reservoir. Thus, tertiary migration occurs in order to reach this equilibrium. It includes following stages: a transport of fluids from higher to lower pressures, distribution of fluids to normal gravitational positions, a decrease of phase dispersion to the smallest fluid–fluid interface area, and a rearrangement of the present fluids at a micro and macroscale (Minescu et al., 2010).

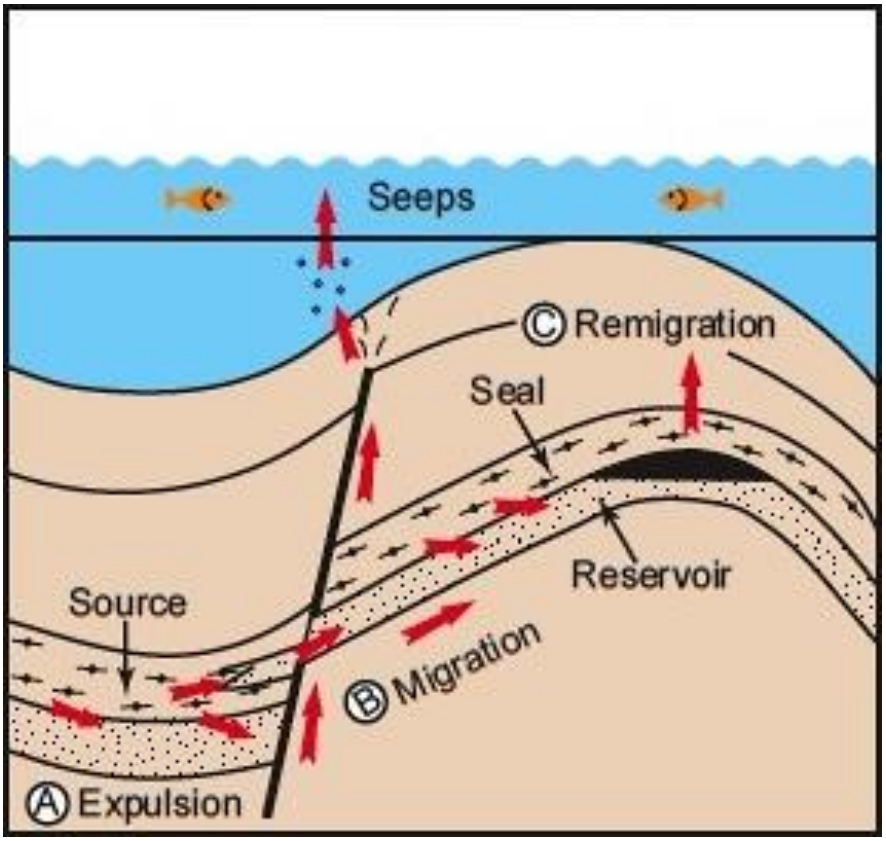

Figure 1-2. *Three migration phases: (A) Primary migration (expulsion); (B) Secondary migration (migration); (C) Tertiary migration (remigration, seeps). Retrieved from Matthews, 2008.*

1.2.2. Mechanisms of fluid migration

Fluid migration is controlled by several mechanisms, known as Darcy Flow, diffusion, and fracture flow (Løseth et al., 2009; Wang et al., 2010).

Darcy Flow

One of the most important mechanisms of fluid flow, which can be applied to describe all types of fluid flow in permeable and porous media, is expressed in Darcy's Law:

$$Q = -\frac{kh \, \Delta \, p}{\mu}$$

Where Q is the total flow/discharge, k- permeability of the rock, i.e. hydraulic conductivity, h- thickness of the geologic strata, $\Delta \, p$- hydraulic potential difference, i.e. hydraulic head, and μ- viscosity, i.e. fluid thickness (Berndt, 2005). Since fluid flows from high pressures to low pressures, negative sign is used in the formula.

Darcy's Law implies that total specific discharge equals the product of the permeability of the rock, total pressure drop and the area where discharge takes place. This law can be applied to describe all types of fluid flow in permeable and porous media, except for the cases when given value of hydraulic conductivity is not valid in reality. For example, fluid flow through the rock containing large number of fractures compared with the area of interest, blow-outs and flows on a microscopic scale (Berndt, 2005).

Diffusion

Diffusion is a fluid transport mechanism based on the concentration gradient. It represent random movement of solute molecules in the fluid because of their kinetic energy and is described by the Fick's First Law:

$$J = -D_d \frac{dC}{dx}$$

Where J is a flux through the medium, D_d is diffusion coefficient for porous media, C- concentration of a solute, x- distance (Šráček and Zachariáš, 2002). Diffusive flow is quite slow, and goes from high to low concentrations in order to reach a state of homogeneity (Watson and Baxter, 2007). Concentration differences of pore-fluid components induce diffusive flux in almost the same manner as pore-pressure differences cause fluid flow within porous and permeable media. (Berndt, 2005).

Fracture flow

Fracture flow represents leakage mechanism occurring along the faults and trough fractures or above small parts of trap. This leakage mechanism takes place in different ways: in spatially limited set of fractures along fault zones, in hydraulic fractures overlying highly overpressured reservoirs (Figure 1-3), on the sides or above salt domes within fractures that formed due to tectonics (Løseth et al., 2009). In order to induce leakage, a reservoir should adjoin the fault in an appropriate place, there hydrocarbons are present and the pore pressure is high enough to reactivate hydrocarbon migration (Wiprut and Zoback, 2002). Faults and fractures may enhance the permeability and porosity of the reservoir and provide high flow rates of hydrocarbons. However, fractures and faults may act as leakage pathways, which can cause depletion of traps that were rich in hydrocarbons within relatively short time (Wennberg et al., 2016; Løseth et al., 2009).

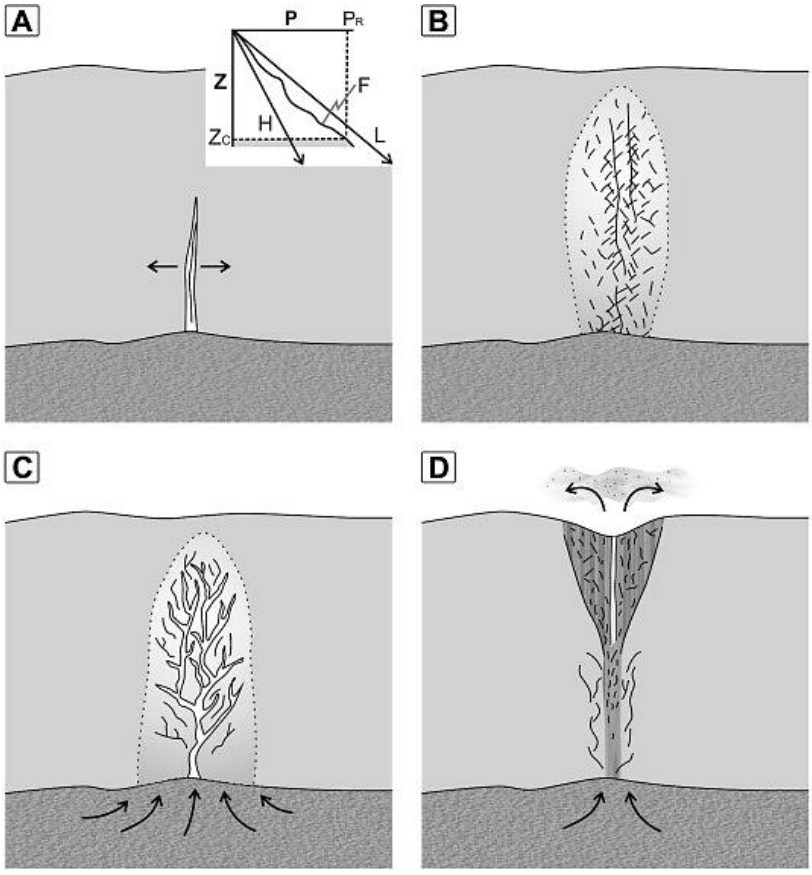

Figure 1-3. *Mechanism of the fluid flow migration through hydro-fractures. A) Fluid pressure exceeds minimum stresses in the overburden and, thus, overpressure is created. First fracture forms. B) Fluid flow starts migrating upwards into the seal due to the pressure difference, causing more fractures to form. C) Constant fluid flow from the reservoir to the seal induces propagation and widening of faults. D) Conduit path for fluid is created that results into possible formation of fluid escape features. Retrieved from Cartwright and Santamarina, 2015.*

1.2.3. Indicators of hydrocarbon fluid migration

Seismic reflections caused by the changes in acoustic impedance that are not attributed to lithological differences within the rock, may be indicators of hydrocarbons and areas with diagenesis (Andreassen, 2009). Following features may serve as indicators of fluid migration:

Acoustic masking

Acoustic masking is one of most common indicators of gas in sediments. On seismic profiles, it appears as vertically oriented wipe-out zone of low amplitude reflections with distorted continuity. Such low amplitude and chaotic continuity of seismic reflections can be explained by impedance contrast resulting from low seismic velocities in gas and much higher seismic velocities in the surrounding sediments. Acoustic masking is usually present on seismic sections in a form of gas chimneys or seepage acoustic pipes (Andreassen, 2009, Arntsen et al., 2007).

Gas chimneys are defined as vertically oriented columns of low amplitude and irregular reflector continuity that are filled with gas, mainly methane (Heggland, 2014). These zones are characterized by wipe-out seismic signal and noise. Gas chimneys are leakage pathways for hydrocarbons and are usually associated with faulting. Arntsen et al. (2007) attribute formation of gas chimneys to three phases. The caprock needs to include fracture network, which gas from the reservoir can migrate through. This gas migration should occur at a constant rate. Further, the diffusion of gas from fractures to adjacent unfractured rocks takes place. Gas accumulations cause fluctuations in seismic velocity and induce scattering of seismic waves.

Cap rock volume, which hydrocarbons migrated to and where gas chimneys or seepage pipes formed, may be referred as a leakage zone. All types of leakage/migration processes take place within this zone. Leakage zone comprises such elements as root, body of the leakage zone, and a top (Figure 1-4). The place at the bottom of a leakage zone, where leakage of hydrocarbons starts, is defined as root. This area is important for hydrocarbon exploration, since its size and character may provide information on leakage processes and hydrocarbon charge of the reservoir. Body of a leakage zone comprises area where hydrocarbons move vertically up to the top, where leakage stops. The place, where uppermost leakage processes occur according to seismic observation- top of the leakage zone, is often located next to or on

the sea floor, and may cause formation of seabed depressions such as pockmarks and craters. Seepage of hydrocarbons results from present active leakage or indicates that leakage has recently been active (Vadakkepuliyambatta et al., 2013; Løseth, 2009).

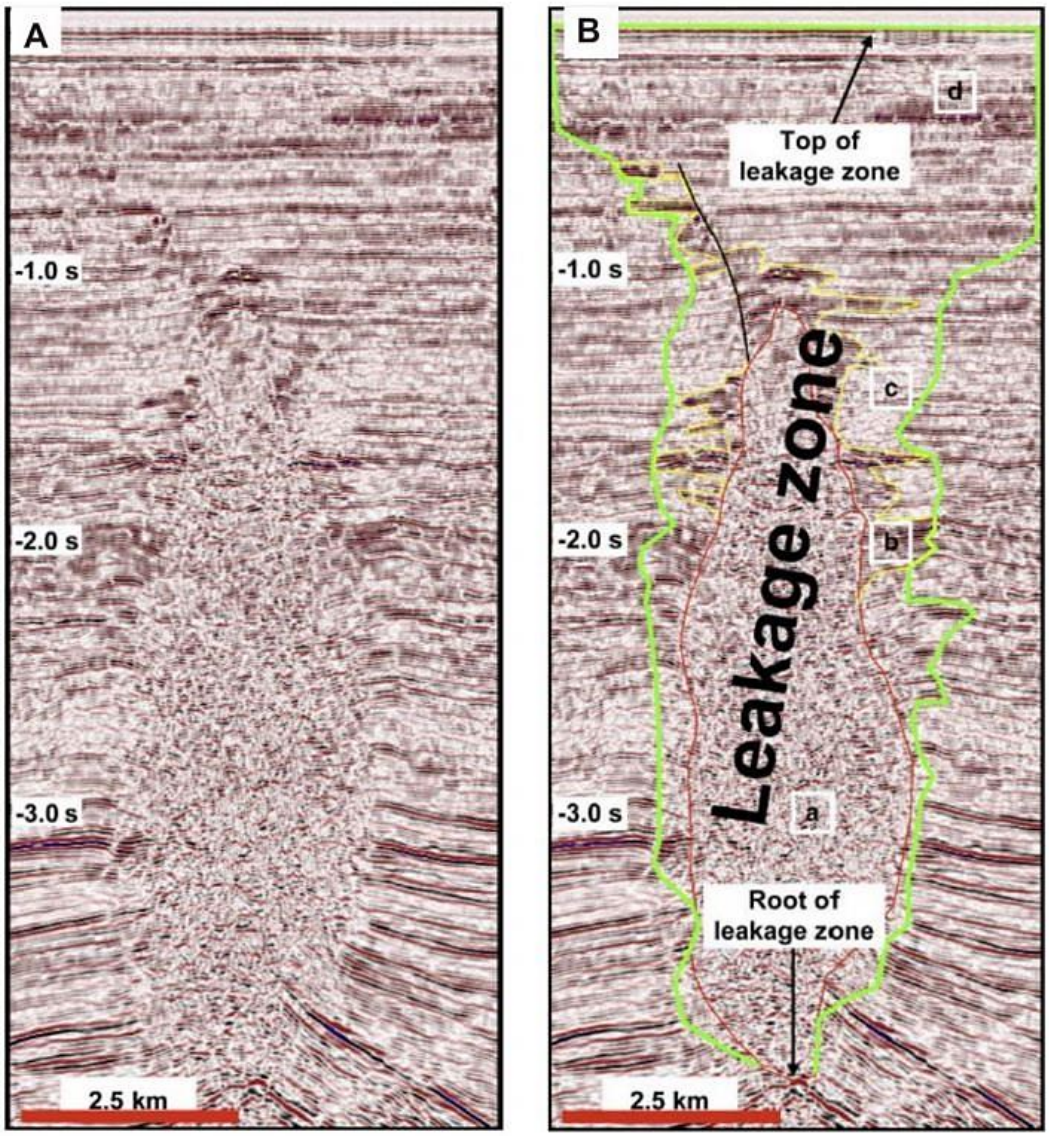

Figure 1-4. *(A) Gas chimney located above a salt dome, (B) Interpretation of the gas chimney with defined leakage zone and its main parts. Retrieved from Andreassen, 2009.*

Seepage acoustic pipes are vertical to sub-vertical, narrow zones of low seismic amplitude and disrupted continuity of reflections. Amplitude anomalies such as acoustic masking and bright spots are typically observed within the pipes as shown in Figure 1-5 and Figure 1-6. Diameter of acoustic pipes varies with depth, as well as inclination of the pipe from a vertical, which may reach up to 60°. Usually diameters of the pipes are about 200 meters; however, they may vary from few tens of meters to even over 500 meters. Height of the pipes lays in a range of 200 to 500 meters with some exceptions that may exceed 2000m or even 5000m. Very often, geometry of the pipes follows fault zones, structural and topographic highs, buried scarps, pinch outs or paleochannels. Surface pockmarks are usually formed in the areas where seepage pipes terminate. Nevertheless, some pipes do not reach the seabed, but form buried pockmarks within the subsurface (Figure 1-5) (Cartwright and Santamarina, 2015).

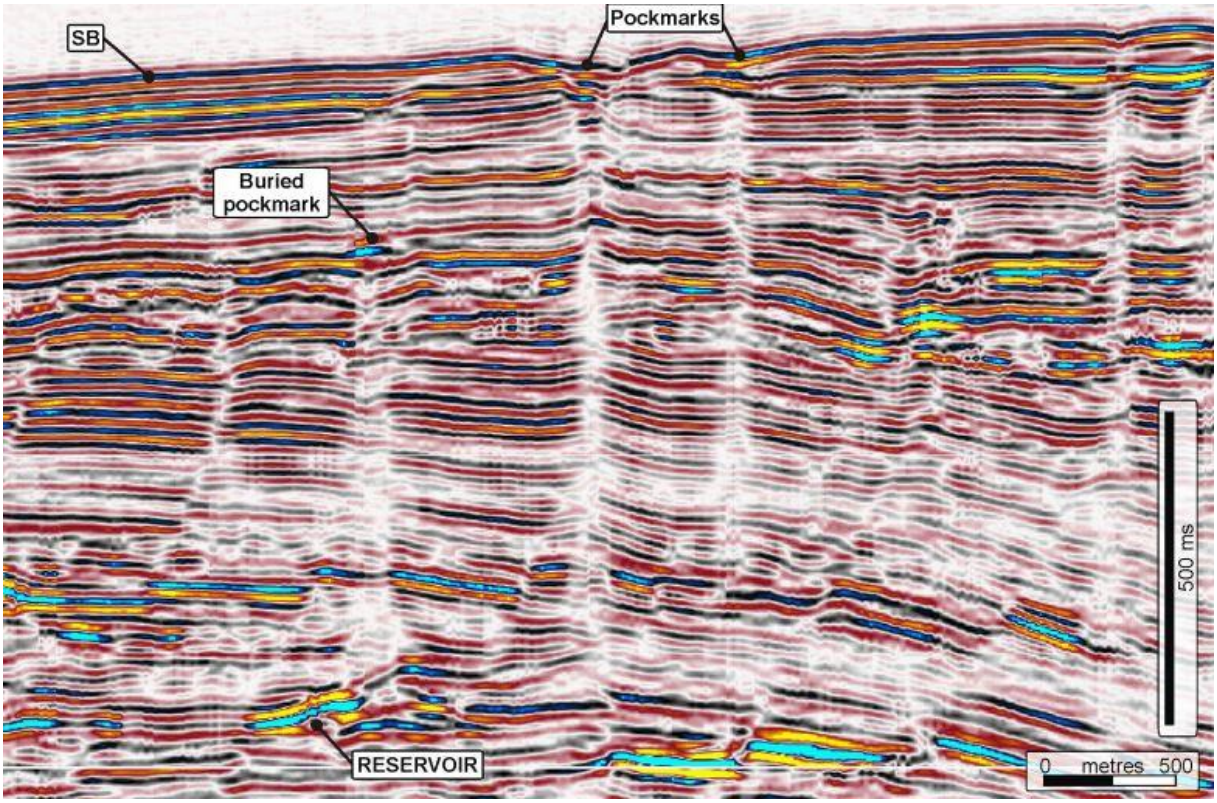

Figure 1-5. *Acoustic pipes with surface pockmark and buried pockmark at the zones of pipes terminations. Retrieved from Cartwright and Santamarina, 2015.*

Fault and fracture zones

Faults and fractures act as good conduits for hydrocarbon migration. Hydrocarbons migrate upwards along the fractures and faults due to increased pressure difference formed after faulting. Hydrocarbons flow into permeable rock layers adjacent to fault zone, but are not likely to be detected within the zone itself. On seismic profiles, they appear as number of high-amplitude anomalies inside permeable layers (Andreassen, 2009).

High amplitude anomalies

Increase in seismic amplitude may be caused by significant changes in lithology or can be an indicator of hydrocarbon presence in the rock. Seismic reflections of high amplitudes are often referred as bright spots (Figure 1-6). They appear on the seismic profile due to sudden changes in acoustic impedance. For example, if shale layer is located above gas sand deposits, the sudden change in acoustic impedance occur and bright spot that serves as a direct hydrocarbon indicator appears on the seismic section (Andreassen, 2009).

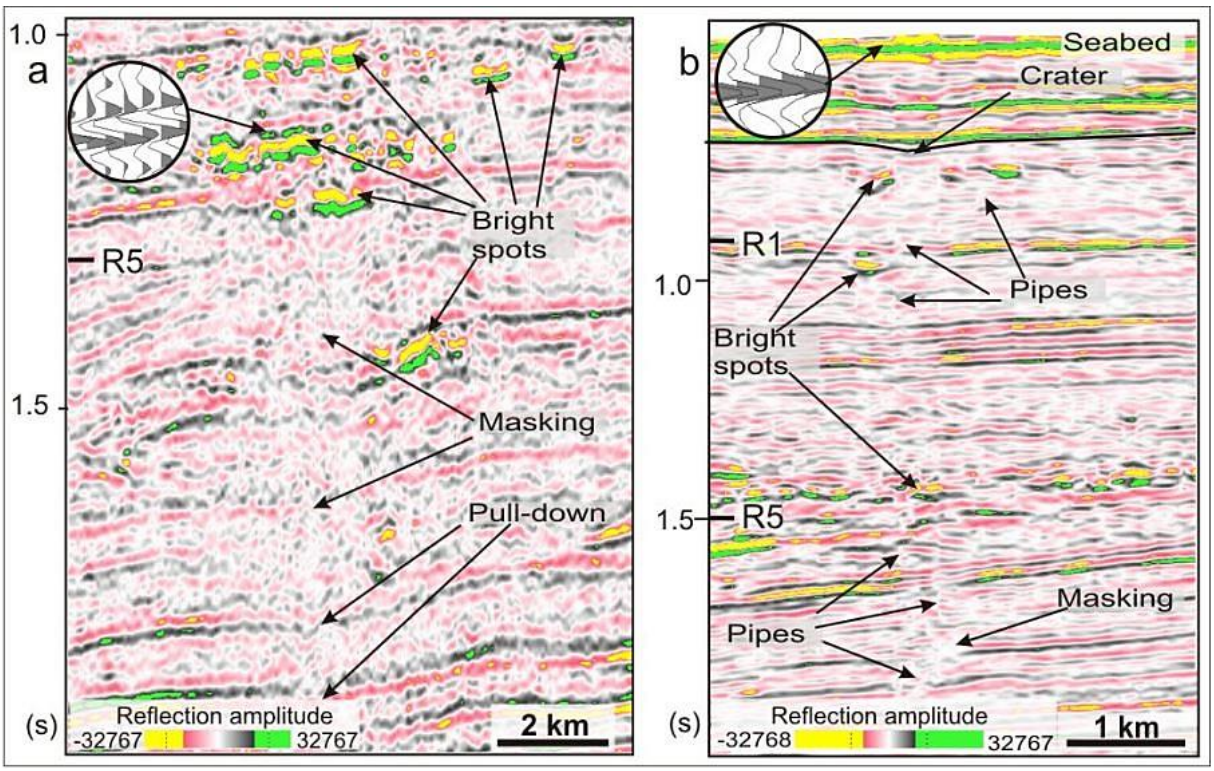

Figure 1-6. *Seismic profile with indicators of hydrocarbon fluid migration including acoustic masking, seepage pipes and high amplitude anomalies. Retrieved from Andreassen et al., 2009.*

Pockmarks

Pockmarks are crater-like depressions on the seafloor formed by the seepage of fluids through the seabed (Hovland, Judd, 1988) (Figure 1-5). They have been detected in many geological environments such as seas, oceans, lakes, etc. Width of pockmarks varies a lot and lays in a range of 1-10 meters (unit pockmarks) and 10-700 meters (normal pockmarks), while height of unit pockmark and normal pockmark is usually less than 0.6 meter and from 1 up to 45 meters, respectively. Pockmarks are usually observed in fine-grained sediments, where they formed due to escape of gas or other fluids (Judd and Hovland, 2007). As it was mentioned above, pockmarks are usually formed at the top of the leakage zone of gas chimneys and acoustic pipes. Thus, pockmarks can act as fluid flow and hydrocarbon indicators, as well as indicators of underground hydraulic activity, subsurface fluid pressure areas in places with high earthquake activity, and potential geohazards such as areas of the seafloor instability with probable slope collapse (Hovland et al., 2002).

Gas hydrates and shallow gas accumulations

In areas with significant number of fluid flow features, gas hydrates are often present. Gas hydrates are crystalline compounds consisting of water and gas, where gas molecules are trapped within a cage-like framework of hydrogen-bounded water molecules (Hovland, 2005). Specific temperature and pressure conditions are needed in order to form gas hydrates. For example, onshore areas in Polar Regions and offshore sediments at the depths of 300-500 meters and with temperatures lower than 10°C are favorable terms for formation of gas hydrates. The zone of subsurface characterized by conditions where gas hydrates may form and be stable is referred as gas hydrate stability zone (GHSZ) (Figure 1-7). (Hovland, 2005; Andreassen, 2009).

Fluid flow migrating upwards or laterally through structural leakage pathways such as polygonal faults, salt diapirs, faults, and gas chimneys can be trapped by the impermeable gas hydrate stability zone leading to the occurrence of a bottom-simulating reflector (BSR) (Wang et al., 2010). BSR is the base of gas hydrate stability zone that follows iso-temperature lines and, thus, appears as a reflection parallel to the seabed on a seismic profile (Figure 1-7). Sudden impedance contrast between layers overlying BSR and containing gas hydrates, where seismic velocity is high, and underlying sediments that are characterized by low seismic velocities due to the presence of free gas, result into BSR reflection. (Andreassen, 2009). If

temperature within GHSZ increases or/and pressure decreases under certain conditions, gas hydrates dissociate and free gas continues to move upwards towards the surface forming shallow gas accumulations (Wang et al., 2010).

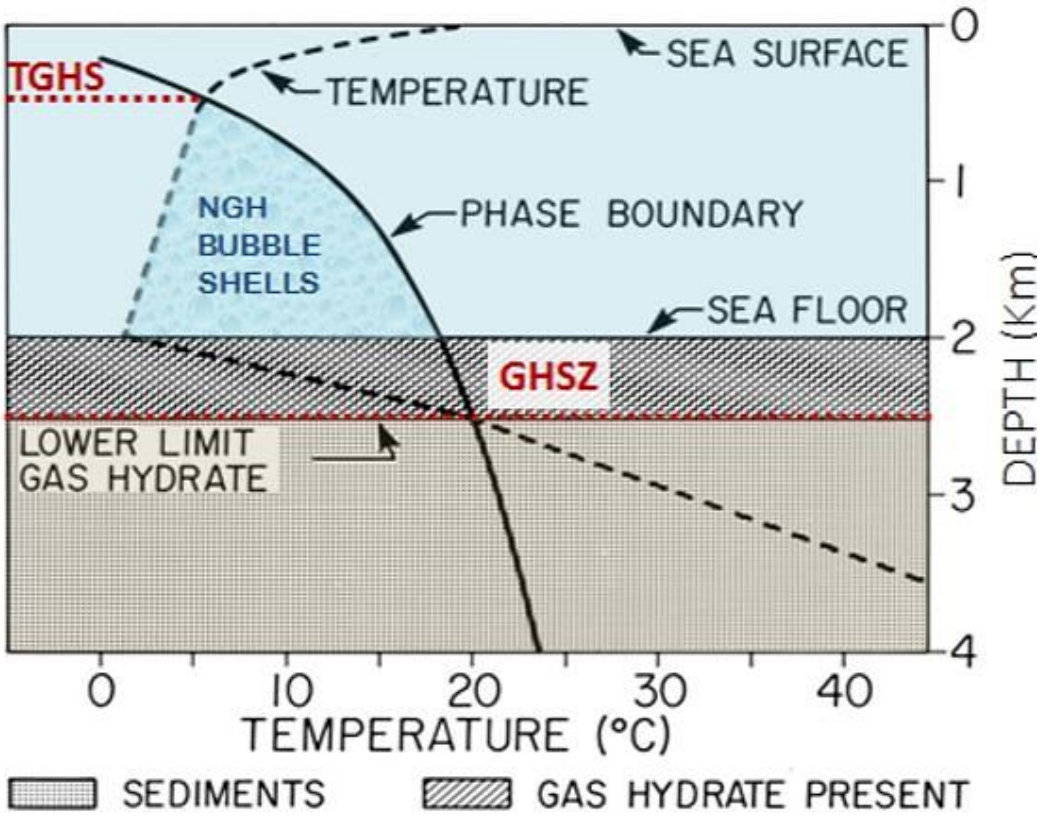

Figure 1-7. *Gas hydrate stability zone (GHSZ) and water column top gas hydrate stability (TGHS) based on relation between temperatures and depth. Retrieved from Barnard et al., 2016.*

1.3. Geology and hydrocarbon potential of the Barents Sea

Barents Sea covers an enormous area edged by the coasts of Russia and northern Norway, Novaya Zemlya, the Atlantic Ocean, Franz Josef Land and Svalbard archipelagos towards the Arctic Ocean (Figure 1-8). It covers 1.3 million km^2 and has average water depths of only 300 m. Barents Sea is situated in an intracratonic setting, and has been affected by several tectonic events since post-Caledonian to Cenozoic times. Barents Sea can be roughly divided into two provinces: Western and Eastern Barents Sea (Figure 1-9). Tectonic and stratigraphic development of the western and eastern part of the Barents Sea differs distinctly with time, magnitude and orientation. There are also major differences in sediment thickness and basin characteristics, as well as in underlying lithospheric mantle density between Western and Eastern Barents Sea that caused a different crustal and lithospheric configuration (Smelror et al., 2009).

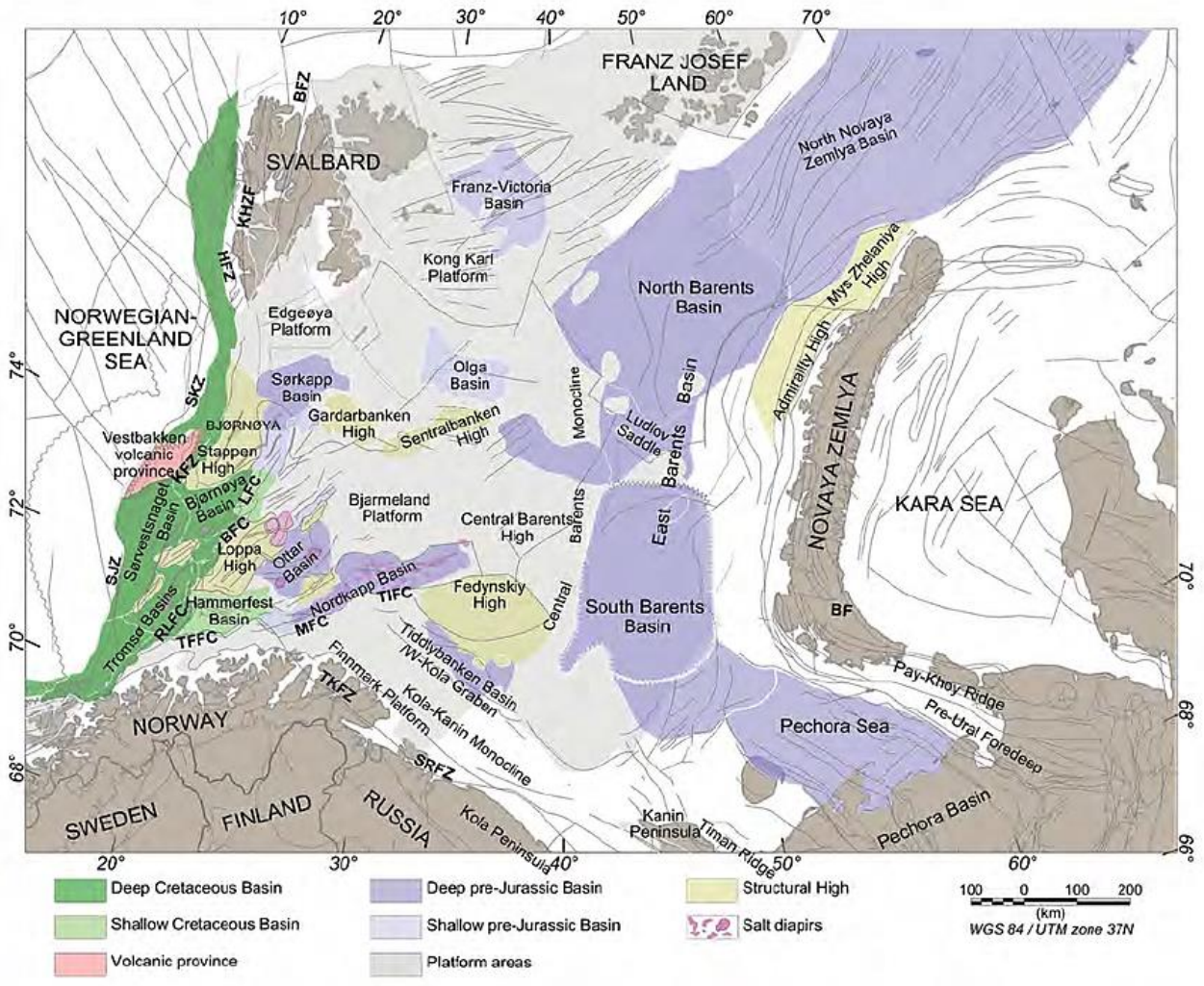

Figure 1-8. *Structural map of the Barents Sea. Retrieved from Marello et al., 2013*.

Geology of the Eastern Barents Sea was dominated by the complex tectonic events of Novaya Zemlya, Pechora Basin, and by Uralian Orogeny. Geological setting of the Eastern Barents Sea was quite stable after Caledonian Orogeny and less affected by tectonic events compared to the Western Barents Sea. Geological history of the western province was mainly defined by major post-Caledonian rifting and later rifting events that resulted into continental breakup along the northwestern margin of the Eurasian plate (Smelror et al., 2009).

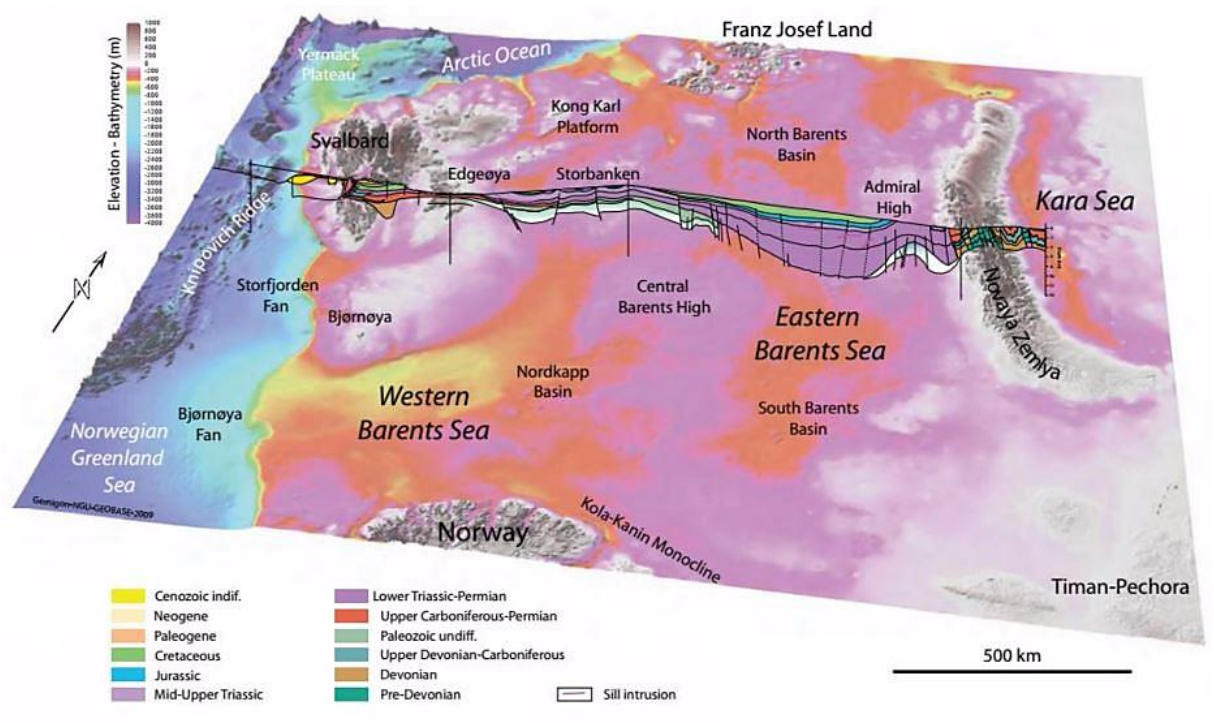

Figure 1-9. *Bathymetry of the Barents Sea with a rough division into western and eastern province; regional geological profile. Retrieved from Smelror et al., 2009.*

Late Mesozoic and Cenozoic times are characterized by significantly active tectonic development in the Western Barents Sea with high deposition rate within sediment sequences of Cretaceous, Paleogene and Neogene sediments in the Harstad, Tromsø and Bjørnøya Basins. While rifting influenced the Western Barents Sea basin development, the basins of the Eastern Barents Sea lay on a stable continental platform. This may imply that a suture zone exists between Eastern and Western Barents Sea. However, such a transition zone between Western and Eastern Barents Sea still remains an open question, as well as the location of the Caledonian suture of this transition zone in the southwestern Barents Sea and its extension into the Eastern Barents Sea (Ebbing et al., 2007).

Such a transition zone could be defined by dominating fault trends that are mainly N-S to NNE-SSW within Ringvassøy-Loppa and Bjørnøyrenna Fault Complexes. The area to the west of transition zone is dominated by NNE-SSW, NE-SW and locally N-S fault trends, while E-W, WNW-ESE to ENE-SSW fault trends prevail in the southeastern Barents Sea, where thick sediment piles accumulated during Upper Paleozoic and Mesozoic (NPD).

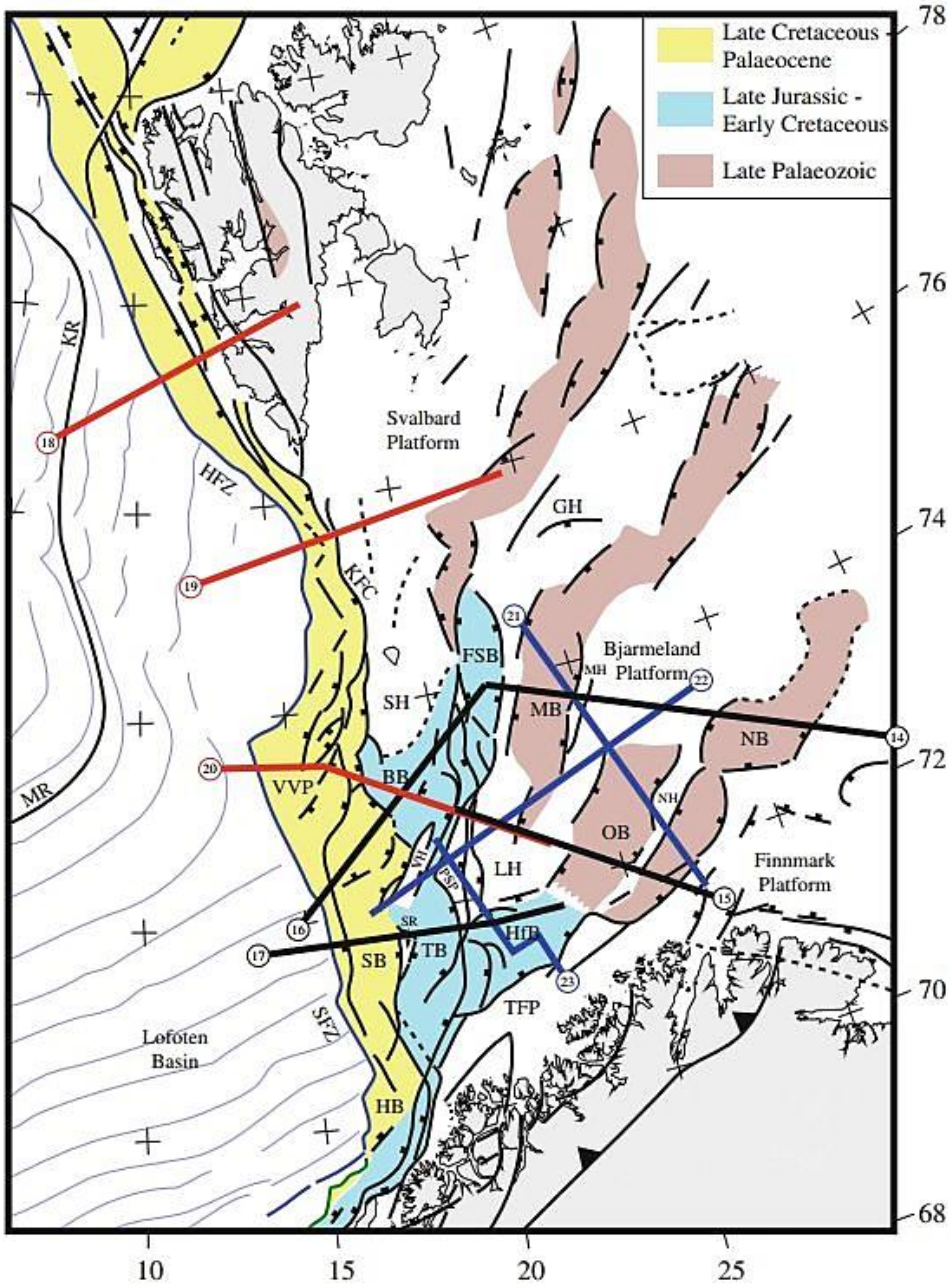

Figure 1-10. *Main structural elements in the western Barents Sea. Retrieved from Faleide et al., 2010.*

Western Barents Sea has a thick sediment sequence of Upper Palaeozoic to Cenozoic rocks. As seen from Figure 1-10, Upper Palaeozoic and Mesozoic sediments, particularly Triassic, dominate on Svalbard Platform. Their paleo surfaces are quite flat and without any traces of strong tectonic activity molding area.

The area to the south of the Svalbard Platform and towards the east, i.e. Norwegian coast comprises numerous small basins and structural highs in the central region within Late Jurassic- Early Cretaceous sediments, and Palaeocene-Eocene successions in the western basins (Figure 1-10). The continental margin includes a southern Senja transform margin, a central rifted margin on the southwest of Bjørnøya related to Early-Tertiary volcanic activity, and a northern margin along the Hornsund Fault Zone that was first transfered and afterwards rifted. A crustal transition zone is limited by a narrow zone along the margin south of Svalbard, which is overlain by a thick Upper Cenozoic sedimentary wedge (Faleide et al., 2010; Eldholm et al., 1987).

Hydrocarbon exploration of the Barents Sea started in 1980 with the first discovery made in 1981. It has been proven that the Barents Sea has a hydrocarbon potential due to its geological setting. Late Jurassic and Triassic formations are considered to be most favorable source rocks for the production of hydrocarbons. Late Jurassic Hekkingen Formation has highest oil and gas potential, and is the largest source rock in the western Barents Sea. Snadd and Havert Triassic Formations have high hydrocarbon potential as well. Largest gas discoveries of the western Barents Sea have been found within these source rocks (Vadakkepuliyambatta et al., 2013). Nevertheless, there are still many discussions on the prospectivity of the Barents Sea including tectonostratigraphic developments. Distribution of reservoirs and source rocks in the Barents Sea is mainly connected to three tectonic stages: Paleozoic Caledonian Orogeny, Late Paleozoic- Mesozoic Uralide Orogeny, and major Late Mesozoic- Cenozoic rift episodes and tectonic breakup in the western part of the Barents Sea (Henriksen, 2011). Formation of the Barents Sea occurred due to two major continental collisions followed by continental separation, i.e. collision of Baltica and Laurentia during mid-Paleozoic, subsequent Mesozoic rifting events and Cenozoic sundering (Doré, 1995; Gernigon et al., 2014). Barents Sea was subject to major tectonic uplift and erosion during Cenozoic times after the opening of the Norwegian-Greenland Sea at approximately 55 Ma. Magnitude of both uplift and erosion varies largely within regions of the Barents Sea. Net erosion values are estimated to be in a

range of 0 and 3000 meters. The age of the erosion and uplift of the Barents Sea has been a subject of significant discussion among scientists, since these events play an important role for hydrocarbon prospect evaluation. Moreover, results of erosion and uplift effect reservoir quality, source rock maturity and migration pathways of hydrocarbons. They increase the risk of leakage and gas cap expansion (Henriksen et al., 2011b).

2. Geological framework of the Western Barents Sea

2.1. Tectonostratigraphic evolution of the Western Barents Sea

The western Barents Sea is part of the continental shelf of northwestern Eurasia, situated north of Fennoscandian Peninsula adjoining the Norwegian-Greenland Sea and Svalbard in the west. Western Barents Sea geology has been affected by several tectonic events, rift episodes, from post-Caledonian to Cenozoic times that formed present complex of basins and platform areas. The western Barents Sea rift system is considered to be the centre of the Caledonide orogen that has a dominating NE-SW strike direction (Faleide et al., 2010; Ritzmann et al., 2007). Development of the southwestern Barents Sea geology comprises such main tectonic phases as the Timanian, Caledonian, and Uralian orogenies, proto-Atlantic Late Permian-Mesozoic rifting in the western part, and the breakup and opening of the Northern North Atlantic Ocean along the western margin of the shelf (Gernigon et al., 2014).

2.1.1 Paleozoic

The history of development of the Western Barents Sea starts with a mountain-building tectonic event known as Paleozoic Caledonian Orogeny that occurred about 400 Ma, started in the Middle Ordovician and culminated in the Silurian. It caused rift development of the southwestern Barents Sea, uplift to the west and distribution of sediments across the shelf in the direction of carbonate platforms to the east (Henriksen et al., 2011). Paleozoic Caledonian Orogeny resulted from gradual convergence of Baltica and Laurentia continents and their subsequent collision, during which margin of Baltica subducted beneath the Laurentia in Silurian to Early Devonian times and Iapetus Ocean closed (Figure 2-1). Because of the collision, the Laurentian plate (Greenland, North America) and the Baltic plate (Scandinavia, western Russia) consolidated into the Laurasian continent. Early Palaeozoic tectonic events formed the Scandinavian Caledonides that represent a large number of thrust sheets of diverse composition, origin and grade of metamorphism (Roberts, 2003). The Caledonide Orogen outcrops are present in Norway, westernmost Finland, western Sweden, on Svalbard and in northeast Greenland. In Norway, they extend for about 2000 km from the Stavanger region in the south to the Barents Sea region in the north. The Caledonide Orogen of the Barents Shelf is exposed on Svalbard along most of the northern and western coasts of the

main islands Spitsbergen and Nordaustandet with general strike in N-S direction (Gee et al., 2008).

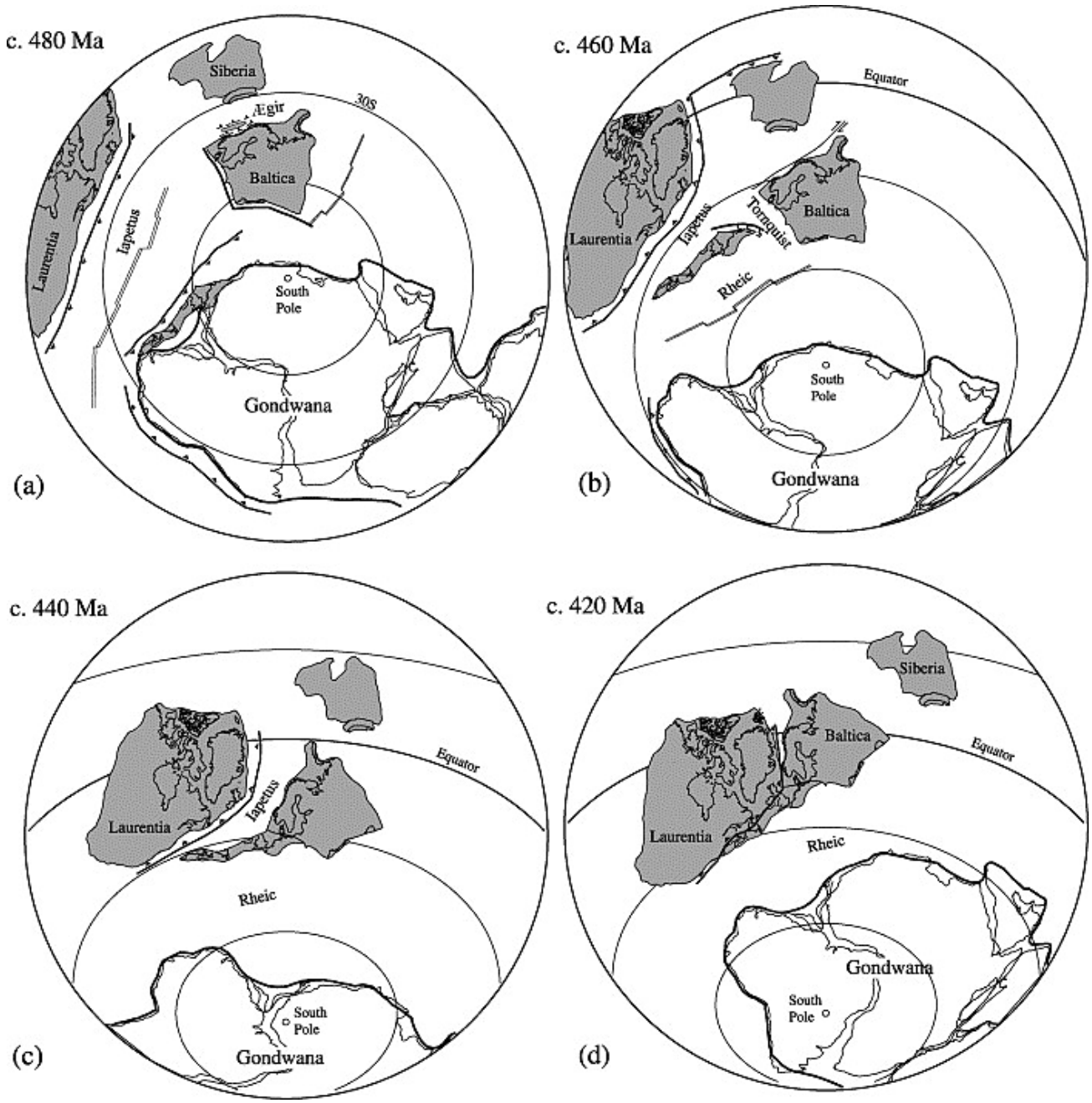

Figure 2-1. *Convergence and subsequent collision paths of Baltica and Laurentia continents from Early Ordovician to Late Silurian time, based on paleomagnetic reconstructions. Retrieved from Roberts, 2003.*

Further collision between Laurasian continent and Western Siberia formed the eastern margin of the Barents Sea during the latest Permian-earliest Triassic with Uralian orogeny at the junction of this collision and its northern extension, Novaya Zemlya. During Permian-Triassic times the Uralide orogeny became the last stage in the formation of the supercontinent Pangea (Roberts, 2003). Further tectonostratigraphic evolution of the area was dominated by an interaction between marine transgression and series of tectonic episodes that resulted in the break-up of the Pangea supercontinent (Dore, 1991).

Crustal extensional tectonic events characterized development of the western Barents Sea during the Late Palaeozoic and Mesozoic, particularly in The Early-Middle Devonian, Carboniferous, Permian, Triassic and late Jurassic-Early Cretaceous periods. They comprised collapse of the Caledonian and Uralian orogenic belts and subsequent break-up of the Pangea supercontinent. Rifting had a general westward migration trend. As a result, major rift basins crossing the Barents Shelf and a range of intermediate platforms and structural highs formed, well-defined rifts and pull-apart basins were created in the southwest, and the belt of strike-slip faults developed in the north. Late Palaeozoic crustal extension accounted for the formation of half graben structures and a subsequent regional sag basin, covering largest parts of the present Barents Shelf. Tectonic conditions on Svalbard Platform and the eastern part of the regional basin have been relatively stable since Late Palaeozoic. However, the area was subject to epeirogenic movements that resulted in elevation differences in present geological setting (Dore, 1995; Faleide et al., 2010).

2.1.2. Mesozoic

A significant Early Triassic rift episode occurred in the western Barents Sea. While further, tectonically quiet conditions and post-rift thermal regional subsidence characterized the geological history during the Triassic period in the western Barents Sea. However, minor tectonic events took place on the Bjarmeland and Finnmark platforms (Smelror et al., 2009; Faleide et al, 1984). Western margin, where Loppa High was subject to uplift and erosion in the Early Triassic, comprises larger number of active faults. Loppa High has undergone several phases of inversion. Sequence patterns from the Loppa High display that it became a site of maximum deposition in the sedimentary basin in Late Triassic, but was afterwards uplifted as a high in Late Jurassic.

Svalbard and Bjørnøya tectonic regimes were calm, and clastic marine sedimentation dominated the areas from the Sverdrup Basin to the Pechora Basin. The area between Greenland and Norway was subject to rifting processes in a form of discrete pulses in the Jurassic, for which direct evidence exists on Svalbard. Rifting during Middle to Late Jurassic times dominated on the Hammerfest Basin and generally along the western margin due to the westward extensional regime directed towards Atlantic rift system (Gabrielsen et al. 1993). Tectonic activity increased through the Late Jurassic in the western Barents Sea and culminated in the Early Cretaceous. It resulted in formation of the present day structural configuration of basins and highs (Gabrielsen et al. 1990). The main rifting in the Barents Sea was associated with basins in the western part, including the Hammerfest Basin and Finnmark Platform (Henriksen et al., 2011a). The Late Jurassic-earliest Cretaceous regional extension prevailed in SW Barents Sea and triggered the development of Bjørnøya, Harstad and Tromsø basins as prominent rift basins (Faleide et al., 2010).

Early Cretaceous time in the northern Barents Sea is characterized by prevalent magmatism without any significant traces of faulting. Large intrusions and extrusions are present both onshore (Svalbard and Franz Josef Land) and offshore north of the Barents Sea. This volcanism was associated with the opening of the Arctic Ocean during Late Mesozoic, in particular rifting and breakup in Amerasia Basin and the development of Alpha Ridge. It caused uplift of the northern margin and formation of southward-prograding delta sequences. Thus, major part of the Barents Sea was a high platform in Late Cretaceous and Cenozoic (Faleide et al., 2010; Polteau, 2016; Smelror et al., 2009). Rifting episodes resulted in a rapid subsidence along the western margin during Early Cretaceous and deposition of a very thick Cretaceous sediment succession in Tromsø, Harstad, Bjørnøya and Sørvestnaget basins (Henriksen et al., 2011a). During the Late Cretaceous- Paleocene, pull-apart basins formed in the westernmost parts of the Barents Sea due to significant rifting between Norway and Greenland and strike-slip movements and deformation on the De Geer zone, mega-shear system connecting Late Mesozoic- early Cenozoic crustal extension in North Atlantic and Arctic region (Smelror et al., 2009; Roberts et al., 2012).

2.1.3. Cenozoic

Cenozoic times are associated with continental breakup of the North Atlantic margins, opening of the Norwegian- Greenland Sea, and formation of the sheared western Barents Sea continental margin.

Norwegian-Greenland Sea and Eurasia Basin sea floor spreading started around 55-53 Ma during Paleocene-Eocene transition. At the same time, a significant magmatic event occurred that resulted in formation of volcanic rifted margins on Lofoten and northeastern Greenland shelves (Smelror et al., 2009). Such a magmatic event at ca. 56 Ma is the major base for the "Paleocene-Eocene Thermal Maximum (PETM)": hypotheses, during which huge amounts of methane and CO2 reached the atmosphere causing a global temperature increase by 5 – 8 °C (Frieling et al., 2016).

A megashear zone connecting the Norwegian- Greenland Sea and Eurasia Basin served as a basis for formation of the western Barents Sea- Svalbard margin during Eocene extensional regime. Compressional deformation occurred within the Spitsbergen Fold and Thrust Belt due to the continental strike-slip system between Svalbard and Greenland, which was active during Paleocene- Eocene. Stress resulted from this transgression to the west of Svalbard acted over large distances, and caused compressional deformation on the eastern part of Svalbard as well. In addition, it is assumed that this compression is also responsible for development of domal structures present in the Eastern Barents Sea (Faleide et al., 2010).

Since Oligocene Greenland and North America moved in a more westerly direction compared to Eurasia continent. Thus, extensional regime started in the Greenland Sea to the west of Svalbard inducing opening of the Fram Strait, which afterwards established the only deep-water gateway between the North Atlantic and Arctic during the Miocene.

Northern Hemisphere glaciations during the Late Pliocene created major unconformities within sediment formations of the western Barents Shelf. Pliocene-Pleistocene times are associated with an uplift and extensive glacial erosion of Cenozoic and some part of underlying sediments on the Barents Shelf. The erosion was more prominent in the western Barents Sea, particularly in the northwest. Here, about 3000 meters of sediment succession was eroded on Svalbard. Erosion rate in the southwestern Barents Sea varies between 1000 and 1500 meters. Large amounts of eroded sediments were transported towards the shelf margins and

accumulated on the continental slope as thick wedges of clastic sediments, in a form of trough mouth fans (Bjørnøya and Storfjorden fans) (Smelror et al., 2009, Faleide et al., 2010).

2.2. Uplift and erosion of the Barents Sea since the Cenozoic

Today, an active discussion is going on about the uplift and erosion of the Barents Sea. First ideas on Barents Sea uplift and erosion appeared in the beginning of 20th century and were suggested by Fridtjof Nansen, based on his observations of bathymetry and geological setting of surrounding areas. In 1980's when hydrocarbon exploration in the Barents Sea began and a first well was drilled, these ideas on uplift and erosion were confirmed. Based on coal petrographic studies on Svalbard several years later, it was confirmed that the area was subject to a significant uplift and erosion of about 1700 m. Data from the first wells in Hammerfest Basin indicated an uplift as well, based on unusually low sandstone porosities at present depth. Scientists assume that the sediments must have been buried at much greater depths, as for example at least 1000-1500 m deeper. The same conclusion was derived from the maturity level of the rocks, which is too high for the present burial depth. Despite the fact that a lot of data has been acquired in the Barents Sea since 1980's, there are still many ongoing debates, particularly related to time frames of uplift and erosion, mechanisms of uplift and location of the major uplifts (Nyland et al., 1992).

Uplift and erosion in the northern North Atlantic region, and in the Barents Sea in particular, during Cenozoic was induced by both tectonic and glacial processes. It includes at least two main phases of uplift and erosion: the first one during late Paleogene and the second during the Quaternary. The first event was caused by the opening of the Norwegian- Greenland Sea and formation of the sheared western Barents Sea continental margin, the second event is considered to be attributed to glaciations and isostasy. (Butt et al., 2002). Magnitude of uplift varies depending on location and lays in a range of 0 to 500 meters (Henriksen et al., 2011b). Tectonic uplift and erosion related to plate reorganization in the Norwegian- Greenland Sea took place at the time of Eocene-Oligocene transition and Neogene times. The uplift is considered to be more prominent in the Svalbard area, where it resulted from a deep-rooted thermal anomaly. Uplift in the shear zone area of the southwestern Barents Sea was less pronounced and was caused by thermomechanical coupling (Laberg et al., 2011).

Barents Sea was subaerially exposed until the Early Pleistocene due to Miocene-Pliocene uplift, and consequently was subjected to severe erosion. Thus, eroded sediments were shed into low-relief areas at that time, i.e. southwards and eastwards across Barents Shelf. The net Cenozoic erosion of the western Barents Sea, defined as the difference between total erosion and total deposition thickness, lays in a range of 0 and 3 km, and varies from place to place, but with most prominent erosion in the northwestern part. There is a discussion on mechanisms that contributed most to this erosion; was it either dominated by tectonics or glacial processes (Zieba et al., 2016; Solheim et al., 1996; Butt et al., 2002).

Based on the results from Ocean Drilling Program, it was indicated that glaciation in the northern hemisphere may have begun around 5.5 Ma or earlier. Products of glacial erosion deposited on the outer shelf and continental slopes of the Barents Sea allowed calculating the magnitude of glacial erosion. Erosion during Late Cenozoic glaciations and interglacial-glacial changes makes up two-thirds of the total Cenozoic erosion in the Barents Sea. Therefore, despite the influence of other mechanisms, glacial erosion is considered to be a predominant erosion mechanism at Late Cenozoic times (Butt et al., 2002).

Larsen et al. (2003) divided glaciations and erosion of the Late Cenozoic (2.5 Ma-present times) into three phases: onshore, transitional, and shelf phase. During the times prior to Pliocene-Pleistocene glaciations, major part of the Barents Sea was lowland and located at about present sea level. On the contrary, northern part of the Barents shelf and Svalbard region was exposed with elevations up to 1500 m. Because of this fact, glaciations started in the mountain areas of Svalbard and subsequently extended and covered larger distances due to decrease in global temperatures at the time of Middle Pleistocene, reaching western and northern shelf edges of the Barents Sea. Scandinavian mainland was ice covered as well. However, most of the parts of Barents Sea remained ice-free. At places that were ice-free and emergent, fluvial processes acted as a major erosion mechanism. This phase of glaciation occurred about 2.5-1.5 Ma, and is referred as an onshore phase (Larsen et al., 2003).

The next, transitional glaciation phase occurred around 1.5-0.5 Ma and implied further ice sheet extension under decreasing temperatures. Scandinavian Ice Sheet induced erosion only next to the coast of Scandinavia. Shelf edge at the mouth of the Bear Island Trough was significantly eroded due to advance and retreat movements of glaciers. Ice Sheets on Scandinavian mainland and the Barents Sea were probably not connected at that time. Erosion

and sedimentation rates during this phase are estimated to reach its maximum based on the observations of deposits in the Bear Island Fan (Larsen et al., 2003).

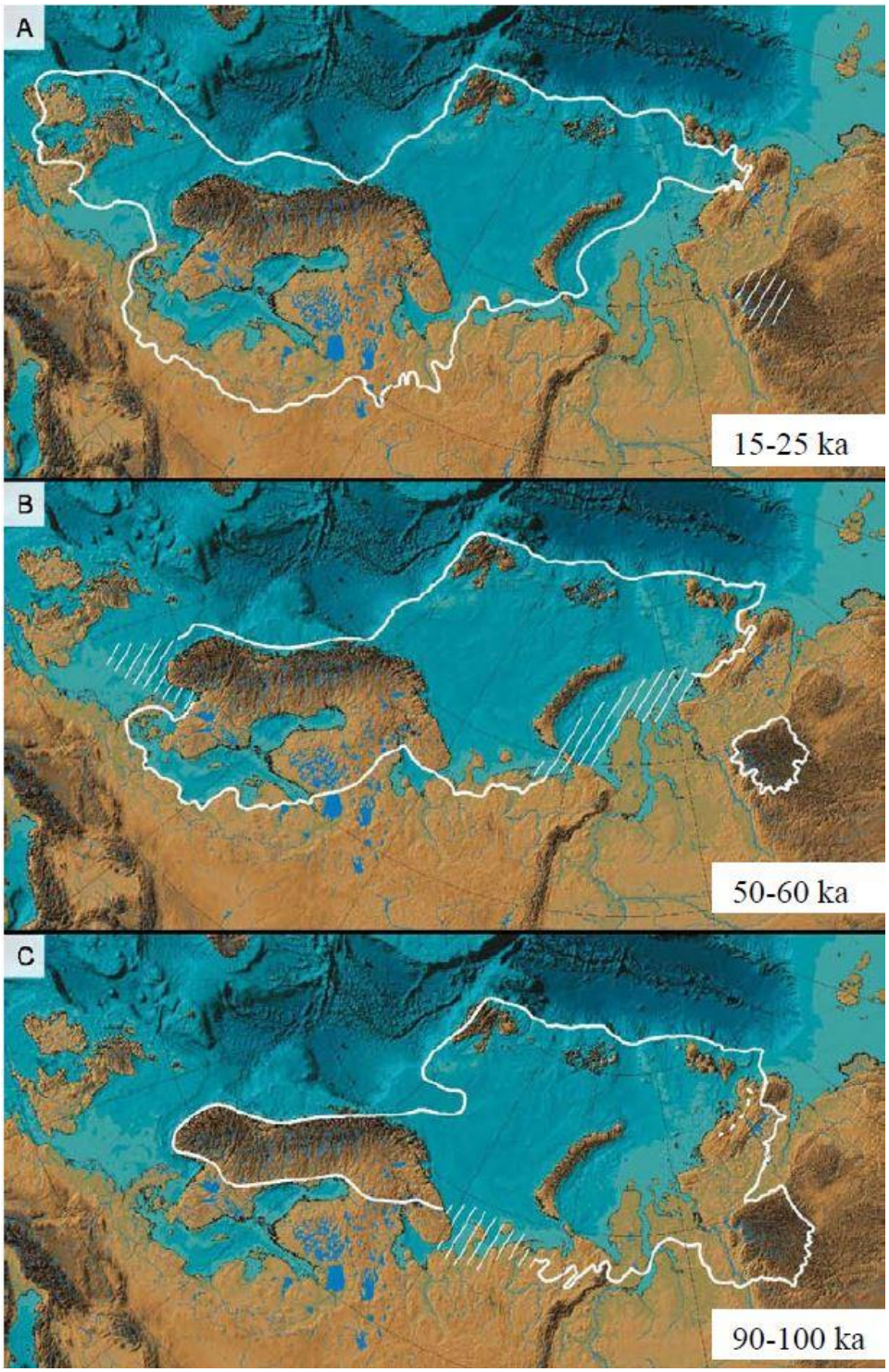

Figure 112. *Ice sheet extent during different places of Weichselian glaciation. a) Ice limits during Last Glacial Maximum. Retrieved from Larsen at al., 2003.*

The last phase of glaciation and erosion, a shelf phase, occurred around 0.5 Ma. Sediments were eroded along the entire Barents shelf during this phase, and vast ice-sheet drainage towards the shelf edge occurred (Larsen et al., 2003).

Zieba et al. (2016) indicated that glaciation of the western Barents Sea can be correlated with marine isotope stages, so-called MIS. Oxygen isotope ratios (O16/O18) of planktonic foraminiferas resemble change in ice volume and sea level and thus glacial interglacial changes (e.g. Shackleton, 1987). Zieba et al. (2016) identifies four stages: MIS 16 (635.6-624.7 ka), MIS 12 (438.7-428.0 ka), MIS 6 (138.6-134.6 ka), and MIS 2 (19.3-16.0 ka). Stage MIS 6, the Saalian glaciation, is associated with distribution of ice sheet on the entire Barents Sea and deposition of regional till deposits. This glaciation was the largest one compared to subsequent glaciations. Weichselian glaciations are divided into three main phases with different maximum glacial limits and shifting glaciation centres. In the Early Weichselian (100-90 ka) southwestern Barents Sea became ice-free, while glaciation continued in the northern and eastern parts. Western and northern shelf breaks became glaciated around 70-65 ka, i.e. during Middle Weichselian. Afterwards, around 25-15 ka at Late Weichselian, the whole Barents Sea was again covered with an ice-sheet, what created highly compacted sediments on the shelf. The earliest Weichselian glaciation was largest in the eastern part of the Barents Sea, while the latest one was largest in the southwestern part. Ice sheet positions during three phases of Weichselian glaciation are shown in Figure 2-. Period from 14 ka to 11 ka is considered to be Last Glacial Maximum (Zieba et al., 2016; Larsen et al., 2003).

Pleistocene glaciations sufficiently influenced the geomorphology of the Barents Sea. Ice sheet dynamics caused erosion on the entire shelf area and transport of eroded sediments to the present day margins. Modern geomorphology of the Barents Sea comprises shallow banks of about 100-200 m below sea level and deep troughs up to 500 meters below sea level. Large amount of glacial material was moved into the major depocenters, which now form a system of large submarine glacial fans along the continental margin. Correlation between ice flow pathways and development of submarine troughs is evident in Figure **2**2-3, where the largest fan in the Arctic region is the Bear Island Trough Mouth Fan (Zieba et al., 2016; Laberg et al., 2011; Vorren et al., 1991).

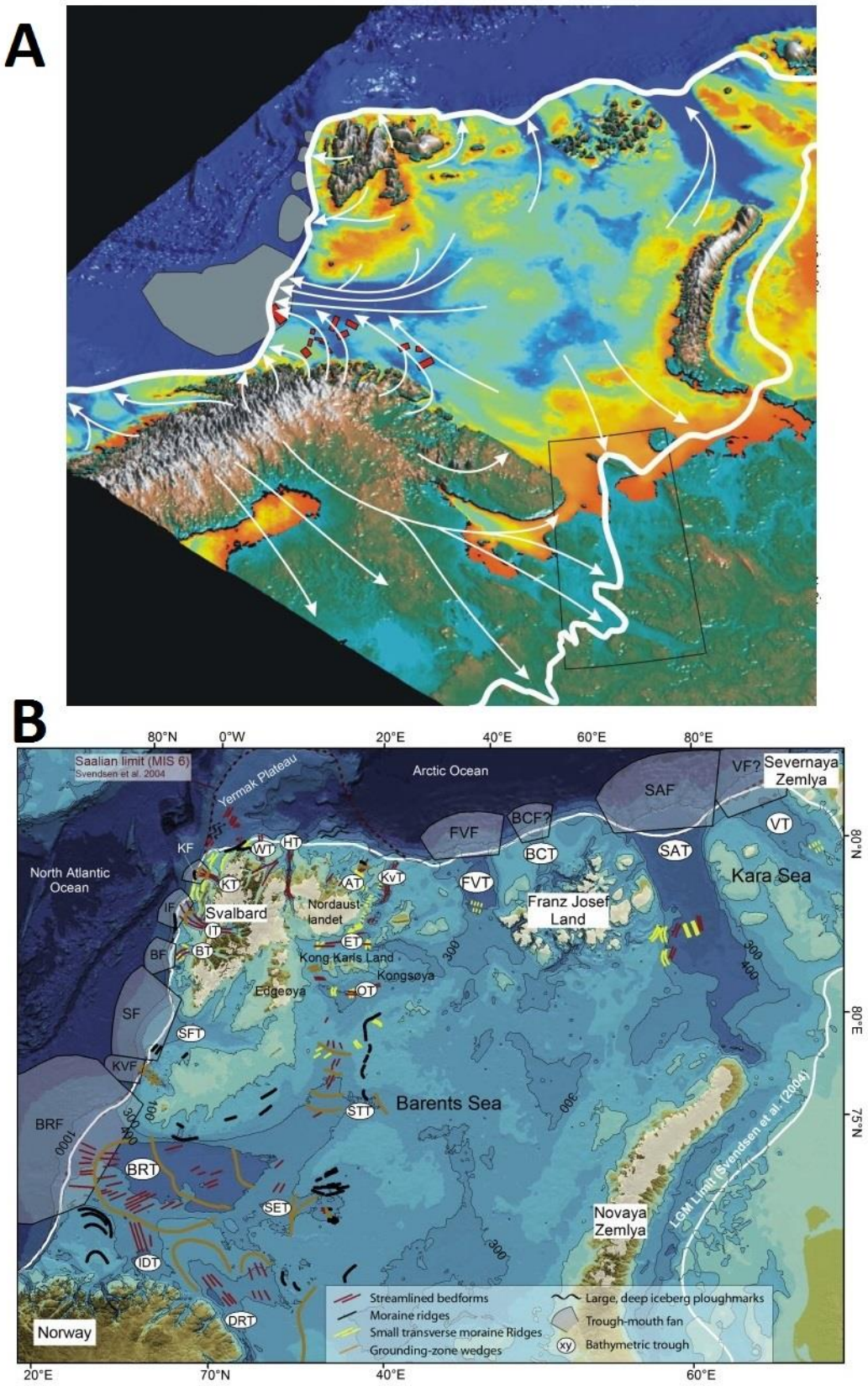

Figure 12-3. *A) Bathymetry map of the Barents Sea with marked glaciation extent (white line) and ice-flow pathways (arrows) during the Last Glacial Maximum. Retrieved from Larsen et al., 2003. B) Map of main submarine glacial landforms. Retrieved from Jakobssen et al., 2014.*

Plio-Pleistocene deposits along western Svalbard-Barents Sea margin form a large unconformity with pre-glacial sediments below and glacial sediments on top (Figure2-4, Figure **2-5**2-5). A strong reflector, known as the upper regional unconformity (URU) represents erosional base for several glaciations. It was formed around 2.5 Ma. Within the Plio-Pleistocene deposits seven reflectors identify regional smaller unconformities: R7- R1. Dominant reflectors R7, R5 and R1 divide the sedimentary succession into three major packages: GI, GII, and GIII, which correspond to Naust Formation of the Nordland Group (Larsen et al., 2003). The regional unconformity corresponds to reflectors R1, R3, R5 in the Bear Island Fan, Storfjorden Fan, and Isfjorden Fan, respectively (Figure 2-5). This correlation, thus, shows the time of the last major glacial erosion reaching the URU level. This time is assumed to correspond with an age of R5 adjacent to Svalbard and later to the central Barents Sea (Larsen et al., 2003).

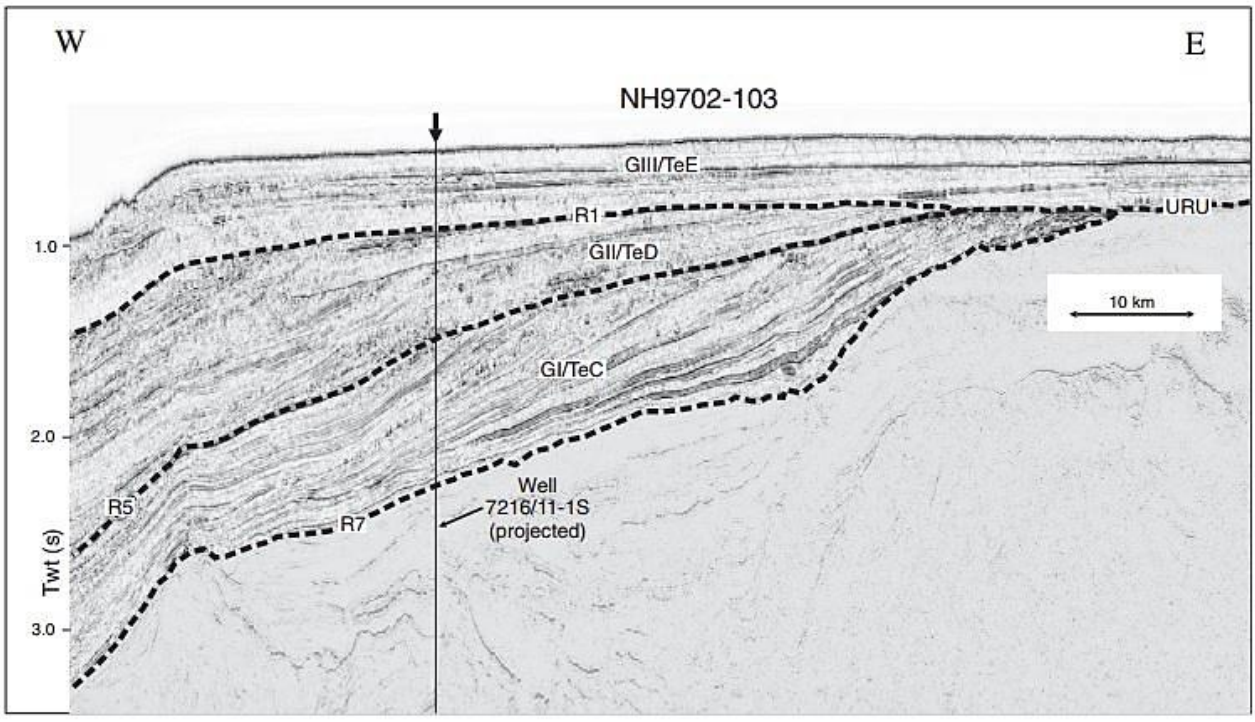

Figure 2-4. *Seismic line through southwestern Barents Sea continental margin. Main sediment packages GI, GII, and GIII are bounded by most prominent regional reflectors R7, R5, and R1. URU, the upper regional unconformity, defines the border between pre-glacial and glacial deposits. Retrieved from Laberg et al., 2011*

Sediment package GI, overlying reflector R7, consists of products of fluvial and glaciofluvial erosion of the Barents Sea. Sediments were eroded and deposited during the period from ca. 2.7 to 1.5 Ma, when Barents Sea remained ice-free, but Svalbard and Northern Scandinavia were covered by an ice sheet. Unconformity R7 marks the onset of glacial sediment deposition around 2.3 Ma and consequently an increase in general sedimentation rate, and corresponds with the base of trough mouth fans on the western margin. During that time, major parts of the Barents Sea have probably emerged, therefore, fluvial sediment transport processes dominated in the area (Zieba et al., 2016; Larsen et al., 2003).

Packages GII and GII contain deposits that resulted from Barents Sea shelf erosion by glacial ice-sheet advances. These sediments were deposited on the outer shelf and on the Barents Sea continental slope. It is estimated that the first glacial advance in the western part of Svalbard occurred around 1.6 Ma, while at the Bear Island Trough Margin at ca. 1.4-1.5 Ma. Glacial erosion since 1.5 Ma ranged from 330 to 420 m. Magnitude of glacial deposition at that time is unknown because of the absence of on-shelf sediments at present time (Zieba et al., 2016).

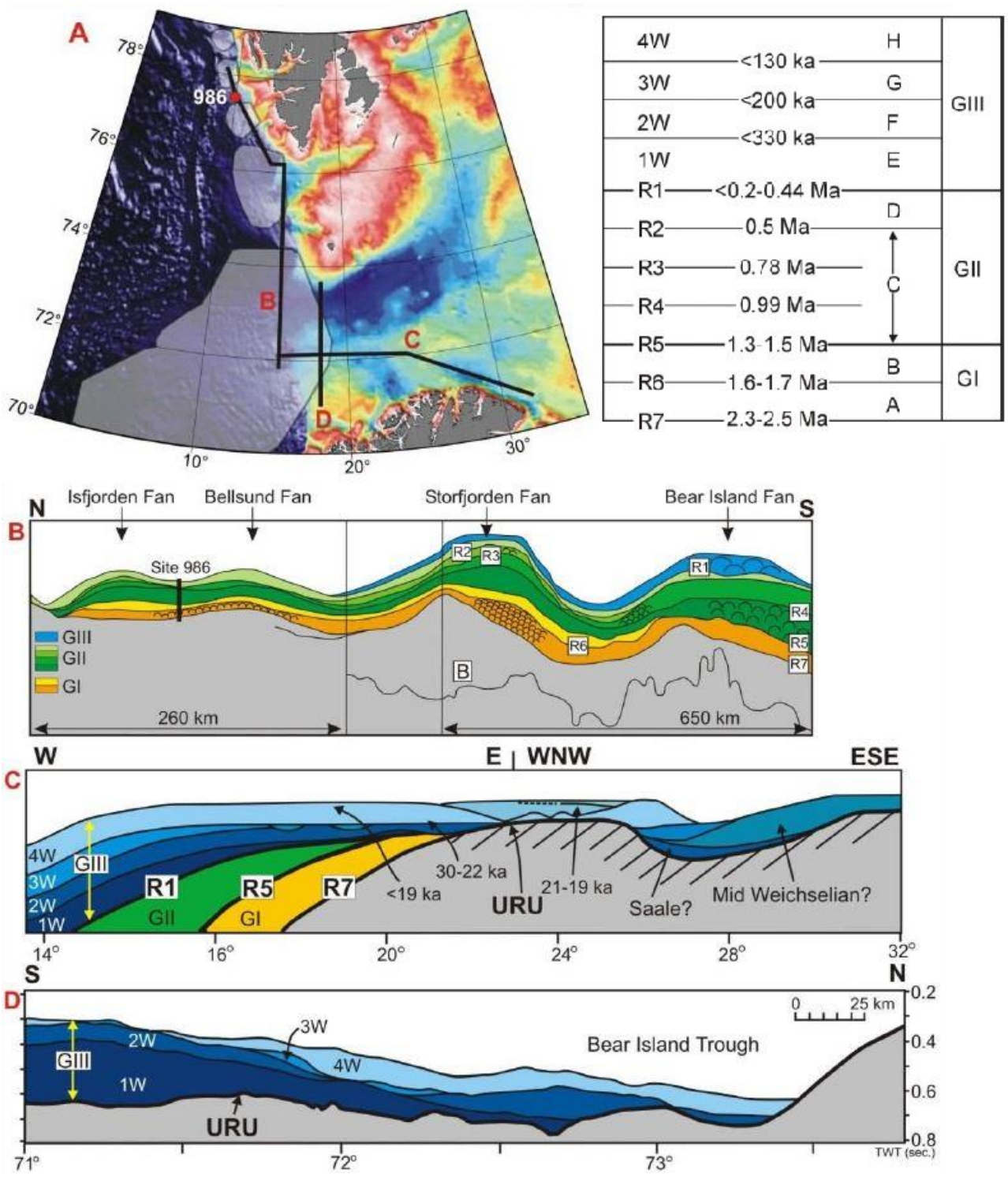

Figure 2-5. *Stratigraphic succession of the late Pliocene to Pleistocene deposits with displayed seven major reflectors, R7-R1, and three main sediment packages GI, GII, and GIII, and a table of age correlations. Modified from Larsen et al., 2003.*

3. Fluid migration indications and development in the W Barents Sea

Western Barents Sea has been subject to many tectonic events, rifting episodes, uplift, and glacial and erosional processes from post-Caledonian to Cenozoic times. Deep sedimentary basins, platforms and structural highs, fault and fracture complexes have been formed in the western Barents Sea due to these tectonic peculiarities. Moreover, depositional environment has been favorable for the formation of mature and hydrocarbon rich source rocks that are located at relatively shallow depths due to the Cenozoic uplift. All these factors form a solid base for fluid migration development in the western Barents Sea. Such features indicating fluid migration as gas chimneys, leakage along fault and fracture zones, seepage pipes, pockmark-like depressions, and accumulations of shallow gas and gas hydrates have been observed in the western Barents Sea (Vadakkepuliyambatta et al., 2013).

Upward migration of hydrocarbons, their seepage through the seafloor and accumulation of gas at shallow depths are mainly attributed to Cenozoic uplift and erosion (Doré, 1995). These processes decreased pressure within the sediments and, consequently, induced liberation of dissolved gas from formation water and its remigration to shallower structures (Dore and Jensen, 1996; Vadakkepuliyambatta et al., 2013).

Cenozoic glaciations influenced fluid migration to a lesser extent than erosional processes and uplift. Nevertheless, changes in generation and migration of oil and gas, redistribution of hydrocarbons within the reservoirs and their spills have probably occurred due to the thermal fluctuations within the ice-underlying sediments. Such fluctuations resulted from series of rapid buildups and subsequent removals of ice sheet (Vadakkepuliyambatta et al., 2013).

It has been observed that fluid migration indicators are usually observed above oil and gas discoveries. For example, researches from Loppa High show still ongoing gas migration along faults and gas seepage through the seabed, what is a positive sign for hydrocarbon exploration. In this way, studying fluid migration indications is crucial and necessary procedure for petroleum industry (Vadakkepuliyambatta et al., 2013; Chand et al., 2008).

4. Study area: Samson Dome

There are many structural features in western Barents Sea that are associated with hydrocarbon fluid-flow, occupying areas varying from 1 to 600 km^2. These structural features include basins, highs, platforms, as well as salt structures and accumulations (Vadakkepuliyambatta et al., 2013) (Figure 4-1).

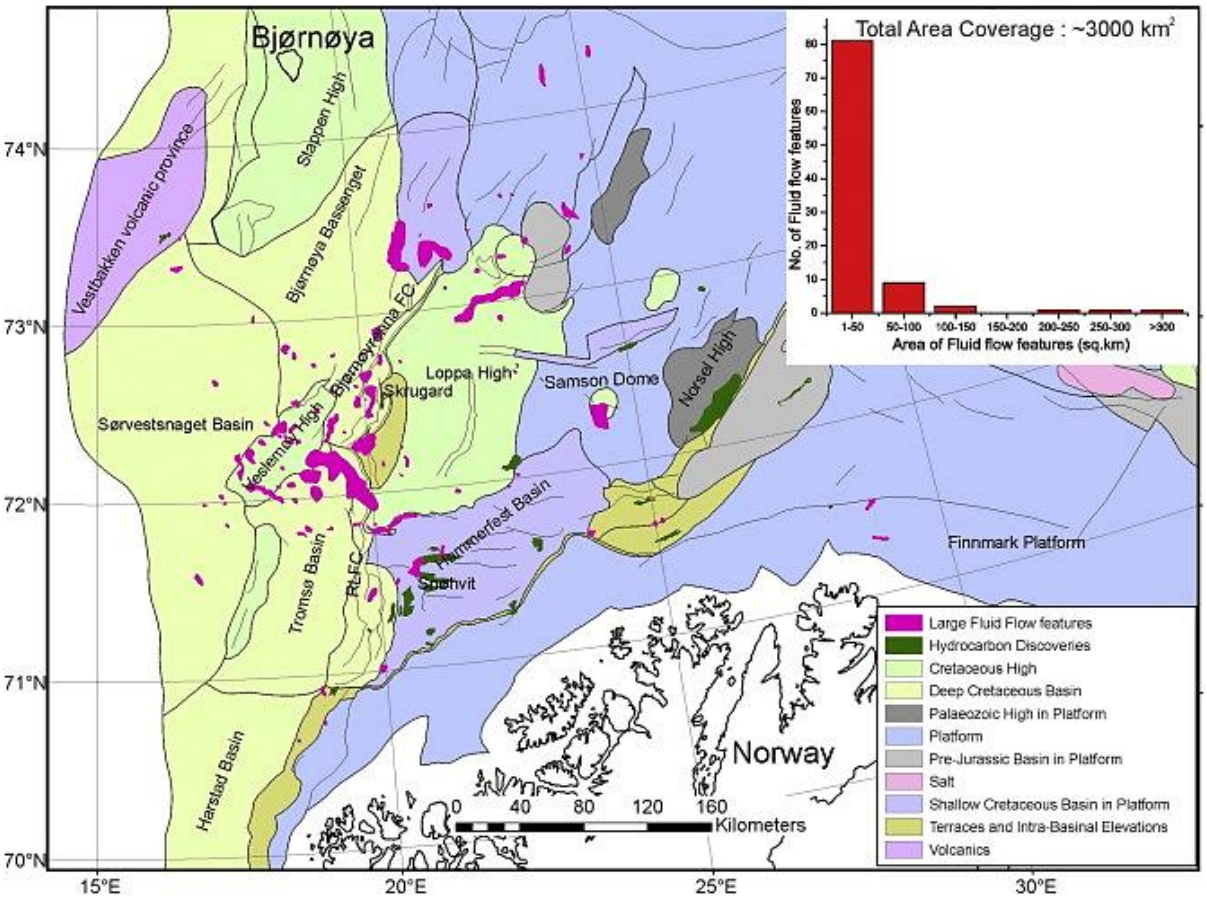

Figure 4-1. *Structural features in western Barents Sea with approximate total area coverage. Retrieved from Vadakkepuliyambatta et al., 2013.*

The area chosen for further studies, Samson Dome, is located in the south-western part of the Ottar Basin and represents a structural high on the Upper Paleozoic depocentre of the Bjarmeland Platform (Breivik et al., 1995). Presence of large salt amounts within the area of the Ottar Basin has been proved and estimated to be approximately 6800 km^3 based on the gravity anomaly observations. Estimations of salt volume beneath the Samson Dome are in a

range of 500 to 600 km^3. Due to its large size and significant salt accumulations, the Ottar Basin is considered as one of the major evaporate basins in Barents Sea, as well as the area above the Samson Dome is the largest fluid-flow feature in the eastern part of western Barents Sea covering approximately 150 km^2 (Breivik et al., 1995; Vadakkepuliyambatta et al., 2013).

5. Data and Methods

5.1. Seismic and well data and Interpretation methods

The dataset used in this master thesis is 3D seismic cube BG1002 and well log data from 7224/7-1 (Figure 5-1, Figure 5-2). ED50-UTM-35 coordinate system was chosen for seismic dataset and well data. Seismic data for the cube BG1002 was acquired in 2013 and is provided by BG Group. The seismic dataset consists of 1099 inlines and 3426 crosslines. The area of this seismic survey is located at Samson Dome and covers about 1170 km^2.

Figure 5-1. *Location of the seismic dataset BG1002 (red rectangular) at Samson Dome, well 7224/7-1 (black dot) and main structural elements next to them. Modified from NPD FactMaps 2016.*

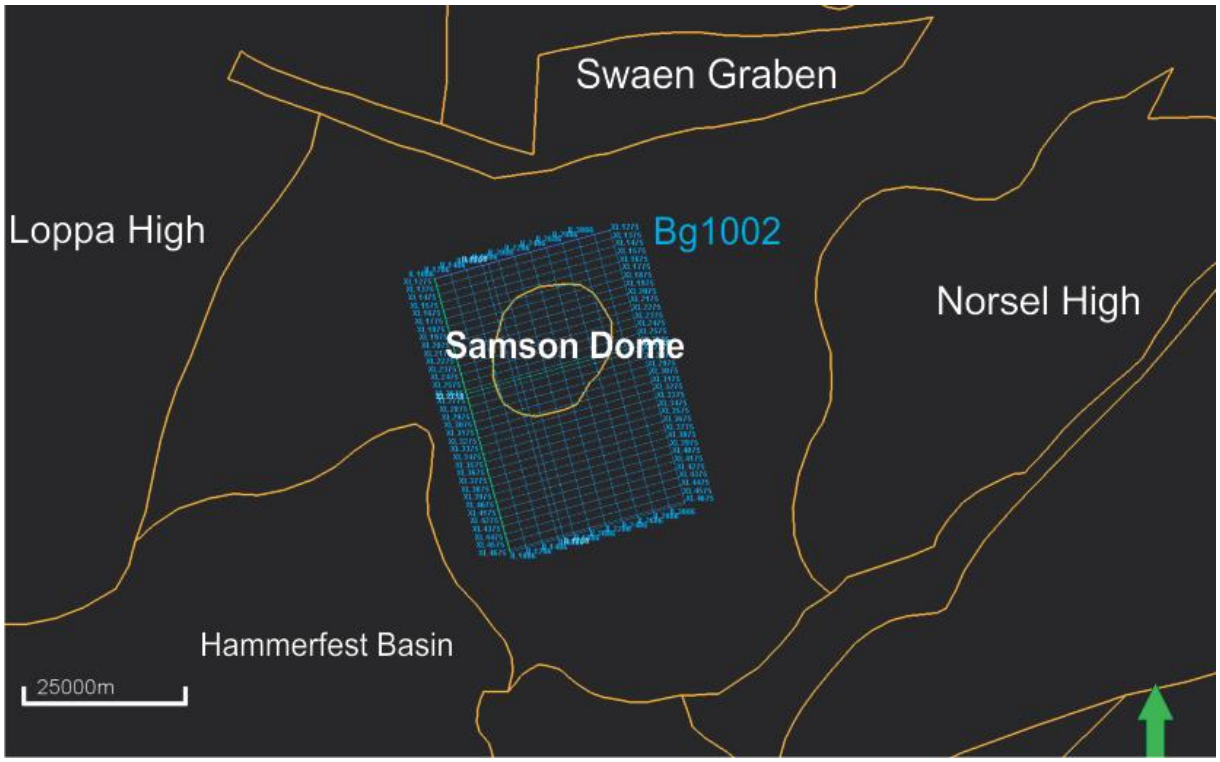

Figure 5-2. *Position of 3D seismic cube BG1002 and main structural elements next to it, illustrated in 2D window in Petrel.*

The well 7224/7-1 was drilled by Statoil (previously Den Norske Stats Oljeselskap A/S) as a wildcat in Lopparyggen Øst area on the Bjarmeland Platform in 1988. It was drilled on the Samson Dome structure with closure on all pre-Oligocene sediments. Well's total vertical depth is 3064 m. Gas-bearing sediments were detected in the intervals from 1660 to 1775 in the Kobbe Formation, and gas shows were recorded on the intervals from 1658 m to 1784 m, 1856 m to 1871 m, and 1922 m to 2027 m. At the same time, permeability of the formation was estimated to be very low and even absent at some sections based on the core analysis and repeat formation tester (RFT) measurements (NPD, factpages).

The data analysis and interpretation have been made by seismic data interpretation of 3D seismic cube BG1002 and well data from the borehole 7224/7-1 in Petrel E&P Software Platform 2015. Methods applied for this data analysis include the use of seismic attributes, interpretation of main seismic horizons, as well as faults and fractures as potential fluid escape paths, and gas accumulation indicators. CorelDraw X8 has been used for editing figures.

The initial 3D dataset BG1002 has been processed to zero-phase, reverse polarity according to SEG polarity standard, where negative reflection coefficient (trough) stands for increase in acoustic impedance (Sheriff, 2006). In order to convert seismic wavelets into more usual format, Phase Shift volume attribute in Petrel was used and new seismic cube processed to zero-phase SEG normal polarity was made, where positive reflection coefficient (peak) corresponds to increase in acoustic impedance (Figure 5-3).

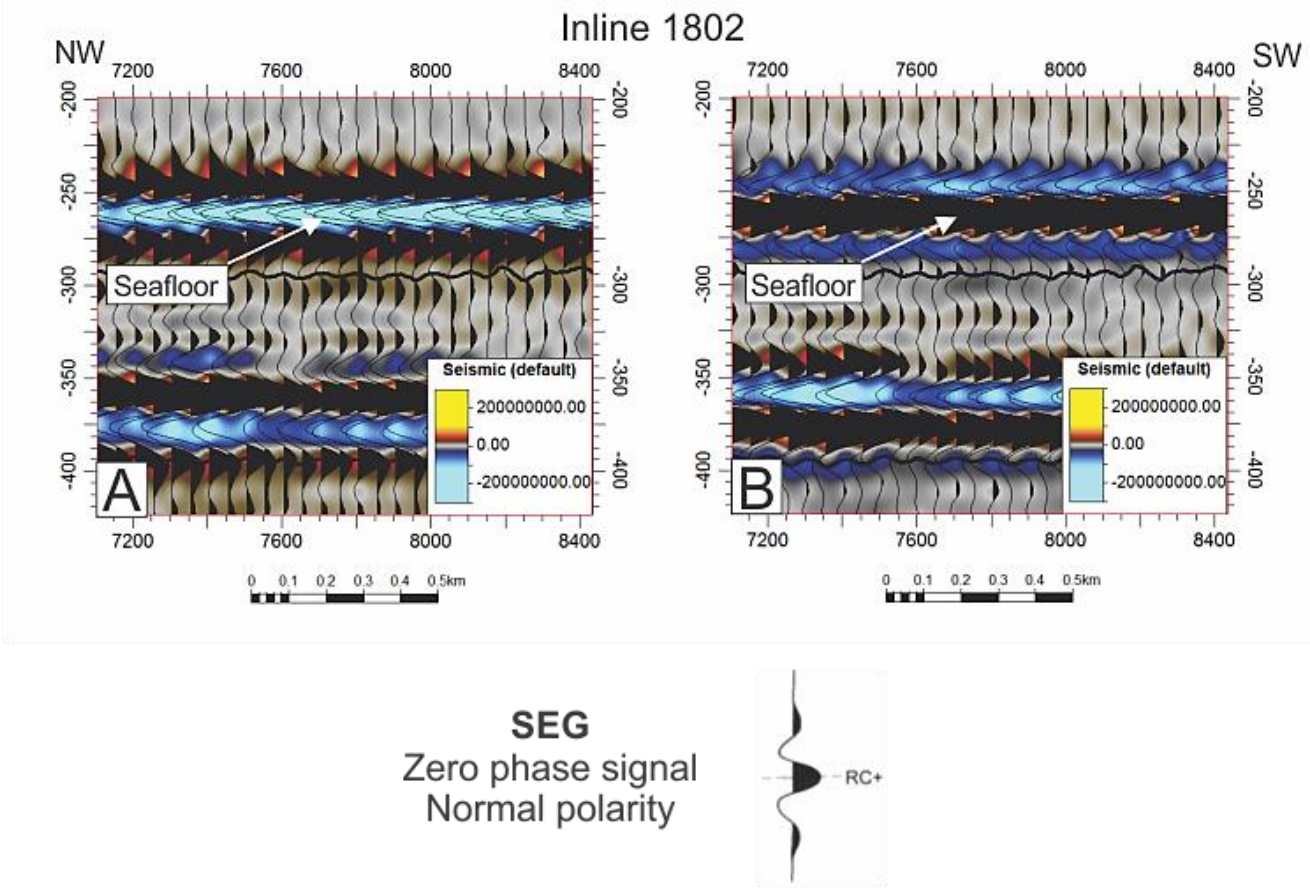

Figure 5-3. *A) Initial phase of seismic signal (SEG zero-phase, reverse polarity) of cube BG1003. B) Phase of the seismic signal of cube BG1002 after applying Phase Shift volume attribute (SEG zero-phase, normal polarity, (Sheriff, 2006)).*

5.2. Seismic resolution

While interpreting seismic data, its resolution plays an important role. “Resolution is the ability to separate two features that are very close together; the minimum separation of two bodies before their individual identities are lost” (Sheriff, 2006).

Seismic exploration uses a method of creation of seismic waves by artificial sources in order to acquire information about geological structures in the subsurface. The method involves observation of the arrival time of the waves reflected from interfaces with a sufficient density-velocity contrast, so called seismic reflectors or acoustic impedance contrasts (Z).

$$Z = \rho \cdot v,$$

Where ρ- is density of the layer, v- velocity of seismic waves in this layer.

Acoustic impedance of subsurface layers is determined by seismic wave velocities. Seismic velocities and wavelengths increase with higher burial depths due to increasing degree of compaction and diagenesis of the sediments. At the same time, frequencies decrease with increasing burial depths. This leads to the fact that seismic resolution is higher at shallow depths and get poorer with increasing depths (Andreassen, 2009; Brown, 1999).

Seismic resolution comprises horizontal resolution and vertical resolution. A geological object of interest have to be larger than vertical or horizontal resolution limit in order to be seen in 3D seismic. Moreover, if two features lay on the large enough distance from each other, anomalies that they produce are easy to be distinguished. When they are located too close to each other, their effects merge and make it very hard to distinguish between them. This conditions are called “resolved”, and “unresolved” respectively (Figure 5-4) (Sheriff, 1997).

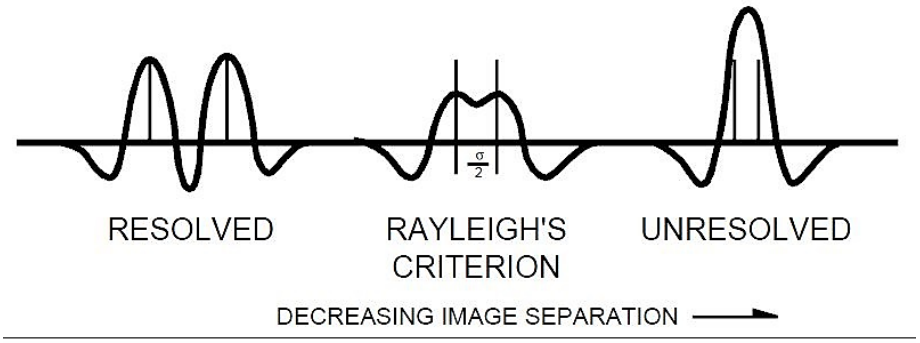

Figure 5-4. *Example on resolved and unresolved condition of two similar geological features depending on the distance between them. Retrieved from Sheriff, 1997.*

5.2.1. Vertical resolution

Vertical resolution is a minimum vertical thickness of a sediment layer necessary to produce a seismic reflection that is visible in seismic. Vertical resolution depends on a wavelength and is defined as:

$$\text{Vertical resolution} = \frac{\lambda}{4} = \frac{v}{4f},$$

Where λ is a wavelength, v- velocity, f- frequency.

Thus, when thickness of the layer is less than a quarter of a wavelength and larger than a limit of visibility, destructive interference occurs. Limit of visibility (λ/30) is a minimum thickness for a bed to produce a reflection distinguishable from the background. If the layer thickness is in the interval between a quarter and a half of a wavelength, constructive interference takes place. No interference occurs and two separate reflections appear in seismic in case if bed thickness exceeds a half of a wavelength (Andreassen, 2009).

5.2.2. Horizontal resolution

Horizontal resolution is defined as the size of the Fresnel zone, roughly circular area from which seismic waves are reflected producing seismic reflection. The Fresnel zone is an interval on the reflector from which seismic signal returns to the hydrophone within a half-cycle after the onset of the reflection (Andreassen, 2009). Following equation helps to define the magnitude of the Fresnel zone:

$$rf = \frac{V}{2} \cdot (\frac{t}{f})^{1/2}$$

Where *rf* is a radius of the Fresnel zone, *V*- average velocity, *t*- two-way travel time, *f*- dominant frequency.

Based on the equation above, we can claim that the radius of the Fresnel zone increases with depth, increasing velocity, and lower frequency. Thus, horizontal resolution decreases with depth, increasing velocity, and lower frequency (Andreassen, 2009).

In order to improve horizontal resolution, migration and shrinking of the Fresnel zone is done. Migration of 2D-seismic data is done along the seismic line resulting in an elliptically-shaped Fresnel zone, while migration of 3D-seismic data is done along the seismic line and

perpendicular to it as well, resulting in a smaller size of the Fresnel zone with a shape of a circle (Figure 5-5).

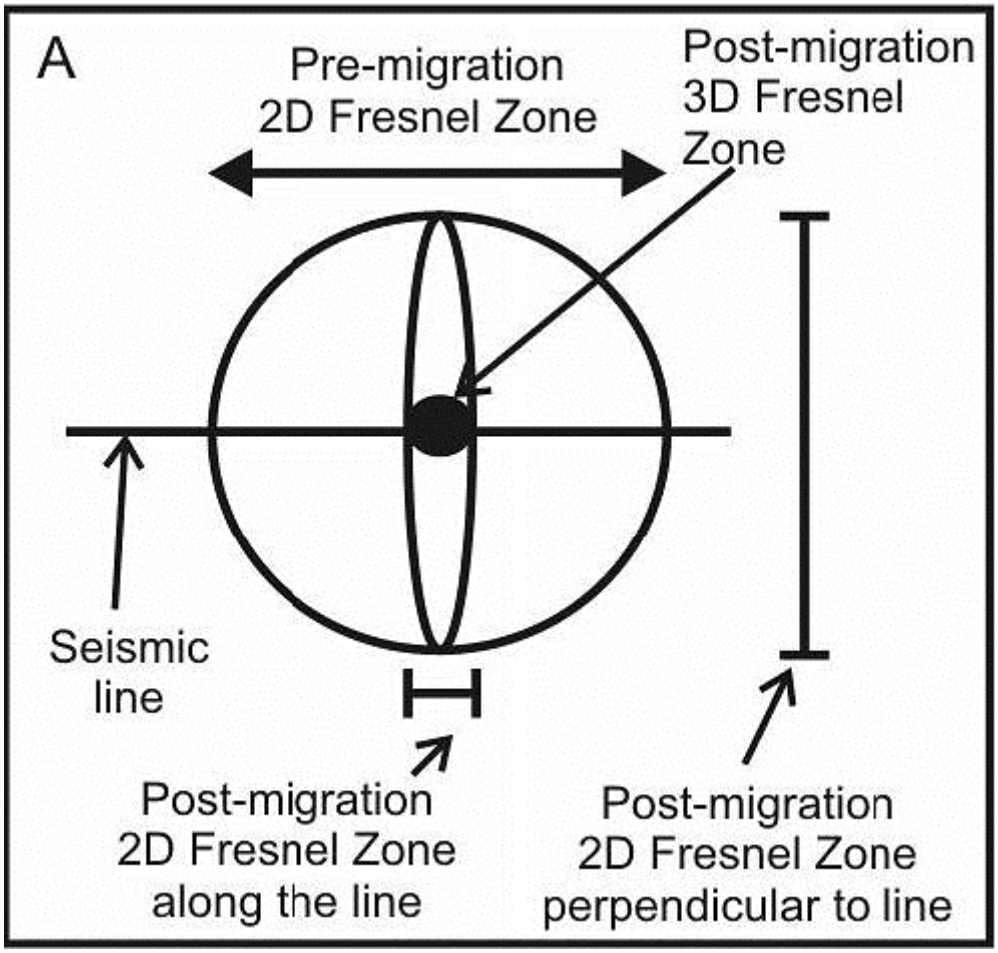

Figure 5-5. *Migration of the Fresnel zone for 2D and 3D seismic data (Andreassen, 2009).*

Frequency spectrum for the 3D dataset BG1002 in shown in Figure 5-6, where dominant frequency is approximately 28 Hz.

Figure 5-6. *Frequency spectrum for dataset BG1002*

Vertical resolution of the seismic dataset BG1002, if we assume wave velocity to be 1800 m/s:

$$\text{Wave length} = \lambda = \frac{1800}{28} \approx 64{,}3\ m$$

$$\text{Vertical resolution} = \frac{\lambda}{4} = \frac{64{,}3}{4} \approx 16\ m$$

Inline spacing for the dataset BG1002 is 25m, crossline spacing is 12.5m, and sampling rate equals 4.

5.3. Seismic attributes

Seismic attributes in Petrel E&P Software Platform 2015 are available in the form of attribute volumes and surface attributes. Seismic attributes are provided as an aid to better visualization and, consequently, superior interpretation of seismic data by improvement, enhancement and correlation of geological information that often is not easily seen in conventional seismic. Surface attributes extract seismic properties out of volumes based on waveform analysis and give an output as a surface. While volume attributes make virtual or realized volumes of the input seismic by extracting information from different properties of the analytical signal (Schlumberger, 2015). Both surface and volume attributes have been applied for seismic data analysis in this master thesis.

5.3.1. RMS (root mean square) Amplitude

An attribute that calculates the square root of the sum of squared amplitudes divided by the number of samples within the specified window. This surface attribute helps to measure reflectivity of the sediments in the chosen area and, thus, to identify potential hydrocarbon-bearing zones by revealing bright spots and amplitude anomalies in the seismic data. Nevertheless, RMS is sensitive to noise since it squares each value within the chosen window (Schlumberger, 2015, Koson et al., 2014).

$$x_{rms} = \sqrt{\frac{1}{N}\sum_{n-1}^{N} w_n x_n^2}$$

Where *N* is number of samples, *x*- trace values, *w* and *n* are window values (Koson et al., 2014).

5.3.2. Variance (Edge Method)

Variance attribute measures local variance in the signal by applying a signal coherence analysis, in other words, it evaluates similarity of traces and wave shapes within the chosen vertical window. This attribute aids detection of faults, fractures, major unconformities and channel infills (Schlumberger, 2015, Pigott et al., 2013).

5.3.3. Ant Tracking

Ant Tracking is a unique algorithm for fault detection and interpretation, which imitates movement of ant colonies while searching for food in the ground. Artificial ants in the program search for fault zones and collect information related to fault associations on their way, and thus, provide necessary data for making an attribute volume cube with sharp and detailed fault features. Variance or Chaos attribute volumes are used as an input data for the Ant Tracking attribute since they are sensitive to faults.

Ant Tracking mechanism include following steps: seismic conditioning by application of structural smoothing tool in order to eliminate background noise, edge detection, and edge enhancement. Ant attribute is an intensive and time-consuming algorithm. Thus, I had to crop a small data section and test different parameters on it before applying the parameters on the primary data set in order to reach the best results (Schlumberger, 2015; Ngeri et al., 2015).

5.3.4. Structural Smoothing

Structural smoothing is a signal-processing tool aimed at enhancing the continuity of the seismic reflectors in the input seismic data and noise reduction, guided by the local structure. It is also applied for detecting flat spots by running smoothing attribute without dip guiding. It is possible to choose between three filter options in parameters of structural smoothing attribute: plain option with regular Gaussian smoother, dip-guided option, which conducts smoothing parallel to dipping in the seismic, and edge enhancement, which runs two filters first and then the least chaotic one is Gaussian filtered again resulting in enhanced edges in the seismic (Schlumberger, 2015).

5.4. Artefacts

Artefact, or seismic acquisition footprint, is a definition for all noise features that appear on the seismic and are not related to geology. They should be taken into consideration during interpretation of the data. Despite the fact that during seismic processing a lot of data noise is being removed, some artefacts remain in the data, and sometimes it is quite hard to distinguish real geological features in the data from artefacts. Main types of artefacts are noise due to the sparseness in acquisition geometry and processing artifacts, which appear if any remained aliased noise is not completely removed and, thus, penetrated into the seismic data (Andreassen, 2009; Mahgoub et al., 2017).

6. Results and Interpretation

In this chapter, I present observations and interpretations of the 3D seismic dataset BG1002 in connection with the well data 7224/7-1. The research focuses on (1) the seismic stratigraphy including definitions of major seismic horizons and units that are correlated to well data, (2) interpretations of seismic amplitude anomalies and (3) detection and interpretations of fault systems and potential fluid flow pathways.

6.1. Seismic stratigraphy

Interpretation of seismic stratigraphy of the study area has been made based on the seismic data from the dataset BG1002 and wellbore information from NPD Factpages, as well as by using previous studies from the area (Mattos et al., 2016; Breivik et al., 1995).

During the interpretation of seismic cross-sections of the dataset BG1002, eight seismic horizons within the study area have been defined (Figure 6-1): Seafloor Horizon, and Horizon 1- Horizon 7. Based on the data from the well 7224/7-1 these horizons have been interpreted to be the tops of the Early Triassic Havert and Klappmyss Formations, Late Triassic Fruholmen Formation, Late Jurassic Hekkingen Formation, Late Cretaceous Kolmule Formation, and Pleistocene Norland Group.

Afterwards, based on the geometry of seismic reflections these horizons have been combined into 5 stratigraphic units (Figure 6-1) corresponding to Permian, Triassic, Jurassic, Cretaceous, and Paleogene- Quaternary geological time sequences.

Unit 1

Unit 1 is interpreted to be a sediment sequence of Paleozoic Era that comprises two sub-units divided by Mid-Permian unconformity (Horizon 1) (Figure 6-1). Well 7224/7-1 does not intersect unit 1, thus, its boundaries and sub-units were defined based on the reflection pattern of the strata as well as previous scientific works in the area (Mattos et al., 2016).

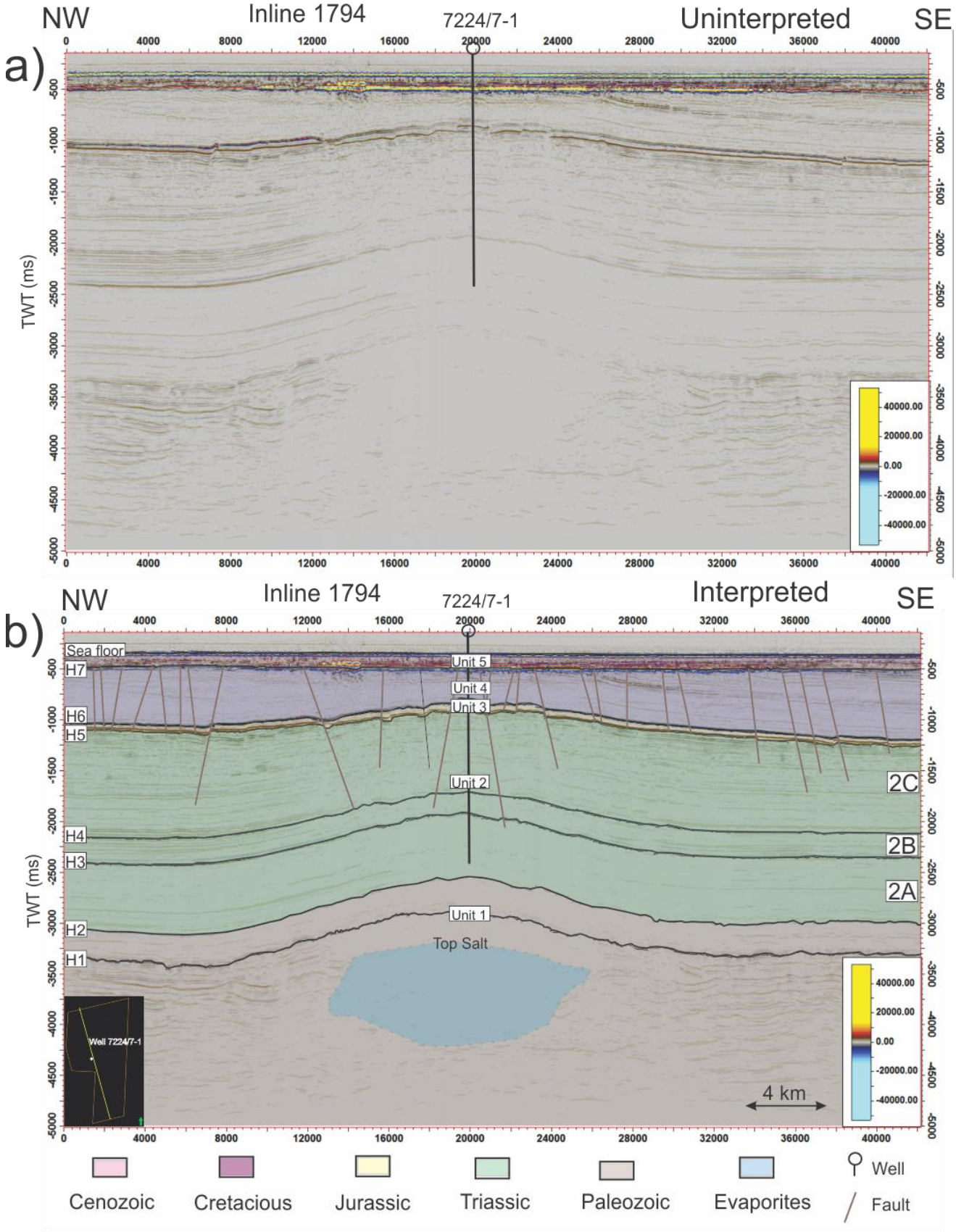

Figure 6-1*. a) Uninterpreted seismic inline 1794 crossing through Samson Dome. b) Interpreted seismic inline 1794 crossing through Samson Dome illustrating five seismic units and eight seismic horizons including sea floor; position of well 7224/7-1; some major faults in the area, and lenticular evaporitic body.*

Mid-Permian unconformity (Horizon 1) represents a negative seismic reflection of medium amplitude and “wavy” geometry (Figure 6-1, Figure 6-8). This horizon divides Unit 1 into two sub-units. The lower one comprises medium-amplitude wavy reflections interpreted as carbonate build-ups. They are illustrated on the thickness map in Figure 6-1 later in the text. Within this sub-unit a structure of lenticular geometry is observed below the carbonate build-ups. On the sides of this structure seismic reflections terminate and show vertical orientation (pull-up). There are almost no seismic reflections within the structure (Figure 6-1). On the top of this structure discontinuous reflections of low to medium amplitude are observed. Due to the absence of seismic reflections within the structure and pull-up effect on its sides, the lenticular structure is interpreted to be an evaporitic body, i. e. the base of the Samson Dome. Discontinuous reflections of low to medium amplitude on its top are interpreted as top salt. Since amplitude of top-salt reflections is not high, we can assume that salt intruded into more compacted sediments (Tarleton State University, 2017).

Horizon 2 is interpreted as Late Permian unconformity and represents a positive seismic reflection of medium amplitude (Figure 6-1, Figure 6-8). This horizon is relatively continuous, however, reflections above the evaporitic body are disturbed and discontinous. These intermittent reflections could be caused by small offset faults formed because of high stress conditions during salt intrusion into overlying sediments. Reflection pattern within this sub-unit is sub-parallel and of low to medium amplitudes.

Unit 2

Unit 2 is interpreted as a sedimentary sequence of Triassic Period (Figure 6-1). The base of Unit 2 is Horizon 2. Based on the reflection pattern and well information, unit 2 was sub-divided into 3 sub-units: 2a, 2b, and 2c.

Top of sub-unit 2a is Horizon 3 that represents positive high-amplitude reflection and coincides with the top of Early Triassic Havert Formation at the depth of 2663 meters according to well information. Horizon 3 is continuous, however, in the area above the Samson Dome structure a loss of reflection continuity is observed. It may be caused by faults formed due to sediment deformation during salt intrusion. Thickness of sub-unit 2a is quite equal throughout the study area, without any major variations. The reflection pattern is characterized by low amplitude reflections with parallel to sub-parallel geometry.

Sub-unit 2b is limited by Horizon 3 (lower boundary) and Horizon 4 (upper boundary). Horizon 4 represents a negative reflection of low to medium amplitude that is located at the depth of 2222 meters in well 7224/7-1 and coincides with the top of Klappmyss Formation. Horizon 4 loses its continuity next to the area of Samson Dome similarly to Horizon 3. Sub-unit 2b is 441m thick, and does not show any major variations in thickness throughout the whole study area.

The upper boundary of sub-unit 2c is a strong negative reflection, which corresponds to Horizon 5 and coincides with the top of Late Triassic Fruholmen Formation at the depth of 931 m in well 7224/7-1. Thickness of the sub-unit varies throughout the study area. Thickness of the sub-unit in the well is calculated to be 1291 meter. It comprises three formations: the Fruholmen, the Snadd, and the Kobe formations. Sub-unit 2c includes higher number of faults in comparison to other sub-units in Unit 2 (Figure 6-18). These faults are of larger geometry and have deeper penetration. Reflection pattern of the sub-unit is characterized by parallel to sub-parallel reflections of medium to strong amplitude and moderate to strong frequency. Reflections are quite continuous, however, there are large number of discontinuities above the area of the Samson Dome that are caused by large offset faults.

Unit 3

Unit 3 represents a quite thin strata with a total thickness of only 139 meter, and is interpreted to be a Jurassic sediment sequence (Figure 6-1). The top of unit 3 is Horizon 6 occurring at the depth of 792 meters below the seafloor. According to the well measurements, Horizon 6 coincides with the top of Hekkingen Formation. The lower boundary of the unit, Horizon 5, marks the top of the Late Triassic sediment sequence. Both of these horizons show reverse polarity and medium to strong amplitude. Reflection pattern of unit 3 is characterized by parallel seismic reflections of high frequency that are quite discontinuous due to the large number of faults that cut it (Figure 6-18).

Unit 4

Unit 4 is interpreted to be the sediment sequence of the Cretaceous Period with Horizon 7 as its top and Horizon 6, the top of Hekkingen Formation, as a lower boundary. According to the wellbore data, unit 4 is 391 m thick. It comprises Knurr and Kolmule Formations. The top of this unit is Horizon 7 interpreted as the top of the Kolmule Formation, the Upper Cretaceous

unconformity at the depth of 401 meters below the seabed. Horizon 7 represents a continuous reflection of high-amplitude and normal polarity that truncates over the crest of the Samson Dome (Figure 6-2). This is the only surface in the study area with a significant degree of erosion. Some high amplitude anomalies cut by faults occur at shallower depths of the unit 4 (Figure 6-2, Figure 6-14). Lower part of unit 4 represents an intensively faulted stratigraphic zone and comprises many of the largest faults. Reflection pattern of this unit varies throughout the study area. Most of reflections are discontinuous and of medium to strong amplitude. In areas above and close to the Samson Dome structure geometry of reflections is quite chaotic (Figure 6-13, Figure 6-14). Reflections in the south and south-east part of the area are of strong amplitude and parallel, but very discontinuous due to the large number of deep faults (Figure 6-15).

Unit 5

Unit 5 is interpreted to be the sequence of Cenozoic Era, Paleogene- Quaternary Period. Thickness of this unit is 108 meters and its top coincides with the seafloor (NPD, Factpages). This unit is 108 meters thick and comprises Nordland and Sotbakken (Torsk Formation) Groups. Reflections of the top and base of this unit are continuous and of high amplitude and normal polarity (Figure 6-2, Figure 6-13).

Horizon 7, the lower boundary of Unit 5, divides Paleogene- Quaternary and Cretaceous strata and marks the large unconformity. Surface of this horizon is the only surface with a significant erosion degree. Wavelet view of horizon 7 shows positive polarity and so does the seafloor reflection (Figure 6-2). Horizon 7 is interpreted to be URU- the upper regional unconformity, the major erosional base for several glaciations.

Reflection pattern within the unit 5 is discontinuous and of medium amplitude. However, quite many discrete high-amplitude anomalies, bright-spots, are present within the unit at the depths of approximately 410-490 ms (Figure 6-13, Figure 6-14). This depth interval has been further chosen for analysis of high-amplitude anomalies in the area and for RMS attribute map. No faults were mapped within this seismic unit.

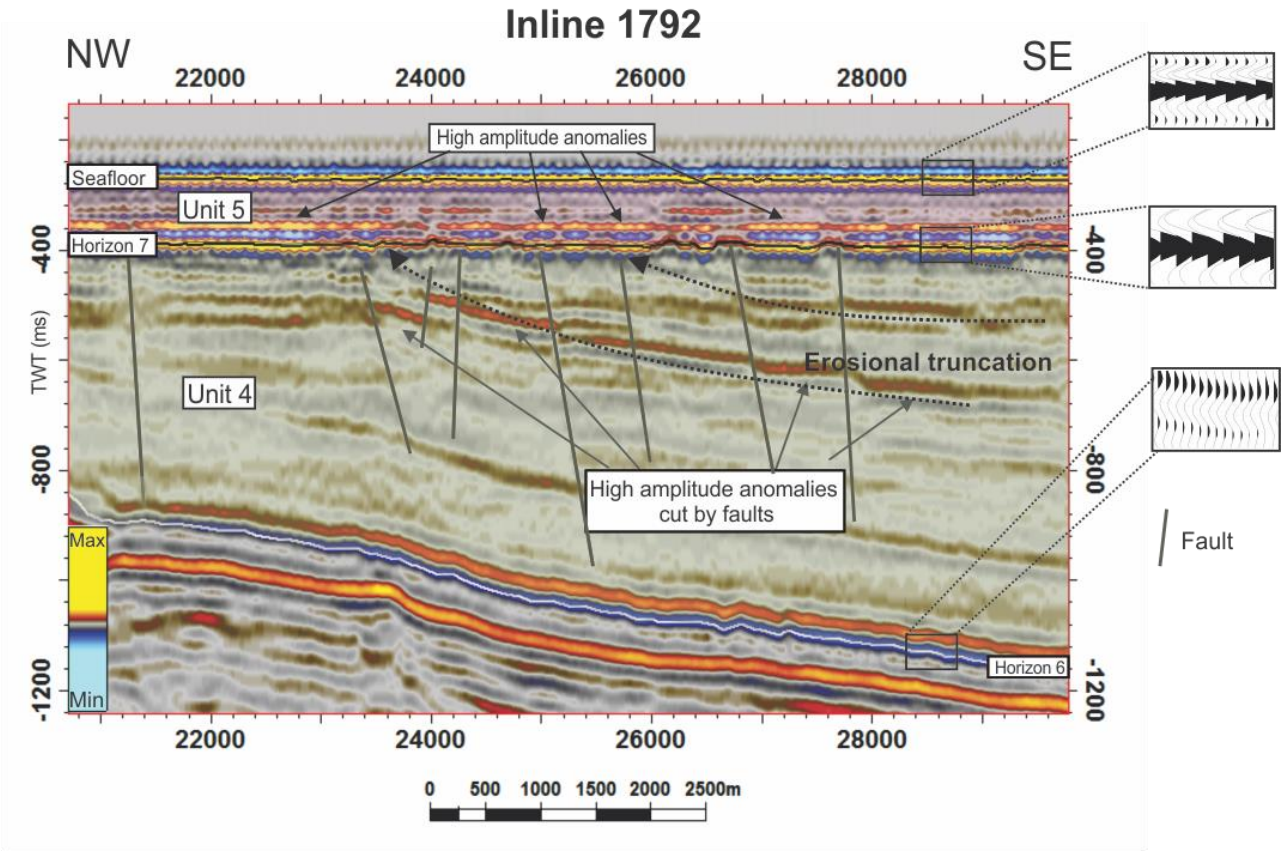

Figure 6-2. *Interpreted seismic profile of inline 1792 with marked horizons, units, high amplitude anomalies, faults, erosional truncation patterns and wavelet view of seismic traces for seafloor, horizon 7, horizon 6 and one of high amplitude anomalies within the unit 5.*

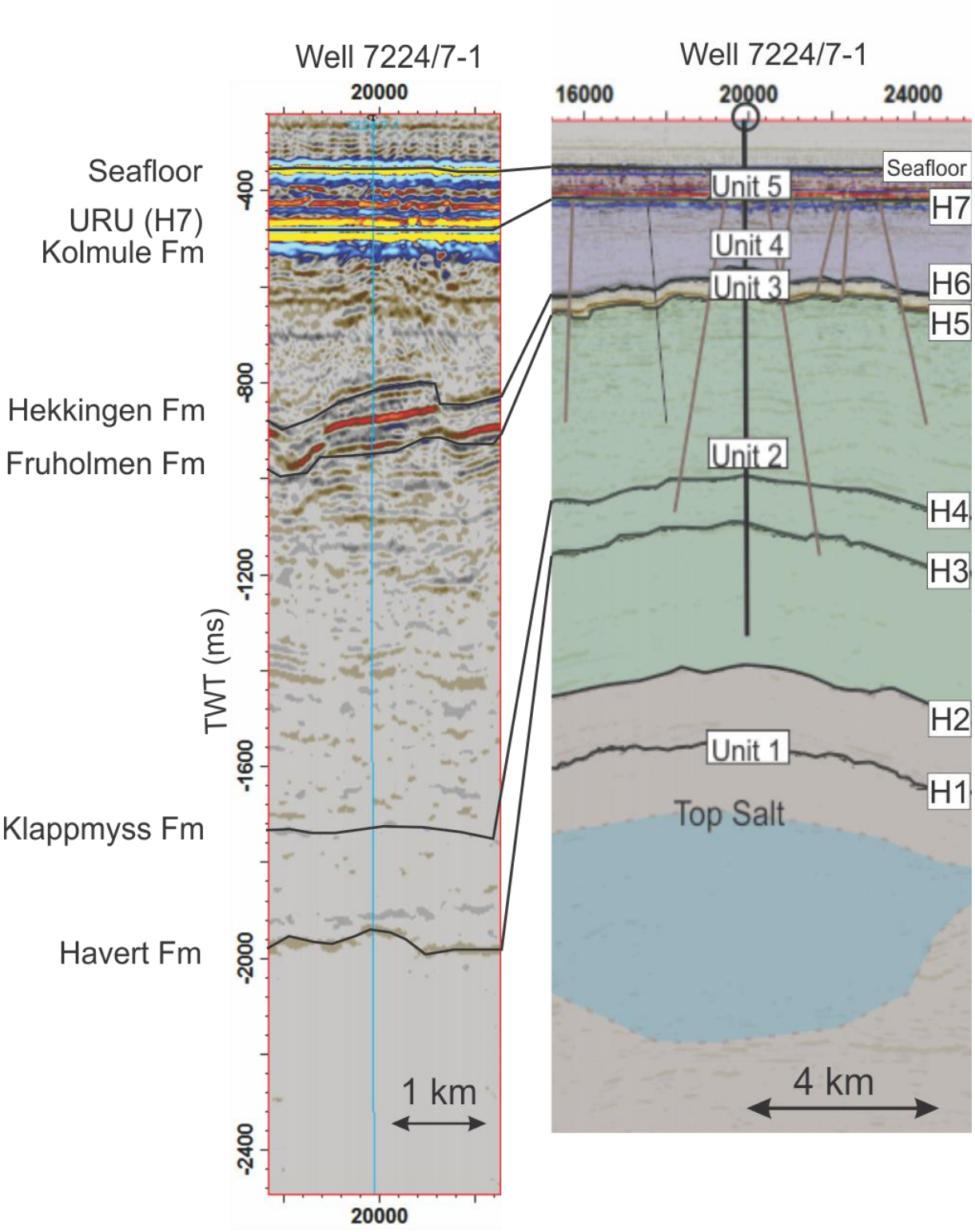

***Figure 6-3**. Seismic section through the well 7224-1 with interpreted horizons and formations.*

6.2. Main surfaces

Surfaces for each horizon have been made in Petrel in order to visualize variations of structural features vertically through the seismic cube. Time structural maps for each surface are presented below in Figure 6-12.

Seafloor

It is clearly seen on the structural map of the seafloor in the study area that the surface has a large number of furrows (Figure 6-4) but also linear continuous artefacts. In contrast to arctefacts, furrows on the seafloor are not parallel to each other and are quite curved. Thus, we can interpret these furrows as plough marks, and not as mega-scale glacial lineations that tend to be more parallel and of a larger scale (tens of km long and several km wide) (Rafaelsen, 2006). Predominant trend of plough marks in the study area is east-west direction.

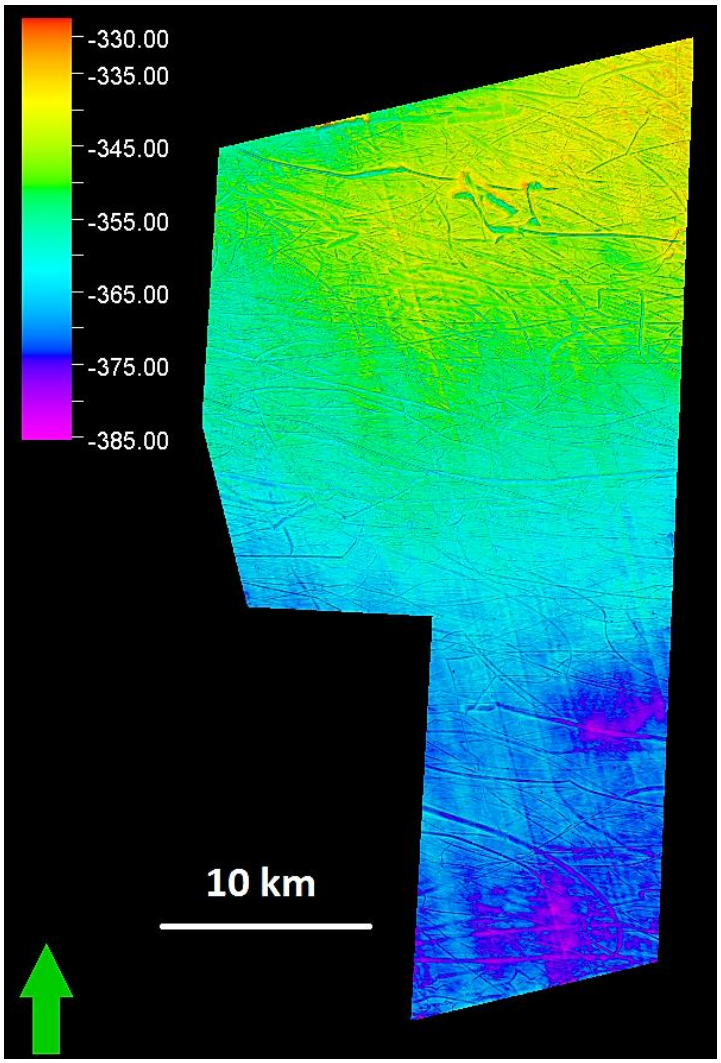

Figure 6-4. *Structural map of the seafloor with high number of plough marks. Vertical exaggeration is set to 3.*

In the study area some pockmark-like depression features are observed (Figure 6-5). They have circular and semi-circular shape and are predominantly located on the plough marks. On the seismic section there are no significant amplitude anomalies beneath these features such as dim spots or gas chimneys (Figure 6-5). Due to the absence of amplitude anomalies and because of the fact that most of the depressions are associated with plough marks, we can interpret these pockmark-like features as morphological depressions formed when iceberg re-adjusts its hydrostatic equilibrium while melting or by ploughing of the ground by large iceberg keels during iceberg movement into shallower waters or during low tidal conditions (Brown et al., 2017). At low tide in shallow waters icebergs may rest on the seafloor forming footprint depressions. They may also swing around being pushed by water and wind currents creating circular and semi-circular depressions on the seabed. These features are usually defined as iceberg pits and can be confused with pockmarks (Judd et al., 2007).

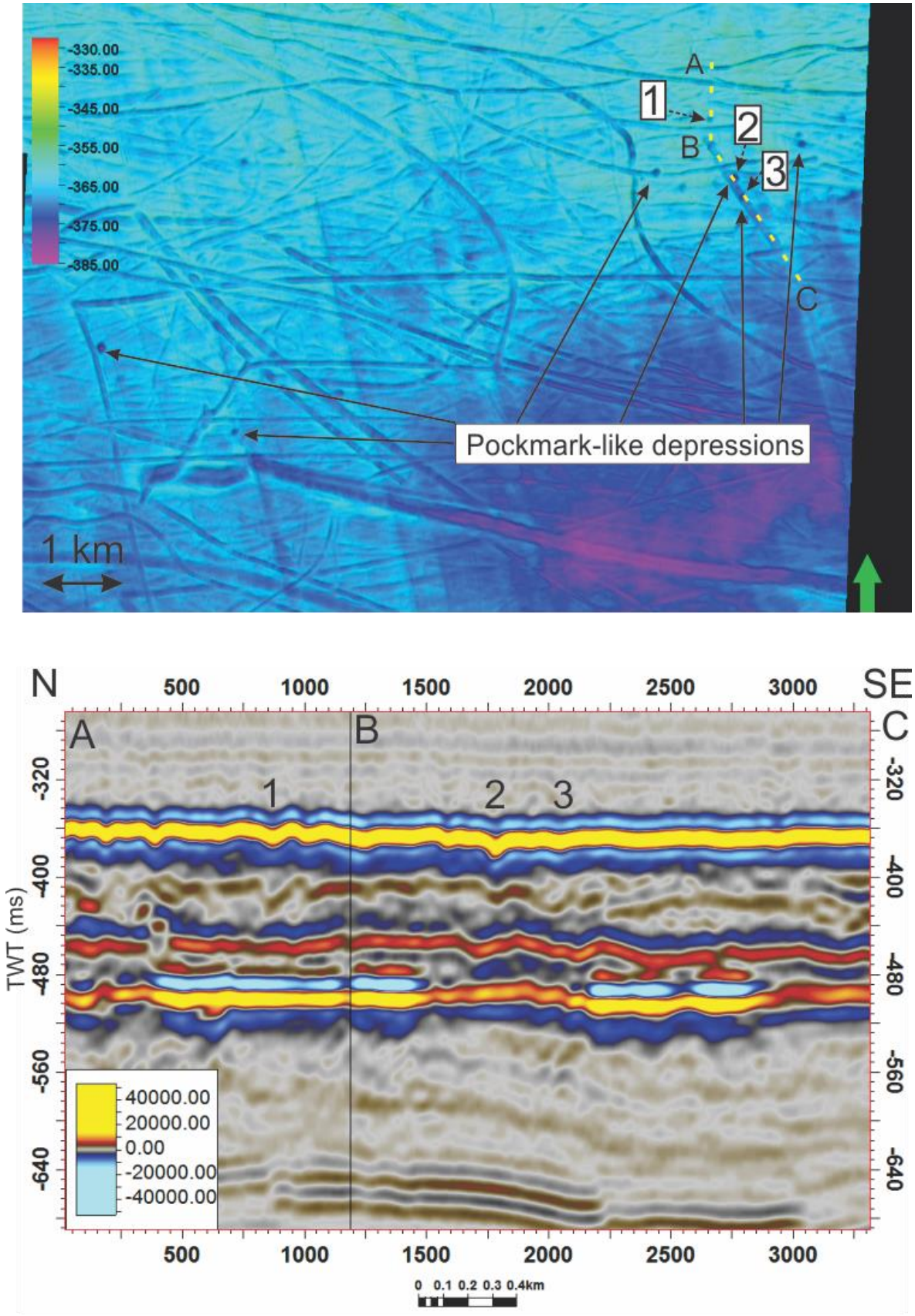

Figure 6-5. *Structural map of the seafloor illustrating pockmark-like depression features associated with plough marks. Seismic profile ABC through three pockmark-like depression features chosen for interpretation.*

Surface H7: Upper Regional Unconformity (URU)

Surface H7, the lower boundary of Unit 5, represents a boundary between Paleogene-Quaternary and Cretaceous strata and marks the large unconformity (Figure 6-6). This surface has one of the highest erosion degree in comparison to other surfaces made based on the previously defined horizons in the area. Erosion rate is unequally distributed within the surface: degree of erosion increases in the direction from the north to the south of the study area.

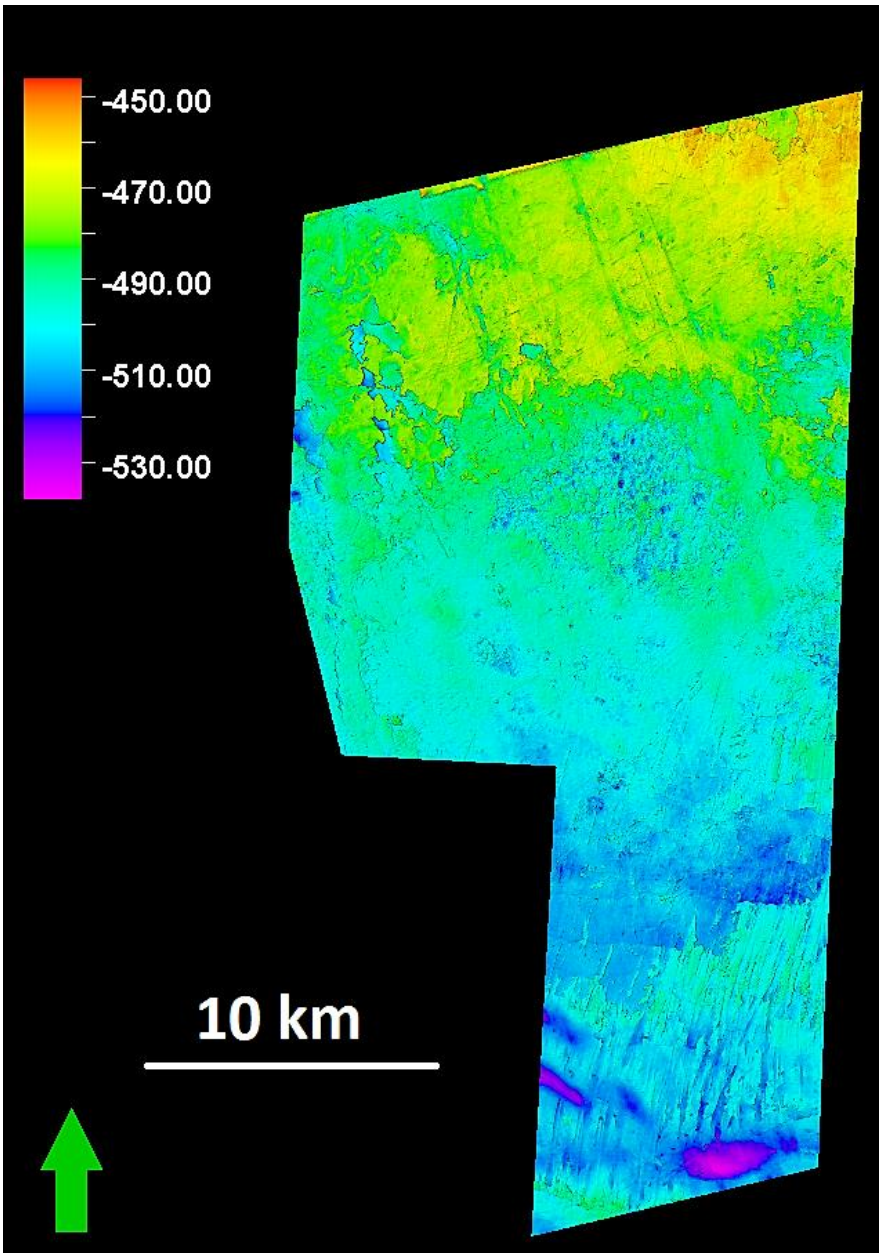

Figure 6-6. *Surface H7 representing Upper Regional Unconformity with a high degree of erosion. Vertical exaggeration is set to 3.*

As it is mentioned before, surface H7 has been interpreted as Upper Regional Unconformity (URU) based on polarity of horizon 7, wellbore information and reflection termination patterns (Figure 6-2). URU represents erosional base for several glaciations and was formed around 2.5 Ma (Larsen et al., 2003). It separates glacial sediments of Cenozoic Era from the pre-glacial bedrock.

Hekkingen Formation (H6) and Fruholmen Formation (H5)

Surface H6 and H5 represent correspondingly upper and lower boundaries of the most faulted stratigraphic unit in the area (Figure 6-7). Large fault patterns are observed on the crest of the Samson Dome and further from its flanks on both surfaces. Faults on the crest of the Samson Dome form radial pattern. Faults to the north from the crest of the dome are more sub-parallel, elongated, and have east-west trend. On the surface H6 some features resembling polygonal faults are observed in the north and north-eastern parts of the study area. Quite high degree of erosion is observed in the south part of the surface H5.

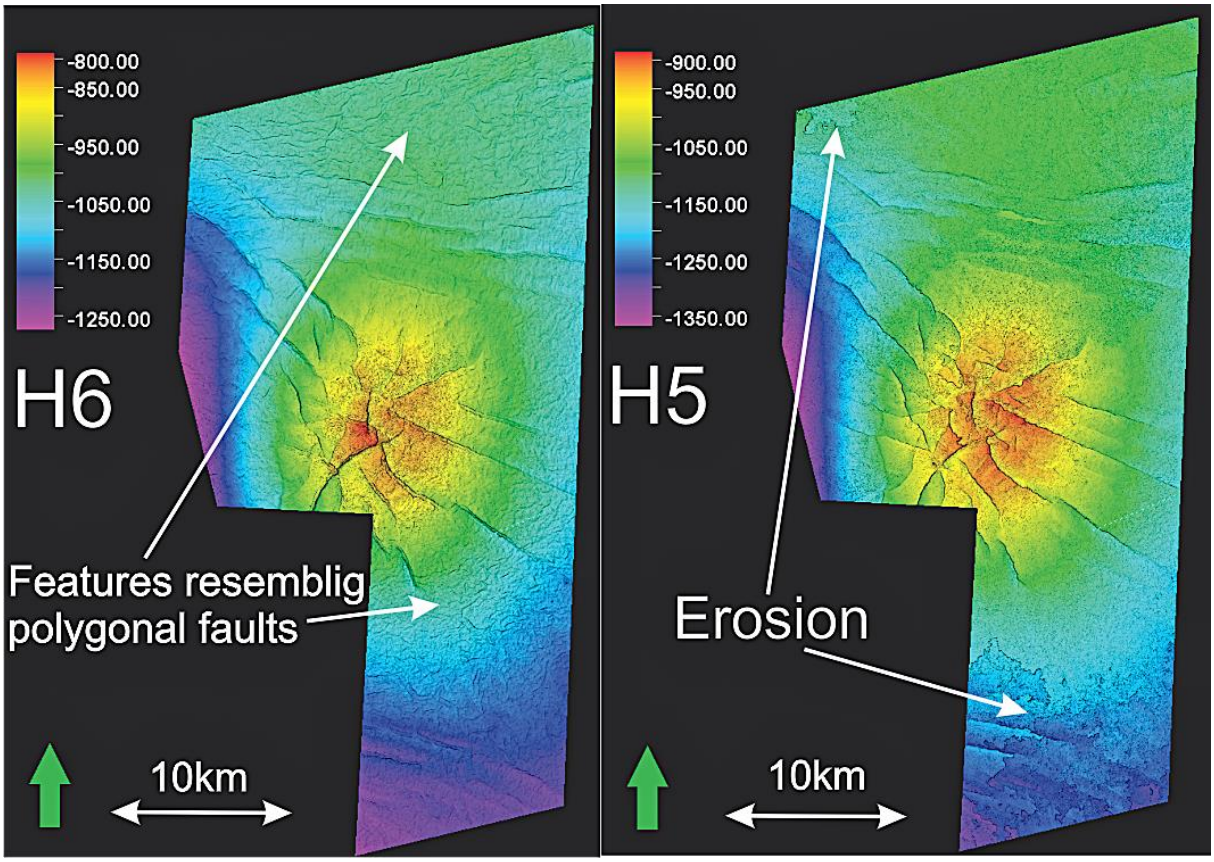

Figure 6-7. *Structural maps of surfaces H6 and H5 illustrating faults patterns in the area: radial pattern on the crest of the Samson Dome, sub-parallel elongated faults to the north of the Samson Dome, and features resembling polygonal faults in the northern part of the area (surface H6).*

Late Permian Unconformity (Surface H2)

Surface H2 that has been previously interpreted as Late Permian Unconformity contains some features of polygonal geometries, interpreted as carbonate polygonal mounds (Figure 6-10, Figure 6-8). Average thickness of these features has been calculates in previous studies (Alves, 2015) and is approximately 151 m. Polygonal mounds dominate to the south and south-east of the Samson Dome, while they are completely absent to the north-west of the Samson Dome. Some polygonal mounds of smaller scale are, however, present in the north-eastern part.

Mid Permian Unconformity (Surface H1)

Surface H1 interpreted as Mid Permian Unconformity is characterized by a major change in geometry of morphology. Large isolated build-ups dominate the morphology of this surface and are located mainly in the south-eastern and north-eastern parts (Figure 6-11). Thickness of these build-ups has been previously calculated in studies of Alves, 2015. Thus, average thickness of observed isolated build-ups has been estimated to be approximately 575 m, and maximum thickness is about 739 m. Isolated build-ups of a maximum thickness are located to the southeast of the Samson Dome. These features appear as wavy reflections of medium to high amplitude on seismic profile (Figure 6-8).

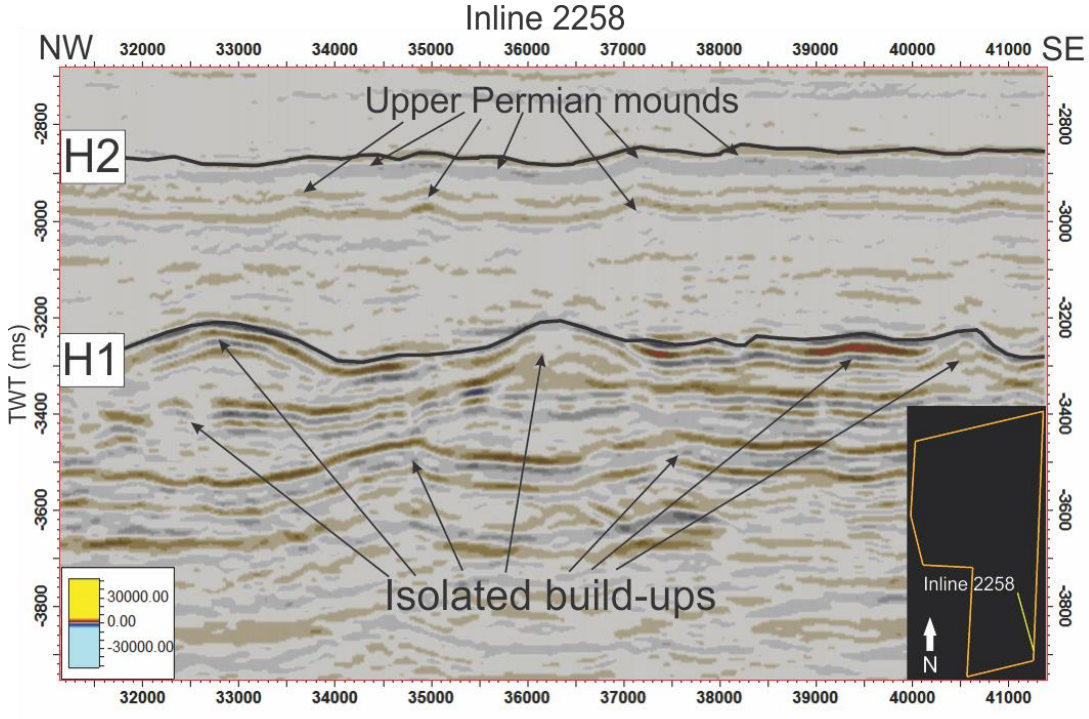

Figure 6-8. *Seismic section through the part of inline 2258 illustrating Upper Permian mounds and isolated build-ups of earlier Permian time.*

Polygonal mounds in Late Permian strata and isolated build-ups in the Earlier Permian strata are observed on slices of variance map as well (Figure 6-9). Two variance maps at the depths of 2992ms and 3312ms illustrating these geological features are presented below.

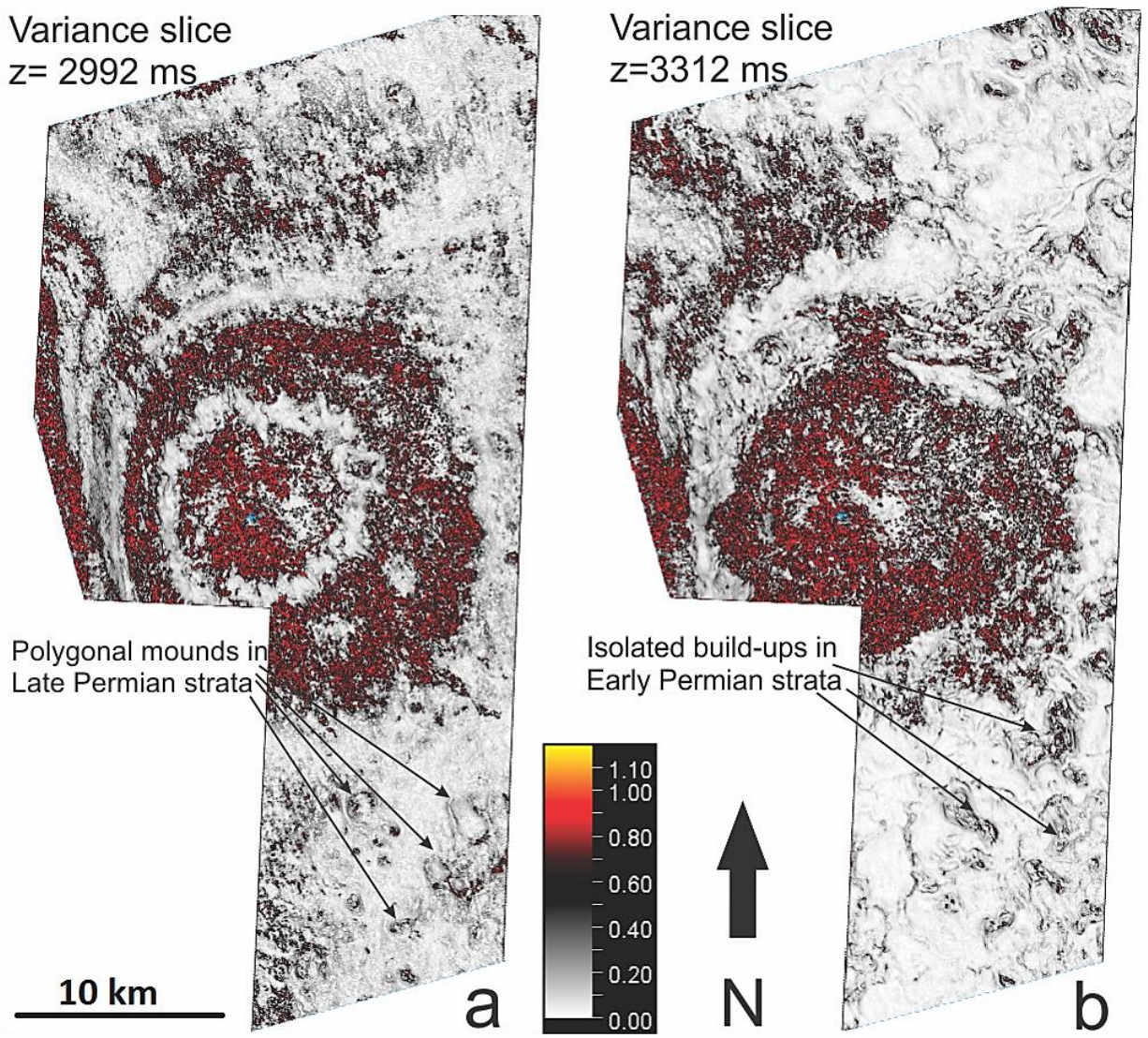

Figure 6-9. *Variance maps showing difference in geometries of the study area within Permian strata. A) Variance slice at the depth of 2992ms illustrating geometries of Late Permian polygonal mounds. B) Variance slice at the depth of 3312ms illustrating geometries of isolated carbonate build-ups within earlier Permian strata.*

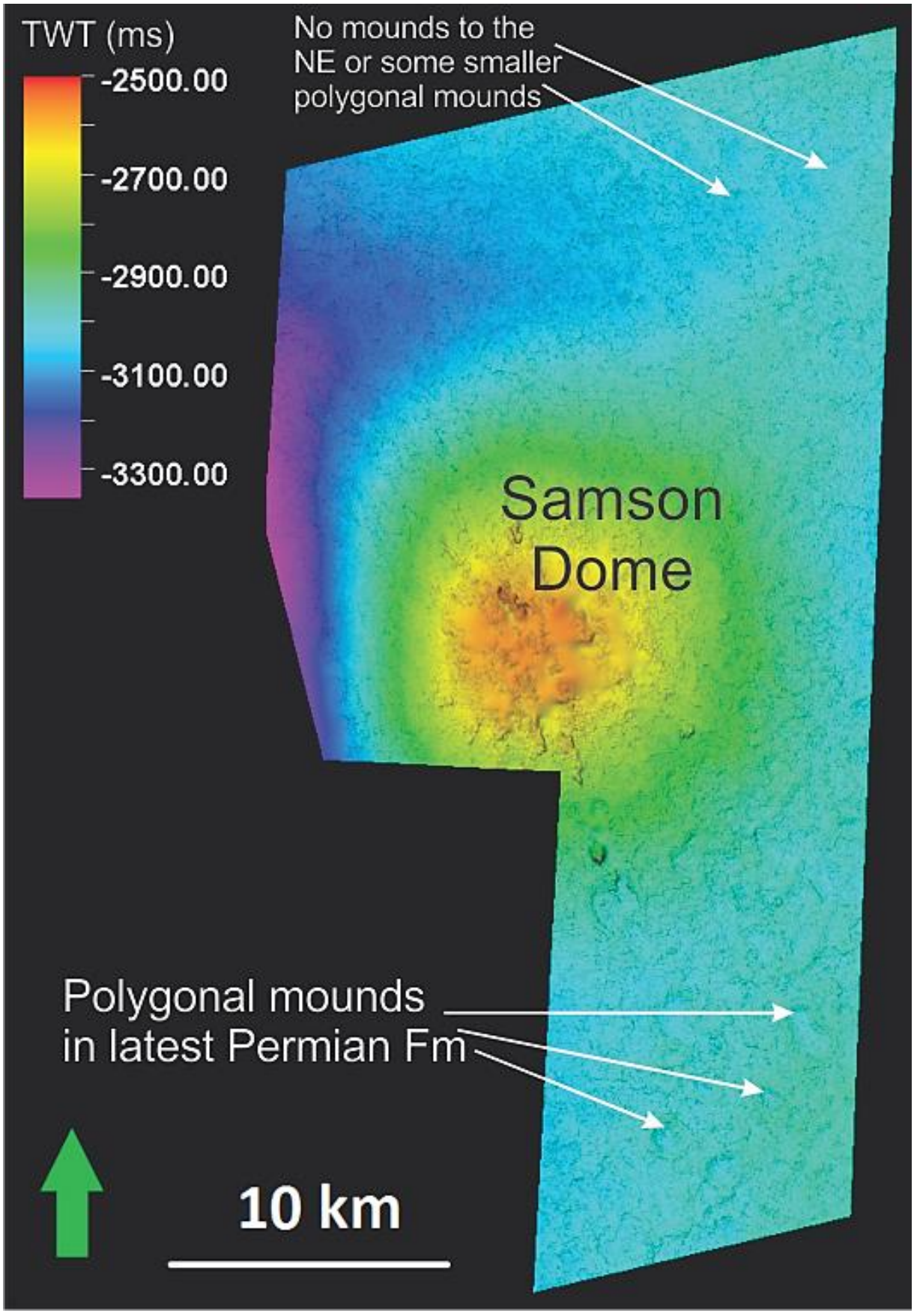

Figure 6-10. *Structural map of surface H2 highlighting polygonal mounds in the Upper Permian strata. Vertical exaggeration is set to 3.*

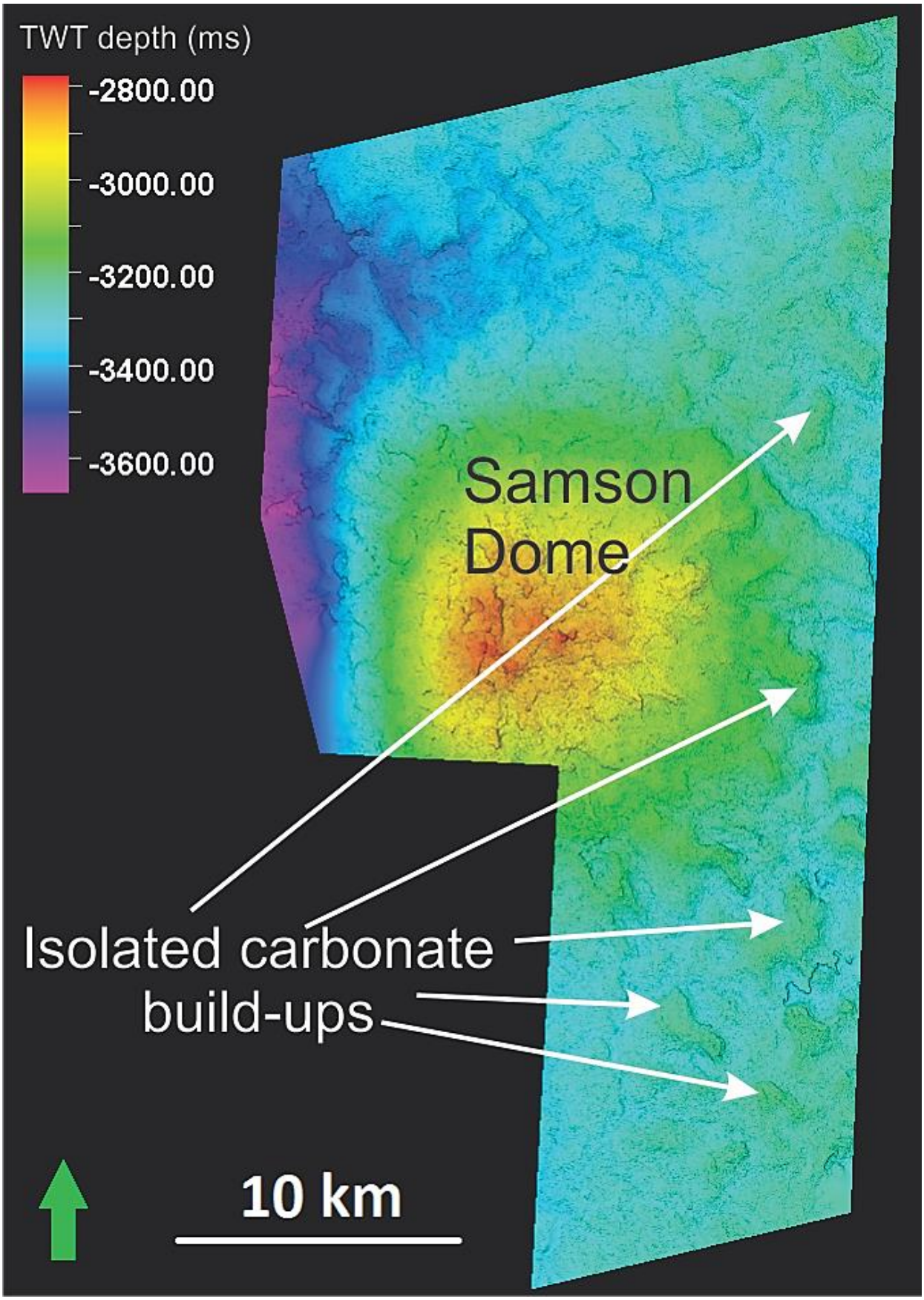

Figure 6-11. *Structural map of surface H1 highlighting isolated carbonate build-ups. Vertical exaggeration is set to 3.*

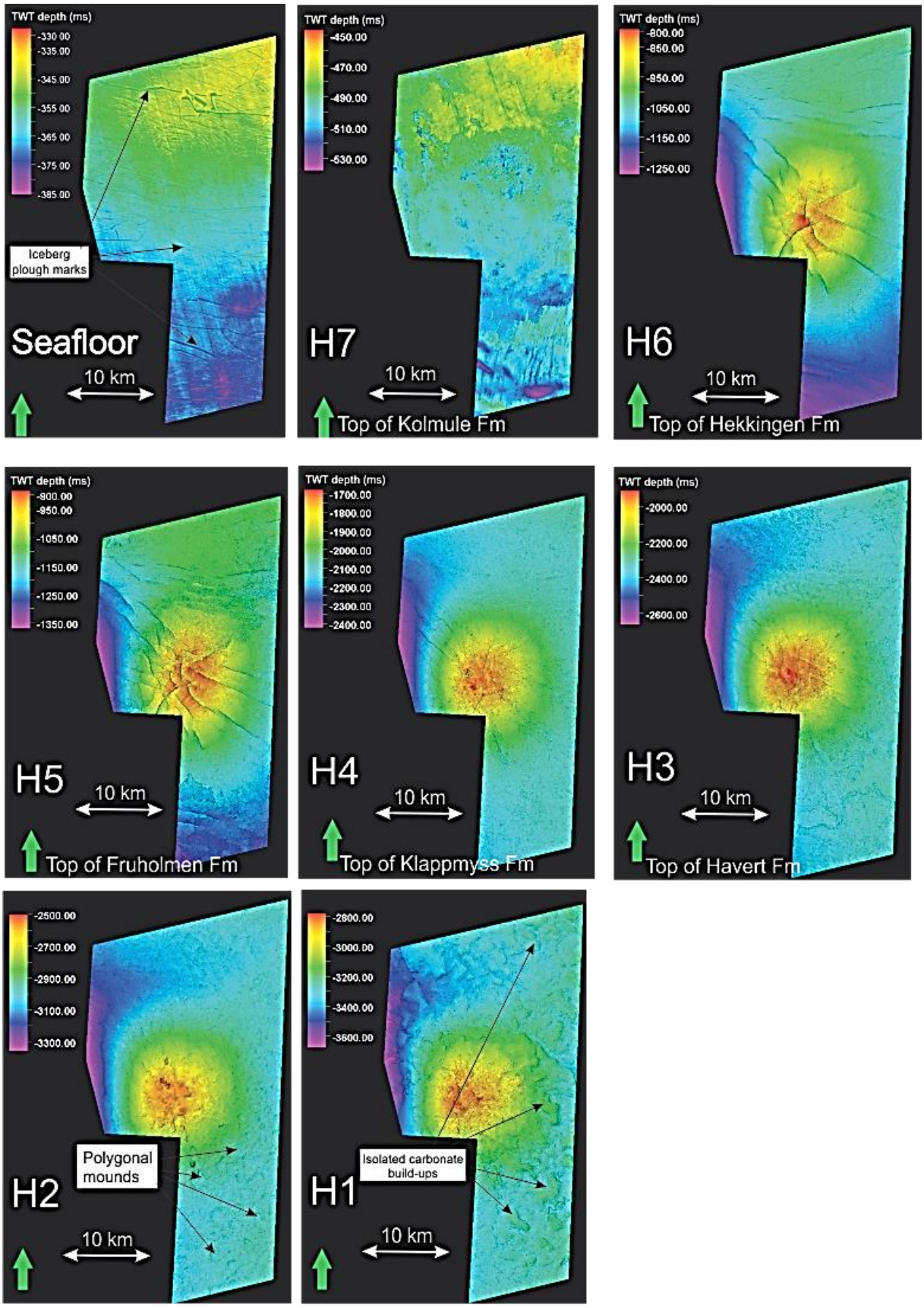

Figure 6-12. *Structural maps for seafloor and H7-H1 surfaces with certain interpreted geological features and formations.*

6.3. Amplitude anomalies

Highest amplitude anomalies in the study area are observed within Unit 5, the Cenozoic strata (Figure 6-13). Most of them are located at the depths of approximately 410 to 490 ms. High amplitude anomalies within these depths occur as many discrete intervals and bright spots. In Figure 6-13 some of these high amplitude anomalies are illustrated and the zoomed section

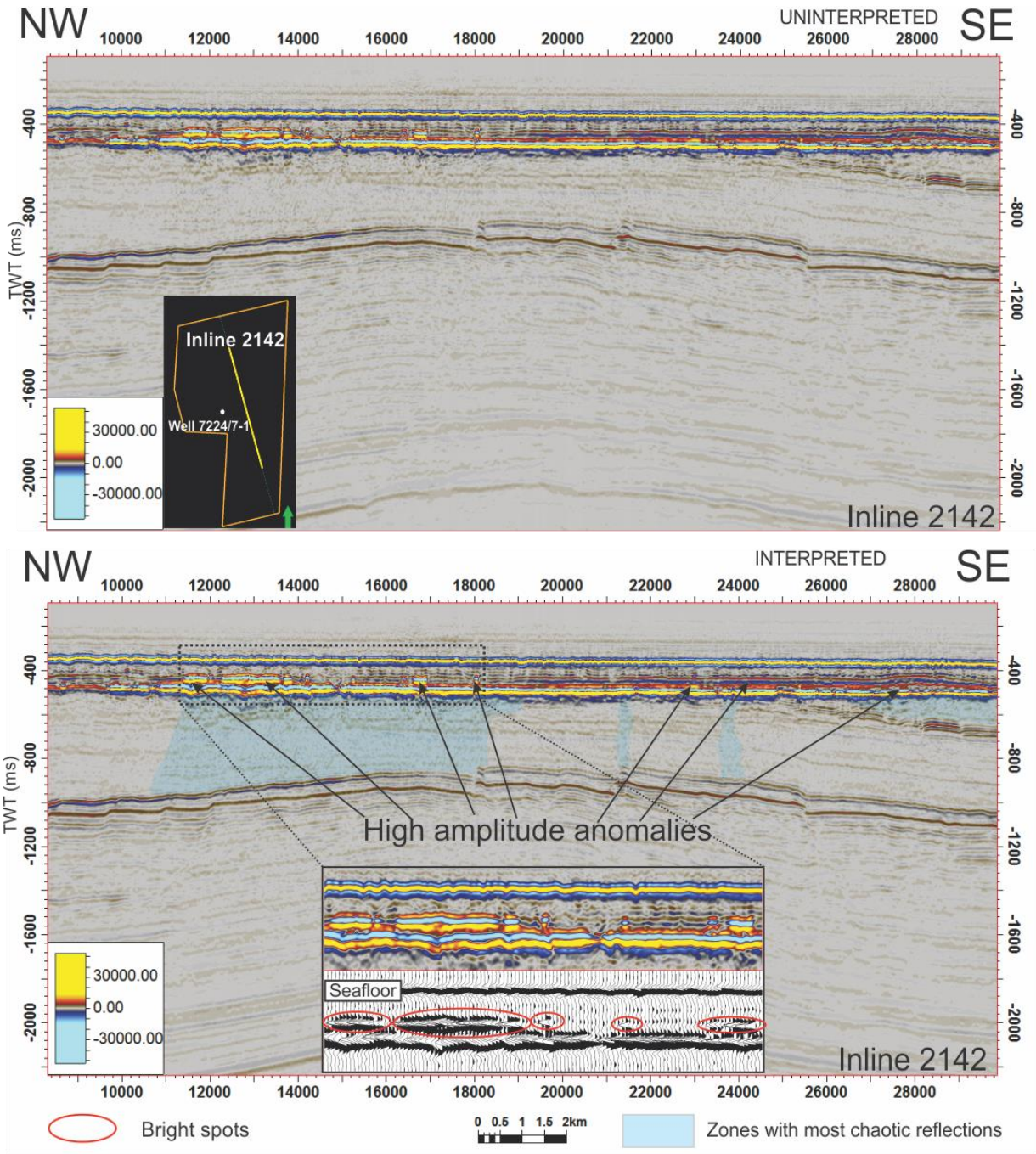

Figure 6-13. *Interpreted and uninterpreted seismic profiles through the middle of the inline 2142 illustrating high amplitude anomalies, zones with most chaotic reflections and zoomed seismic section of brightest reflections with their wavelet profile and some bright spots within the red ellipses.*

of brightest anomalies is presented. In the zoomed section bright sports with reverse polarity are shown (Figure 6-13).

Most of the high amplitude anomalies are located above highly faulted area a bit to the north of the crest of the Samson Dome and to the south and south-east of the Samson Dome above the erosion surface at the transition zone between Cenozoic and Mesozoic strata. Beneath these high amplitude anomalies zones of most chaotic and disturbed reflections are observed. These zones are illustrated in Figure 6-13 and are marked by transparent blue colour. Such chaotic reflections are interpreted to appear due to the frequency loss caused by the presence of high amplitude anomalies above. These chaotic reflections can also be interpreted as areas where upward migration of fluids occurred. Zones of very chaotic reflections that are located above the crest of the Samson Dome have lateral distribution through whole seismic Unit 4, while zones of chaotic reflections to the south and south-east of the Samson Dome occur just in the upper layers of Unit 4 and within the transition zone between Cenozoic and Mesozoic sediments that is characterized by a major erosion event in the study area.

Seismic interval of 80 ms within Unit 5 at the depths of approximately 410 to 490 ms with horizon 7 as a lower boundary has been chosen for the RMS amplitude analysis. The results are present in Figure 6-14. On the RMS map high amplitude anomalies are predominantly observed in the central part of the seismic dataset. Area of their distribution has sub-circular shape and resembles the geometry of the Samson Dome structure and geometry of erosion trace within the transition zone of Cenozoic and Mesozoic sediments (see Figure 6-6). Highest amplitude anomalies occur above the crest of the Samson Dome.

Some high amplitude anomalies are observed above the south-eastern flank of the Samson Dome at shallow depths of the Unit 4 (Figure 6-15). These high amplitude anomalies are cut by large number of faults and occur close to the zone where Horizon 7 is truncated over the crest of the Samson Dome. This area coincides with the area within the transition zone between Cenozoic and Mesozoic sediments that was mostly exposed to erosion.

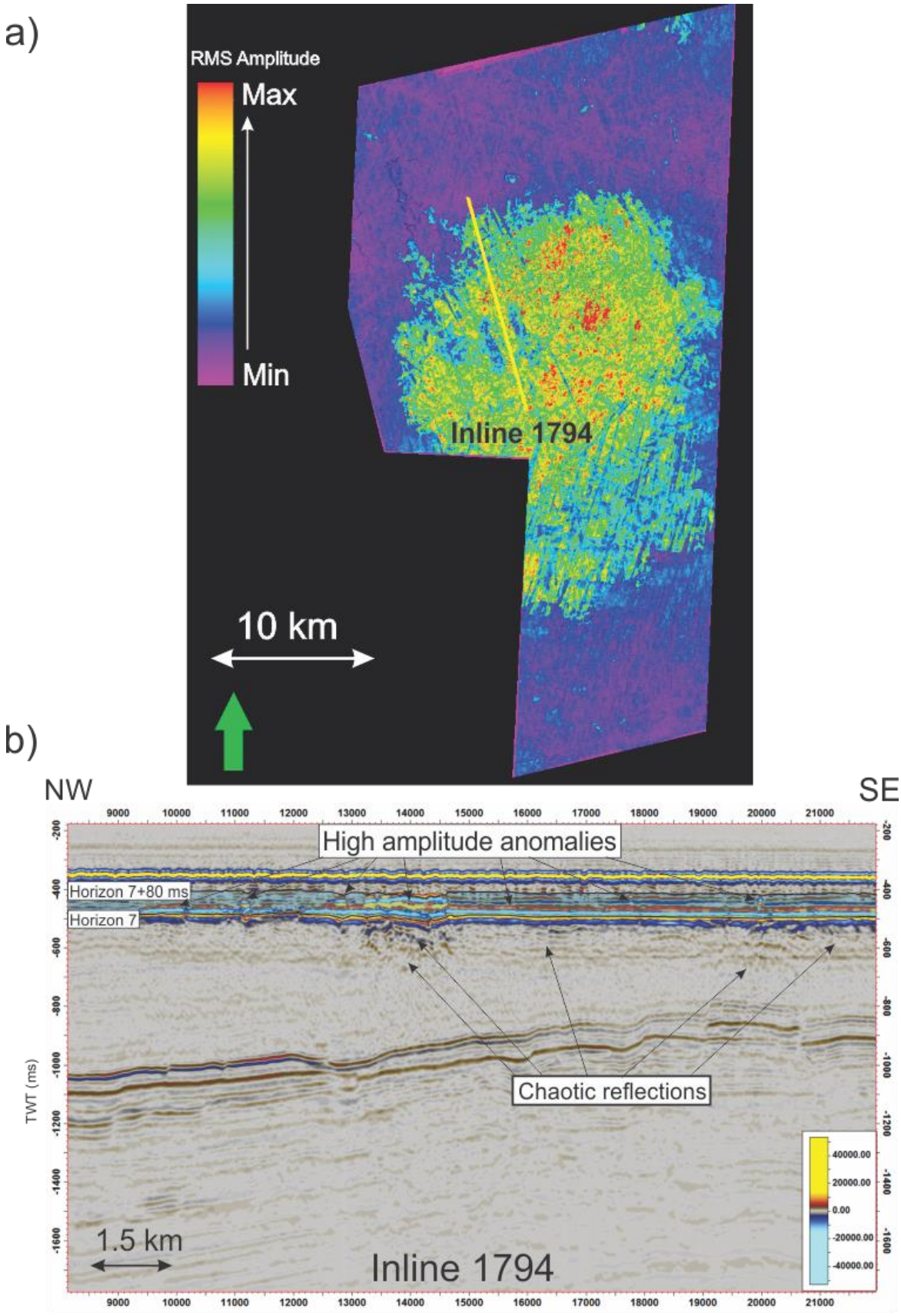

Figure 6-14. *A) RMS-map within Unit 5. Yellow line defines the position of seismic section of inline 1794. B) Seismic section through inline 1794 illustrating seismic window for the RMS-map above (transparent blue colour).*

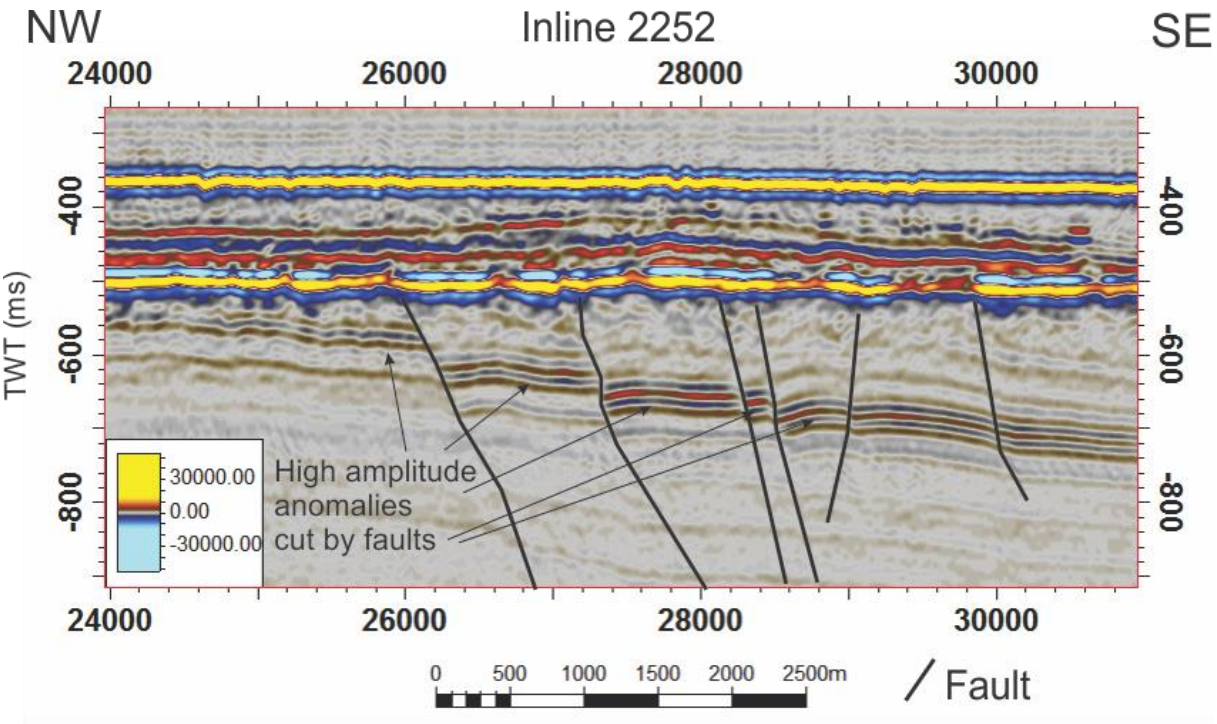

***Figure 6-15**. Seismic profile through the inline 2252 illustrating high amplitude anomalies cut by faults at the upper layers of Unit 4.*

Phase-reversal or Polarity reversal has been observed in the area. It occurs mostly in the Cenozoic strata and acts as a hydrocarbon indicator. Many small dim spots occur within Cenozoic sediments as well (Figure 6-16).

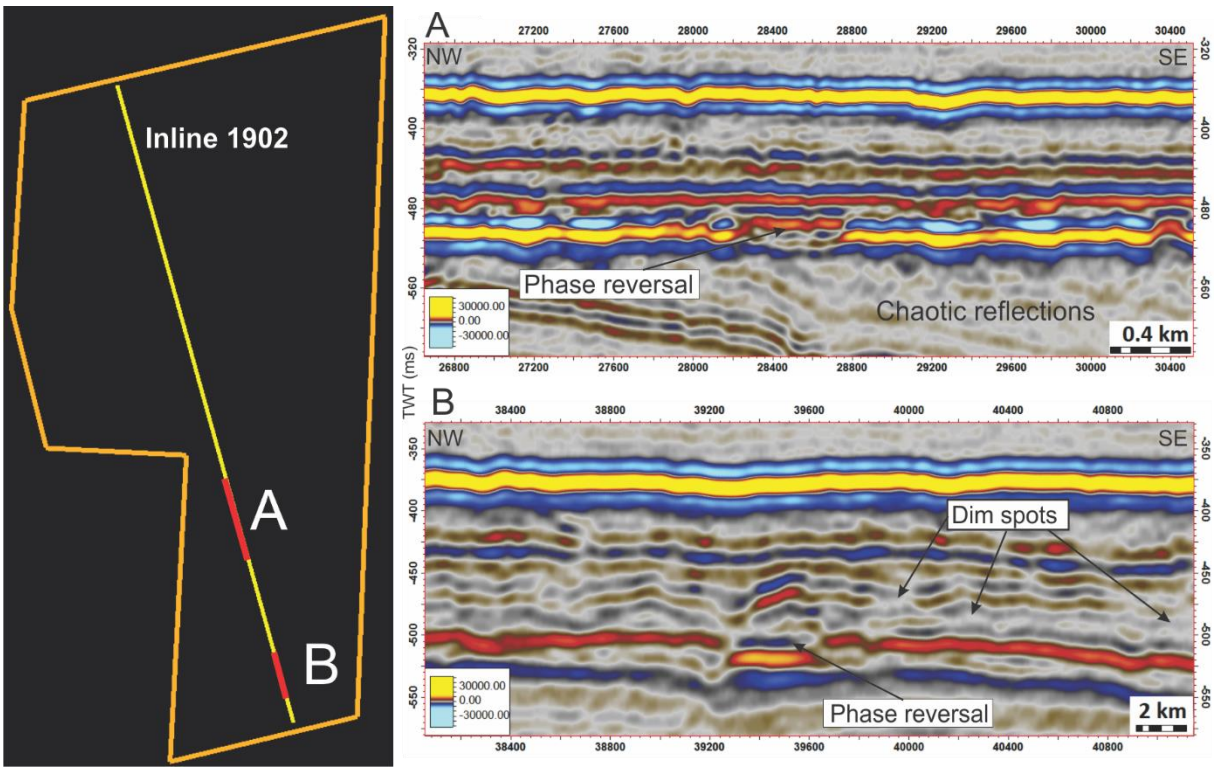

***Figure 6-16.** Seismic profiles through the parts of the seismic inline 1902 illustrating phase reversal and dim spots within Cenozoic strata.*

6.4. Fault system of the Samson Dome

Mapping and interpretation of faults has been made based on the analysis of coherence slices of the seismic cube BG1002 and seismic sections through the study area. Faults in the study area have been divided into three types based on their geometries and strikes: type 1, type 2, and type 3.

Type 1 faults are situated on the crest of the Samson Dome predominantly in the central part of the study area, so-called crestal faults (Figure 6-17). These faults are one of the deepest in the area, and they are observed in the sediments from Early Triassic up to Late Cretaceous Periods. They have a radial pattern in a plan view. Area on the crest of the Samson Dome is most deformed and includes highest number of faults of large geometry. Type 1 faults have predominant NW-SE strike and form half-graben and horst structures. These faults cut unit 2, 3, and 4 and form large tilt-blocks seen on the seismic profile. Example of such faults are faults F2 and F3 (Figure 6-18).

Type 2 faults show sub-parallel, elongated geometry and are located to the north of the Samson Dome (Figure 6-17). These are one of the longest faults in the study area with a length of up to 20 km, and they have dominant E-W strikes. The longest fault of this type in the area is F1 (Figure 6-17). Type 2 faults penetrate through Cretaceous, Jurassic and Triassic strata, but are not as deep as type 1 faults.

Type 3 faults are observed on the variance map and have a geometry resembling polygonal fault patterns (Figure 6-17, Figure 6-19, Figure 6-20, Figure 6-21). These faults are located to the sides from the Samson Dome structure predominantly in the western and northern parts of the study area. Most of them have NW strikes, but faults with NE strike are also present. Polygonal faults to the south of the Samson Dome are of larger geometry but show a smaller penetration. They are observed at depths of approximately 580 to 800 ms (Cretaceous strata), while polygonal faults to the west and to the north of the Samson Dome are observed within entire Cretaceous unit and even in Jurassic strata.

Cartwright & Lonergan (1996) suggested that polygonal faults represent non-tectonic type of faults and form due to sediment contraction and fluid expansion. In addition to polygonal faults in Cretaceous strata, zones of chaotic reflections and high amplitude anomalies within Cretaceous sediments and above them (in the Cenozoic strata) have been observed, as it was

mentioned before. Thus, we can assume that polygonal faults formed during fluid expansion and that they can serve as an indicator for fluid migration in the study area.

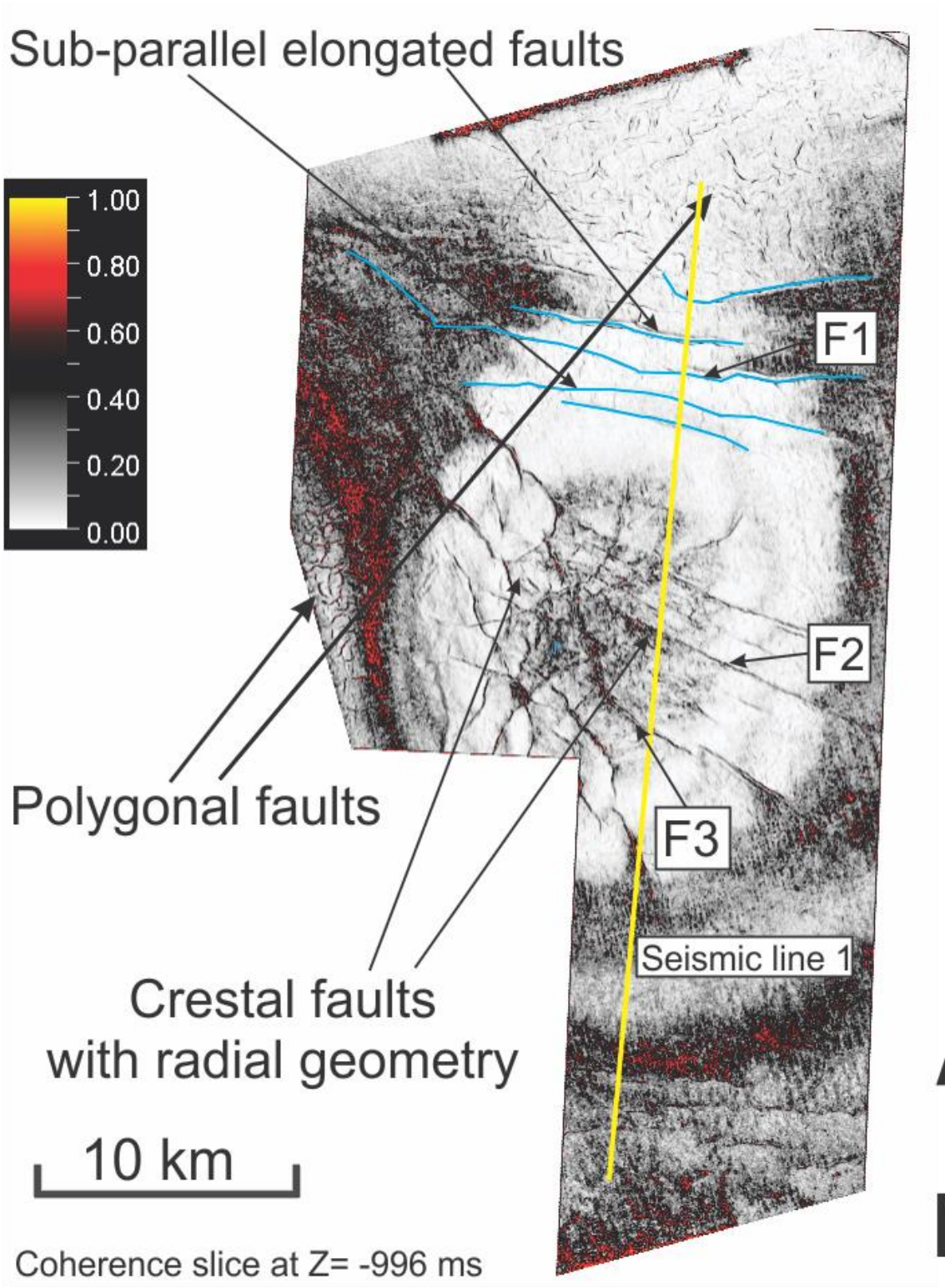

Figure 6-17. *Coherence (variance) map at Z= -996 ms illustrating different types of faults in the study area: polygonal faults to the north and west of the Samson Dome, crestal radial faults on the crest of the Samson Dome, and sub-parallel elongated faults marked as blue lines to the north of the Samson Dome.*

Seismic section through seismic line 1 crossing faults F1, F2, and F3 is shown in Figure 6-18. F1 is elongated sub-parallel fault and F2 and F3 are crestal faults.

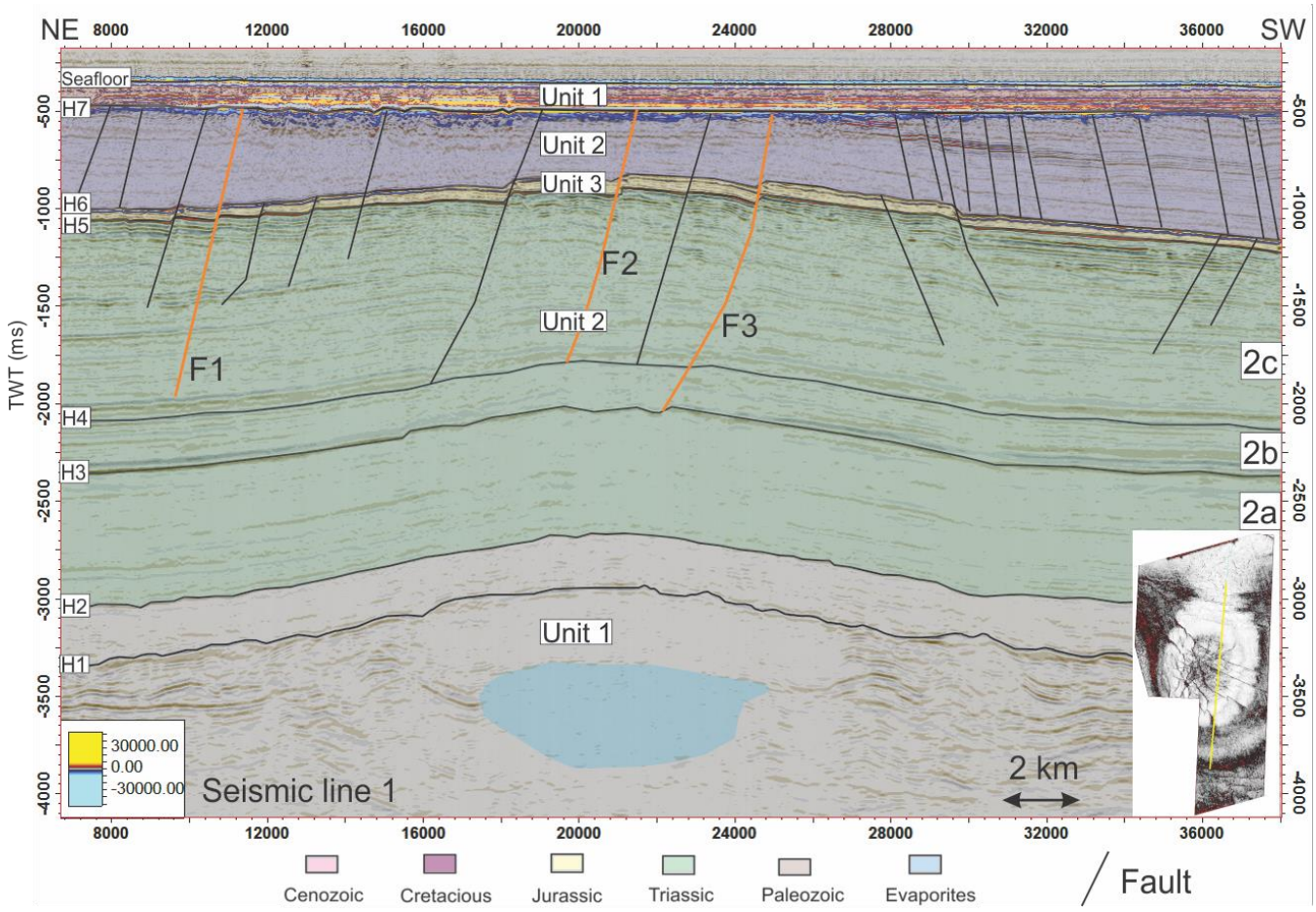

Figure 6-18. *Interpreted seismic section of seismic line 1 crossing faults F1, F2, and F3.*

Polygonal faults surrounding the Samson Dome structure are illustrated in Figure 6-19. Polygonal faults to the south of the Samson Dome have a larger geometry in comparison to the polygonal faults surrounding the Samson Dome from the other sides, but the quantity of polygonal faults to the north and west of the Samson Dome appears to be higher. Polygonal faults are absent on the crest of the Samson Dome. Two seismic lines through polygonal faults

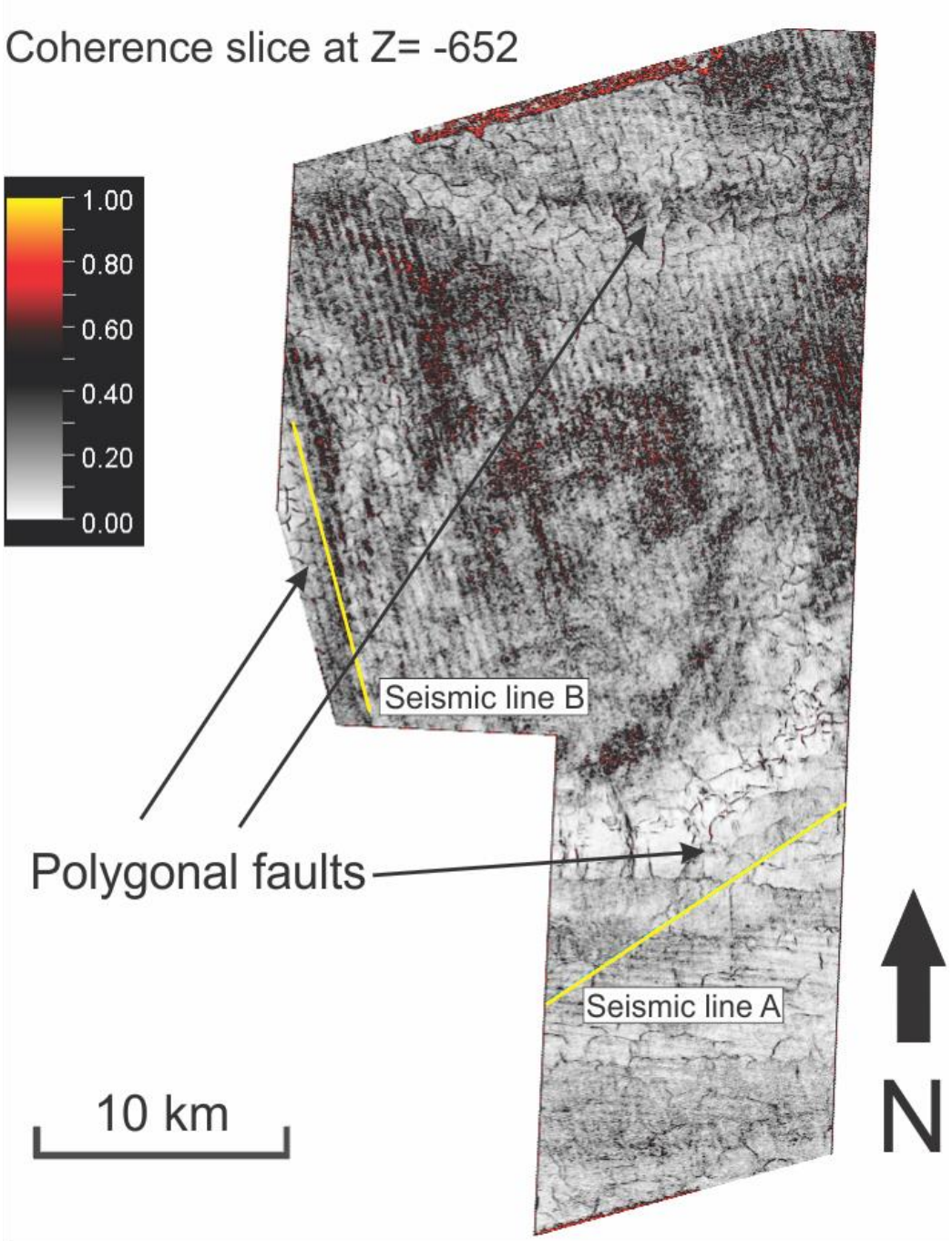

Figure 6-19. *Variance map at the depth of 652 ms highlighting polygonal faults surrounding the Samson Dome with a position of seismic lines A and B chosen for interpretation of the seismic profile through the polygonal faults in the area.*

have been chosen for further interpretation: seismic line A and seismic line B, to the south and to the west of the Samson Dome, correspondingly.

3D cross-section of seismic line A and coherence slice at Z= -752 ms is shown in Figure 6-20. There is a clear correspondence between the pattern of polygonal faults on the variance map and its vertical representation on the seismic profile through line A.

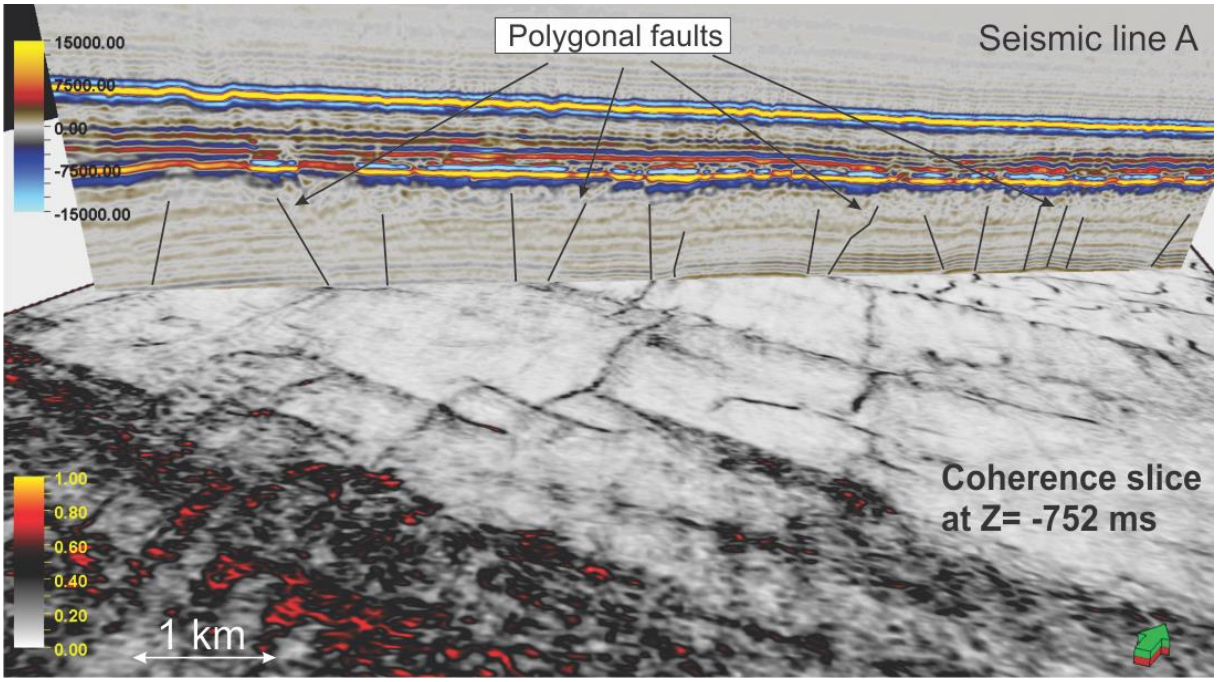

Figure 6-20. *3D seismic cross-section of seismic line A through polygonal faults to the south of the Samson Dome and coherence slice at the depth of 752 ms.*

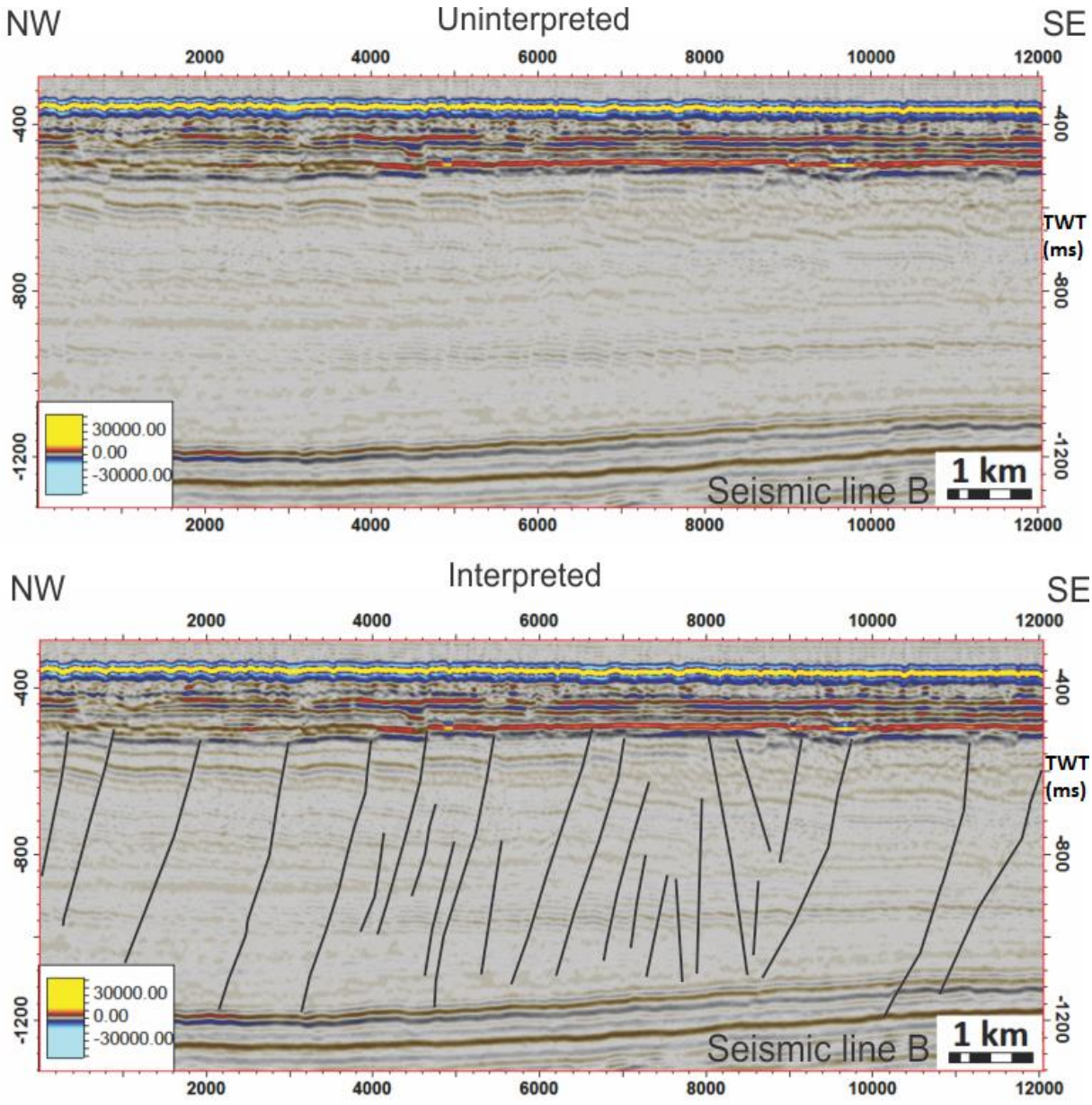

***Figure 6-21**. Uninterpreted and interpreted seismic profiles of the seismic line B through polygonal faults to the west of the Samson Dome.*

We observe a large number of polygonal faults to the west of the Samson Dome, as seen on a seismic profile in Figure 6-21. Average penetration of these faults is approximately 550-600 ms, and most of the faults cut through entire Unit 4.

Running of the Ant-tracking attribute has been tried in order to improve visualization of the faults in the area and extract their fault patches by the use of automatic fault extraction. Results of the Ant-tracking in Figure 6-22 show an example of the ant-tracking slice at a depth of 1056 ms. Despite the fact that data on the Ant-tracking attribute map is quite noisy, crestal faults and elongated sub-parallel faults that have been identified before become somewhat visible. However, the ant-tracking fault data was not clear enough to improve the results distinctly by using automatic fault extraction. Due to the very high number of discontinuities, probably caused by the presence of many polygonal faults, small faults and fractures in the area, number of extracted fault patches was too high, and their distribution was too random in order to merge some of them into larger faults and get better visualization of the faults 3D geometry.

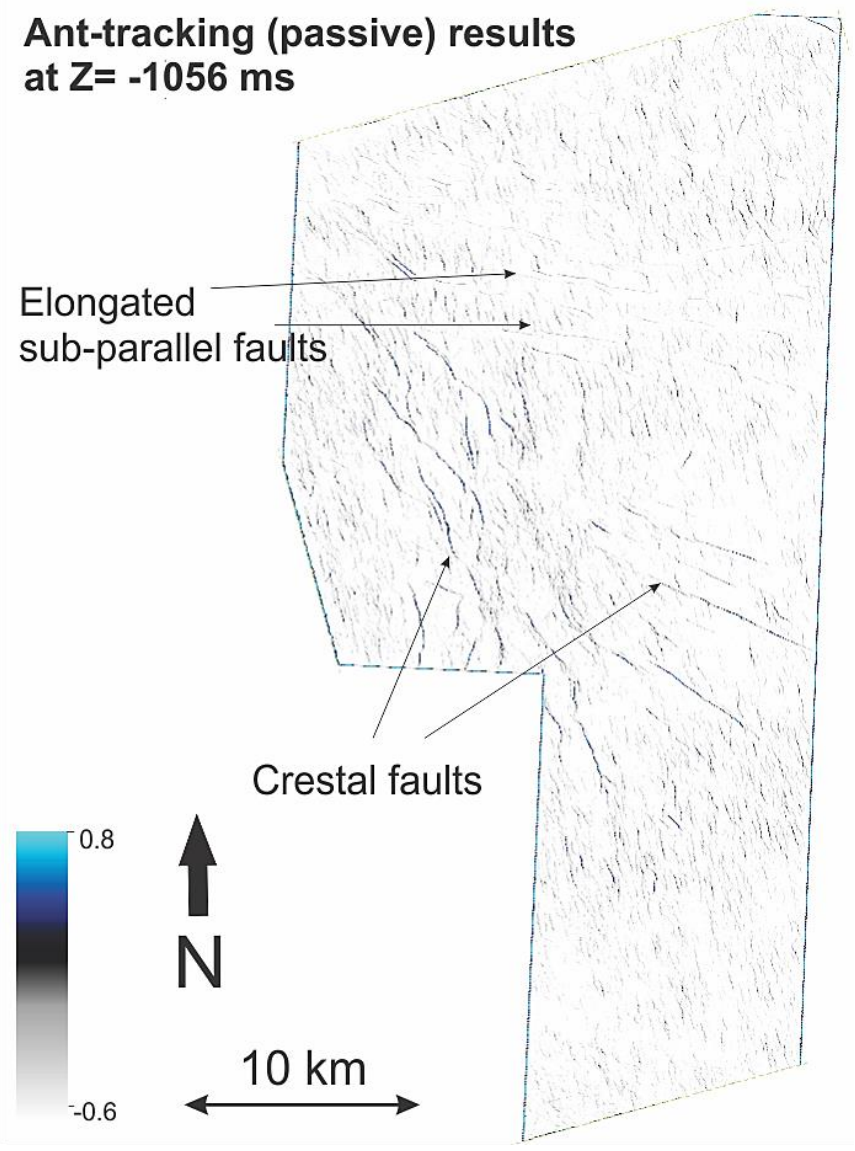

Figure 6-22. *Ant-tracking (passive) slice at the depth of 1056 ms illustrating crestal faults and elongated, sub-parallel faults in the study area.*

7. Discussion

7.1 Tectonostratigraphic evolution of the Samson Dome

Based on the results acquired during the seismic interpretation of the 3D seismic cube BG1002, we can claim that structural evolution of the Samson Dome is closely related to the regional tectonic and stratigraphic development of the western Barents Sea.

The Nordkapp, Tromsø, Njørnøya, Fingerdjupet, Maud, Hammerfest and Ottar basins formed during Late Paleozoic times. Accumulation of thick evaporate deposits in these basins started during Middle Carboniferous Period and reached its peak in the beginning of Permian times (Breivik et al., 1995). On the interpreted seismic profile through the Samson Dome we see these Paleozoic successions comprising lenticular evaporitic accumulations (Figure 6-1).

Structural development of continental margins of the Arctic Ocean has been characterized by many crustal extensional tectonic events during the Late Paleozoic and Mesozoic, particularly in The Early-Middle Devonian, Carboniferous, Permian, Triassic and late Jurassic-Early Cretaceous periods. In the study area of the Samson Dome polygonal mounds and isolated carbonate build-ups observed in the seismic sections within Permian strata (Figure 6-8) could be formed on active structural highs as a result of these rifting events and subsequent break-up of the Pangea supercontinent (Dore, 1995; Alves, 2015).

Permian and Mesozoic strata in the Samson Dome region are quite flat-lying except for the middle part, on the crest of the salt structure where seismic reflectors are concave due to the deformation during halokinesis (Figure 6-1). This confirms the Breivik et al., 1995 suggestion that the Samson Dome was not exposed to active tectonism during Mesozoic Era.

First tectonic salt movements in Ottar basin occurred during Middle to Late Triassic (Breivik et al., 1995; Mattos et al., 2016). However, on the seismic sections through the Samson Dome (Figure 6-18) the only evidence of tectonic movements during that period are few faults reaching horizons H5 and H6. These faults had NE trend and were later reactivated and propagated into upper sedimentary units during late Mesozoic- Early Cenozoic. This fact let us suggest that post-salt deposits in the Samson Dome area were not significantly deformed during Middle to Late halokinetic movements. Faults intersecting Late Triassic- Late

Cretaceous sediments have NW-SE strikes, what coincides with a trend that prevailed in Ottar basin at that times (Mattos et al., 2016).

Major halokinetic movements took place during Late Mesozoic- Early Cenozoic times, which were probably caused by extensional processes in the Barents Sea during opening of the North Atlantic Ocean. This caused not only new salt movements but also reactivation of faults with NE trend (Mattos et al., 2016). As a result of these salt movements large anticline structure formed and deformed overlying sediment sequences. Faults around the Samson Dome offsetting Triassic, Jurassic and Cretaceous strata serve as an evidence for this.

Radial pattern of the faults illustrated on Variance map at the depth of 996ms (Figure 6-17) highlights the geometry of the Samson Dome and defines the area of the dome's crest extension. Faults on the crest of the dome are normal. Circular geometry of the Samson Dome was probably the determining factor for the formation of such radial pattern comprising normal faults. Radial extensional faults formed due to the arching of the overburden. During this process sedimentary strata stretches in the hoop direction (tangential to the peripheral areas of the salt dome) and the radial direction (normal to the peripheral areas of salt dome) (Figure 7-1(b)). Extension is highest in hoop direction around the flanks of a dome. As a result radial faults are formed (Carruthers, 2012; Mandi, 2000).

Polygonal faults in the study area surround the Samson Dome structure and may indicate position of the limit of the hoop stress field (Figure 7-1(a)). Such structures as salt domes surrounded by polygonal faults have been observed before in previous researches (for example in Pierce Diapirs in the Central North Sea, Carruthers, 2012). In Figure 7-1(b) the potential model of formation of radial faults due to hoop stress during arching is presented. This model illustrates how the geometry of polygonal faults surrounding salt domes may be used for the reconstruction of hoop stress dimensions in the area.

Nowadays, the principle of formation of polygonal faults is still a topic for research. We know that this type of faults is not tectonically-related and occurs in fine-grained sediments (Berndt et al., 2003). In the study area polygonal faults are observed within Cretaceous strata, which comprises dark-grey shales and red to yellow-brown claystones in Lower Cretaceous Knurr Formation and brownish grey to dark grey shales interbedded with thin layers of sandstones and siltstones in the Upper Cretaceous Kolmule Formation according to the wellbore data.

These polygonal faults could have developed due to loading and dewatering of the formation, and they are of interest since they might control fluid flow in the region.

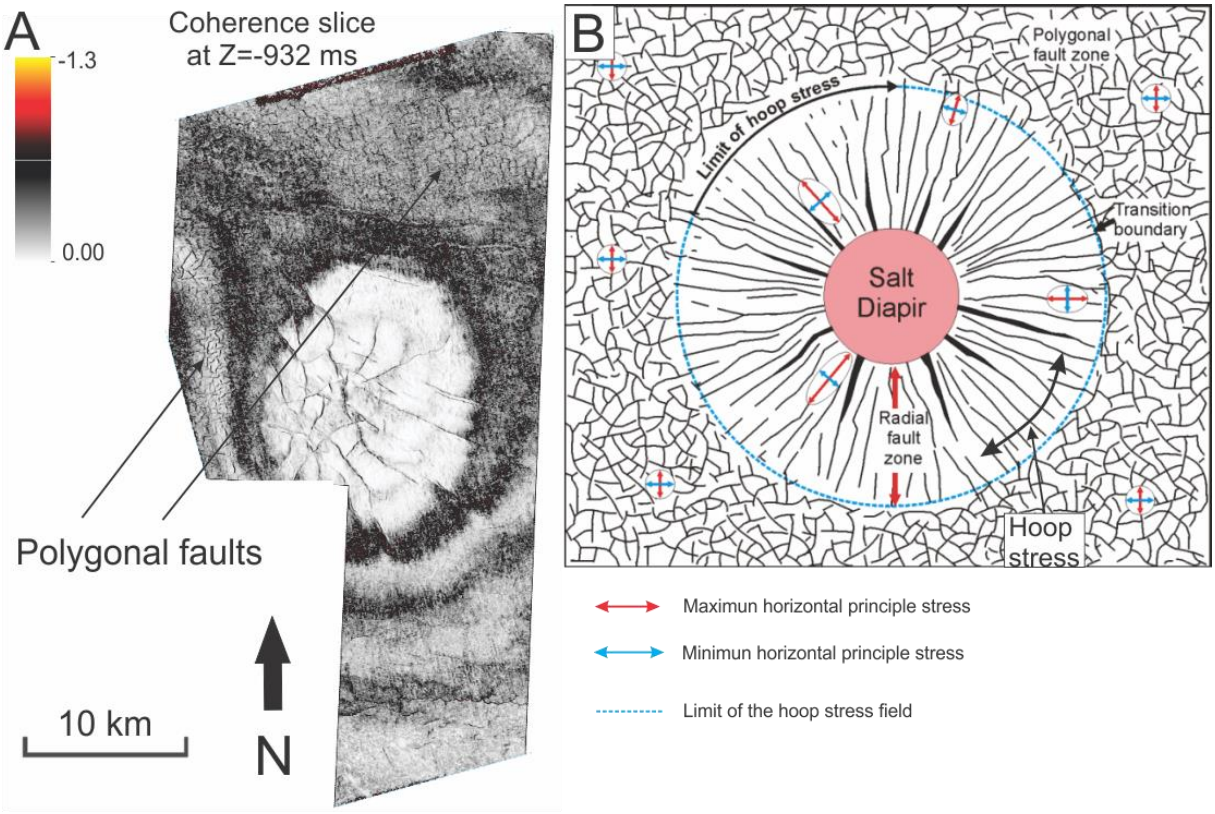

Figure 7-1. *a) Coherence slice at the depth of 932ms illustrating polygonal faults surrounding the Samson Dome structure; b) Illustration of the stresses influencing the overburden during arching and formation of radial fault pattern and geometry of the polygonal faults surrounding the salt diaper structure. Geometry of the polygonal faults may be used for reconstruction of hoop stress field dimensions. Figure 7-1(b) is modified from Carruthers, 2012.*

The surface in the study area with a significantly higher erosion degree in comparison to the other ones is surface H7, which truncates over the crest of the Samson Dome. This surface represents the Upper Regional Unconformity, erosional base for several glaciations formed around 2.5 Ma (Larsen et al., 2003). The surface is thinner in the area at the top of the dome (Figure 6-6). Erosion of this surface and its thickness variations are apparently related to Paleogene uplift and subsequent Paleogene and Neogene erosion, which were induced by Cenozoic tectonic and glacial processes: opening of the Norwegian- Greenland Sea and

formation of the sheared western Barents Sea continental margin, several glaciations and isostasy (Butt et al., 2002). Important part of erosion processes in the area occurred in Quaternary due to the glacial conditions. Evidence for this is represented by plough marks and iceberg pits observed in the study area on the seafloor surface (Figure 6-4, Figure 6-5).

7.2. Fluid flow model for the Samson Dome area

Presence of seismic amplitude anomalies as well as large number of faults, which could act as potential fluid migration pathways, in the 3D seismic cube BG10022 make the area of the Samson Dome interesting for the petroleum industry. Previous studies (Vadakkepuliyambatta et al., 2013; Mattos, 2016) claim that hydrocarbons and fluid flow features are present in the area of the Samson Dome as well.

High amplitude anomalies, bright spots and reflections with phase reversal have been observed only at shallow depths in the study area (Figure 6-13, Figure 6-14, Figure 6-15, Figure 6-16). Large intervals of high amplitude anomalies and many bright spots within the Unit 5 act as hydrocarbon indicators and are probably caused by accumulation of shallow gas within the Cenozoic strata. The largest bright spots and most of the high amplitude anomalies have been observed slightly northward of the crest of the Samson Dome (Figure 7-2). These amplitude anomalies overlie highly faulted area between horizons H7 and H5. In addition, intervals of highly chaotic and disturbed reflections are present below these high amplitude anomalies. Such features serve as hydrocarbon indicators caused by fluid flow in the area. Faults underlying the zone of the largest high amplitude anomalies probably act as potential leakage pathways for hydrocarbons (Figure 7-2). If faults and fractures form, they increase permeability and porosity in the subsurface providing high flow rates for hydrocarbon migrations.

One can assume that a large number of faults that act as potential fluid pathways are present within the chaotic areas as well (Figure 7-2). However, on the seismic profiles through the 3D cube BG1002 faults within that chaotic area have not been observed. The lack of such evidence may be caused by frequency loss and amplitude dimming associated with shallow gas anomalies in the area and migration of the gas through the subsurface.

High amplitude anomalies have been also observed to the south and south-east of the Samson Dome above the erosion surface H7 and above the south-eastern flank of the Samson Dome at shallow depths of the Unit 4 (Figure 6-15) within the transition zone between Cenozoic and Mesozoic strata. The area comprising high amplitude anomalies within the Unit 4 is highly faulted as well, and reflections are discontinuous. So hydrocarbons could probably migrate along these faults from deeper source rocks into shallow layers of Cretaceous strata as well as even further up into the Cenozoic sediments.

Moreover, since high amplitude anomalies within the shallow layers of the Unit 4 are located at the transition zone between Cenozoic and Mesozoic sediments characterized by a major erosion event in the study area, we can suggest that hydrocarbon leakage into shallower layers was likely triggered by the reduction in overburden pressure in the area caused by erosion and periods of the retreat of ice sheets during deglaciations.

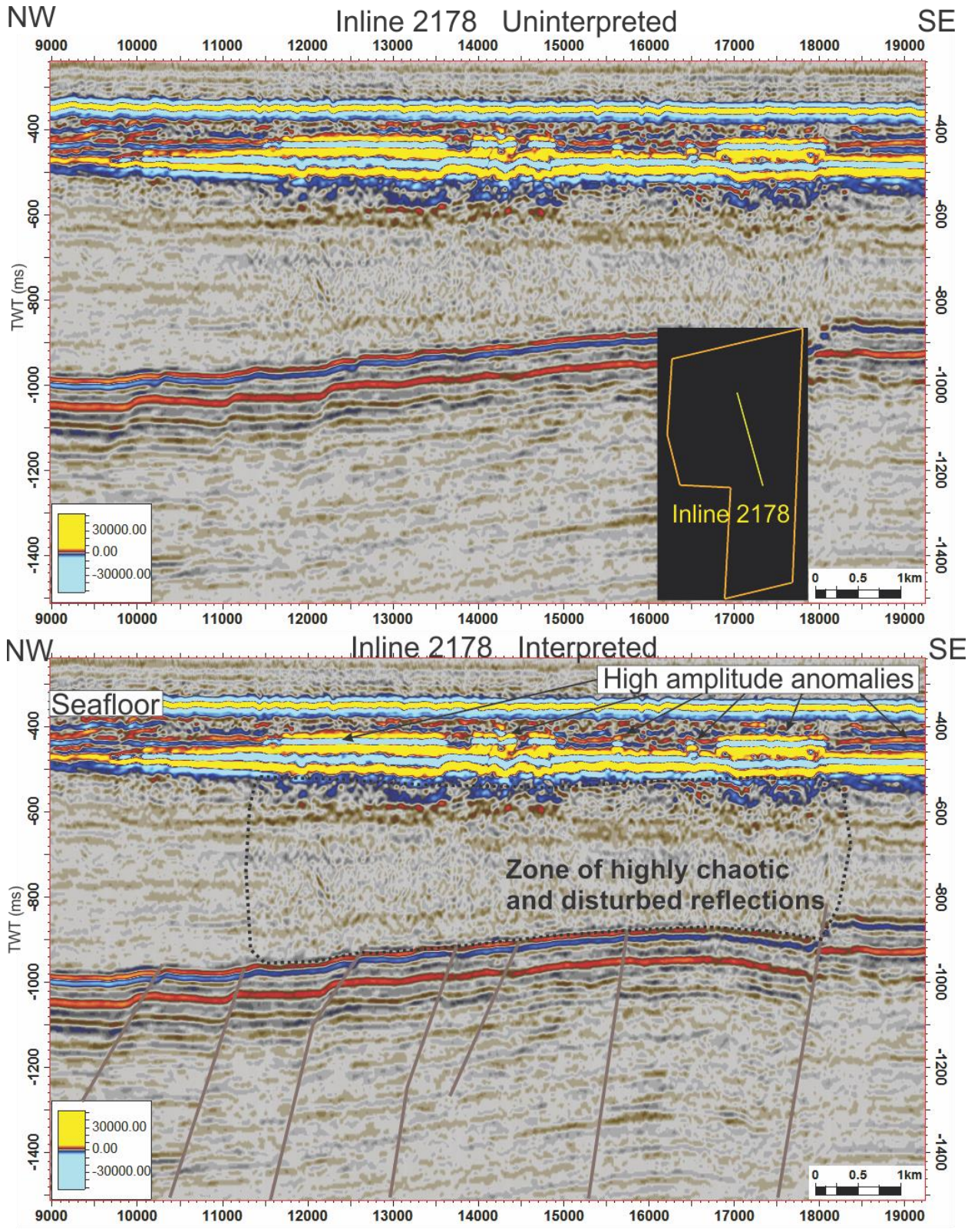

Figure 7-2. *Uninterpreted and Interpreted seismic profile through inline 2178 illustrating zone of highly chaotic reflections overlying faulted area and high amplitude anomalies above them.*

In the study area within the 3D seismic cube BG1002 there have not been observed any obvious gas chimneys or large dim-spots, which were previously detected by Vadakkepuliyambatta et al., 2013 on 2D seismic data in the area of the Samson Dome (Figure 7-3). Nevertheless, hydrocarbon fluid migration indicators such as zones of highly chaotic reflections, high amplitude anomalies, bright spots and reflections with phase reversal, as well as a network of faults in the area acting as potential leakage paths, create the fluid flow model of the Samson Dome area.

Late Jurassic Hekkingen Formation, which has the highest oil and gas potential and is the most prominent source rock in the western Barents Sea, is present in the study area. However, this formation is immature in the Samson Dome region (Dore, 1995; Vadakkepuliyambatta et al., 2013). Most likely potential source rocks for the migrated hydrocarbons in the study area are deep Triassic formations (for example Havert Formation).

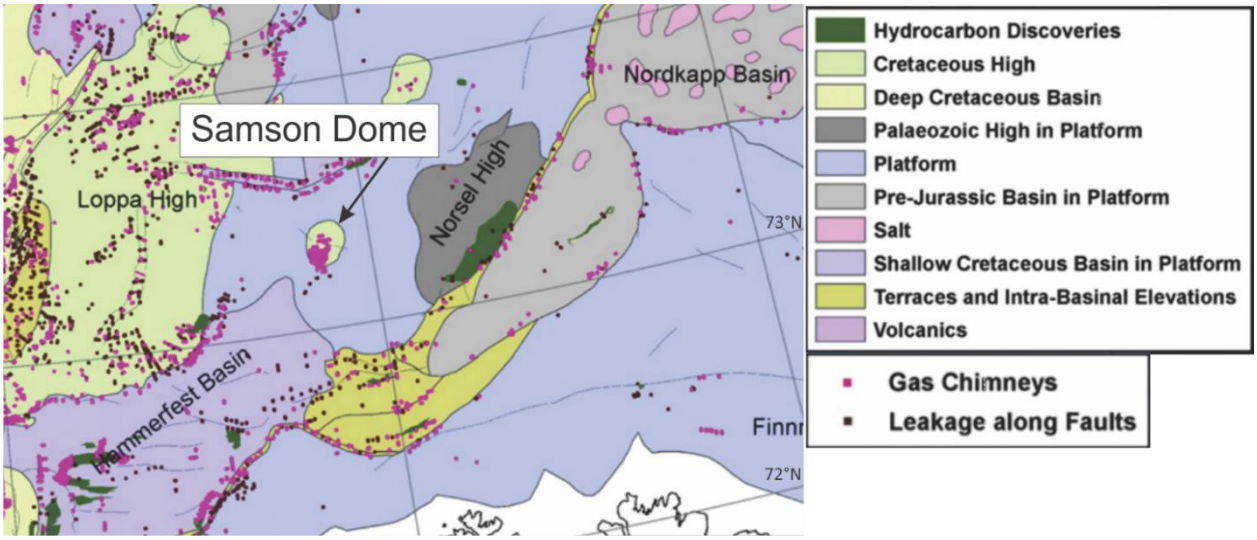

Figure 7-3. *Structural map illustrating position of gas chimneys and zones of leakage along faults in the Samson Dome and some nearby areas in the SW Barents Sea. Modified from Vadakkepuliyambatta et al., 2013.*

8. Conclusions

- Geological evolution of the Samson Dome structure is directly connected to regional tectonic and stratigraphic development of the western Barents Sea. Rifting events, halokinetic movements, uplift and glacial processes heavily influenced the area of the Samson Dome.
- Stratigraphy for the 3D seismic cube BG1002 has been defined and 5 stratigraphic units can be distinguished: Paleozoic strata comprising evaporitic deposits, Triassic, Jurassic, Cretaceous, and Cenozoic sediments.
- Top settings of some of the seismic/stratigraphic units in the study area coincide with the following geological formations: top of Unit 2- Fruholmen Fm, top of Unit 3- Hekkingen Fm, top of Unit 4- Kolmule Fm.
- Faults within the study area show three major types: crestal faults (type 1), elongated sub-parallel faults (type 2), and polygonal faults (type 3).
- Formation of the anticline structure of the Samson Dome started with Middle to Late Triassic halokinetic movements and appearance of NE faults. Subsequent reactivation of these faults occurred in Late Cretaceous induced by opening of the North Atlantic Ocean. Active arching of Cretaceous strata took place in Late Mesozoic- Early Cenozoic due to the salt mobilization that was caused by extension in the Barents Sea.
- Study area has been exposed to Late Mesozoic- Early Cenozoic erosion processes and uplift. The erosional processes are especially evident from the Upper Regional Unconformity surface present in the area, as well as evidence for the glacial erosional processes such as iceberg plough marks and iceberg pits.
- Indicators of hydrocarbon presence exist in the area: high amplitude anomalies, bright spots, reflections with phase reversal, and large zones of chaotic disturbed seismic reflections. Integration of these amplitude anomalies with presence of large faults suggests that hydrocarbons migrated into shallower layers at the Samson Dome through faults and fractures. Hydrocarbon leakage could also be triggered by reduction in overburden stresses during erosion events of Cenozoic times. Potential source rocks for the leaked hydrocarbons in the area are deep Triassic formations (for example Havert Formation).

References

Alves, T. M., (2015). Polygonal mounds in the Barents Sea reveal sustained organic productivity towards the P-T boundary. Terra Nova, 28(1), 50-59. doi:10.1111/ter.12190

Andreassen, K. (2009). Marine geophysics. Lecture notes for GEO-3123. University of Tromsø.

Arntsen, B., Wensaas, L., Løseth, H., Hermanrud, C. (2007). Seismic modeling of gas chimneys. Geophysics, 72(5). doi:10.1190/1.2749570

Barnard, A., Sager, W. W., Snow, J. E., Max, M. D. (2016). A New Look at Seafloor Venting: Natural Gas Hydrate Derivatives. Offshore Technology Conference. doi:10.4043/27283-ms

Berndt, C. (2005). Focused fluid flow in passive continental margins. Philosophical Transactions of the Royal Society A: Mathematical, Physical and Engineering Sciences, 363(1837), 2855-2871. doi:10.1098/rsta.2005.1666

Berndt, C., Bünz, S., Mienert, J. (2003). Polygonal fault systems on the mid-Norwegian margin: A long-term source for fluid flow. In: Subsurface Sediment Deformation van Rensbergen, P., Hillis, R. R., Maltman, A. J. and Morley, C. (eds.) Geological Society of London Special Publication, 216, pp. 283-290.

Breivik, A. J., Gudlaugsson, S. T., Faleide, J. I. (1995). Ottar Basin, SW Barents Sea: a major Upper Palaeozoic rift basin containing large volumes of deeply buried salt. Basin Research, 7(4), 299-312. doi:10.1111/j.1365-2117.1995.tb00119.x

Brown, A.R. (1999): Interpretation of three-dimensional seismic data, 5th edition. AAPG Memoir 42, Tulsa, Oklahoma, pp. 514.

Brown, C. S., Newton, A. M., Huuse, M., Buckley, F. (2017). Iceberg scours, pits, and pockmarks in the North Falkland Basin. Marine Geology, 386, 140-152. doi:10.1016/j.margeo.2017.03.001

Butt, F. A., Drange, H., Elverhøi, A., Otterå, O. H., Solheim, A. (2002). Modelling Late Cenozoic isostatic elevation changes in the Barents Sea and their implications for oceanic and climatic regimes: Preliminary results. Quaternary Science Reviews, 21(14-15), 1643-1660. doi:10.1016/s0277-3791(02)00018-5

Carruthers, T. D., (2012). Interaction of Polygonal Fault Systems with Salt Diapirs.

Cartwright, J. A., Lonergan, L. (1996). Volumetric contraction during the compaction of mudrocks: a mechanism for the development of regional-scale polygonal fault systems. Basin Research, 8(2), 183-193. doi:10.1046/j.1365-2117.1996.01536.x

Cartwright, J., Santamarina, C. (2015). Seismic characteristics of fluid escape pipes in sedimentary basins: Implications for pipe genesis. Marine and Petroleum Geology, 65, 126-140. doi:10.1016/j.marpetgeo.2015.03.023

Doré, A. (1991). The structural foundation and evolution of Mesozoic seaways between Europe and the Arctic. Palaeogeography, Palaeoclimatology, Palaeoecology, 87(1-4), 441-492. doi:10.1016/0031-0182(91)90144-g

Doré, A. (1995). Barents Sea Geology, Petroleum Resources and Commercial Potential. Arctic, 48(3). doi:10.14430/arctic1243

Doré, A., Jensen, L. (1996). The impact of late Cenozoic uplift and erosion on hydrocarbon exploration: Offshore Norway and some other uplifted basins. Global and Planetary Change, 12(1-4), 415-436. doi:10.1016/0921-8181(95)00031-3

Ebbing, J., Braitenberg, C., Wienecke, S. (2007). Insights into the lithospheric structure and tectonic setting of the Barents Sea region from isostatic considerations. Geophysical Journal International, 171(3), 1390-1403. doi:10.1111/j.1365-246x.2007.03602.x

Eldholm, O., Faleide, J. I., Myhre, A. M. (1987). Continent-ocean transition at the western Barents Sea/Svalbard continental margin. Geology, 15(12), 1118. doi:10.1130/0091-7613(1987)152.0.co;2

Faleide, J. I., Bjørlykke, K., Gabrielsen, R. H. (2010). Geology of the Norwegian Continental Shelf. Petroleum Geoscience, 467-499. doi:10.1007/978-3-642-02332-3_22

Faleide, J. I., Gudlaugsson, S. T., Jacquart, G. (1984). Evolution of the western Barents Sea. Marine and Petroleum Geology, 1(2), 123-150. doi:10.1016/0264-8172(84)90082-5

Gee, D. G., Fossen, H., Henriksen, N., Higgins, A. K. (2008). From the Early Paleozoic Platforms of Baltica and Laurentia to the Caledonide Orogen of Scandinavia and Greenland.

Gernigon, L., Brönner, M., Roberts, D., Olesen, O., Nasuti, A., Yamasaki, T. (2014). Crustal and basin evolution of the southwestern Barents Sea: From Caledonian orogeny to continental breakup. Tectonics, 33(4), 347-373. doi:10.1002/2013tc003439

Heggland, R. (2014). Visualization and Interpretation of Gas Chimneys in Exploration for Hydrocarbons. EAGE Shallow Anomalies Workshop. doi:10.3997/2214-4609.20147430

Henriksen, E., Ryseth, A. E., Larssen, G. B., Heide, T., Ronning, K., Sollid, K., Stoupakova, A. V. (2011a). Chapter 10 Tectonostratigraphy of the greater Barents Sea: Implications for petroleum systems. Geological Society, London, Memoirs, 35(1), 163-195. doi:10.1144/m35.10

Henriksen, E., Bjornseth, H. M., Hals, T. K., Heide, T., Kiryukhina, T., Klovjan, O. S., Stoupakova, A. (2011b). Chapter 17 Uplift and erosion of the greater Barents Sea: Impact on prospectivity and petroleum systems. Geological Society, London, Memoirs, 35(1), 271-281. doi:10.1144/m35.17

Hovland, M., Judd, A. G. (1988). Seabed pockmarks and seepages: Impact on geology, biology, and the marine environment. London: Graham & Trotman.

Hovland, M., Gardner, J. V., Judd, A. G. (2002). The significance of pockmarks to understanding fluid flow processes and geohazards. Geofluids, 2(2), 127-136. doi:10.1046/j.1468-8123.2002.00028.x

Hovland, M. (2005). Petroleum Geology: Gas Hydrates. Encyclopedia of Geology, 261-268. doi:10.1016/b0-12-369396-9/00235-5

Jahn, F., Graham, M. (1998). Developments in Petroleum Science, 46. Burlington: Elsevier.

Jakobsson, M., Andreassen, K., Bjarnadottir, L. R., Stein, R. (2014). Arctic Ocean Glacial History.

Judd, A. G., Hovland, M. (2007). Seabed fluid flow: The impact on geology, biology and the marine environment. Cambridge: Cambridge University Press.

Koson et al., (2014). Seismic attributes and seismic geomorphology. Vol. 6, No. 1, 1-9.

Laberg, J. S., Andreassen, K., Vorren, T. O. (2011). Late Cenozoic erosion of the high-latitude southwestern Barents Sea shelf revisited. Geological Society of America Bulletin, 124(1-2), 77-88. doi:10.1130/b30340.1

Larsen, E., Andreassen, K., Nilssen, L. C., Raunholm, S. (2003). The prospectivity of the Barents Sea: Ice ages, erosion and tilting of traps. Geological Survey of Norway.

Løseth, H., Gading, M., Wensaas, L. (2009). Hydrocarbon leakage interpreted on seismic data. Marine and Petroleum Geology, 26(7), 1304-1319. doi:10.1016/j.marpetgeo.2008.09.008

Mahgoub, M., Ghosh, D., Abdullatif, A. H., Neves, F. (2017). Taking Seismic Acquisition Artifacts Beyond Mitigation. Icipeg 2016, 403-412. doi:10.1007/978-981-10-3650-7_34

Mandl, G. (2000). Parallel Faults. Faulting in Brittle Rocks, 376-406. doi:10.1007/978-3-662-04262-5_8

Marello, L., Ebbing, J., Gernigon, L. (2013). Basement inhomogeneities and crustal setting in the Barents Sea from a combined 3D gravity and magnetic model. Geophysical Journal International, 193(2), 557-584. doi:10.1093/gji/ggt018

Matthews, J. (2008). The Origin of Oil-A Creationist Answer. Retrieved December 12, 2016, from https://answersingenesis.org/geology/the-origin-of-oila-creationist-answer/

Mattos, N. H., Alves, T. M., Omosanya, K. O. (2016). Crestal fault geometries reveal late halokinesis and collapse of the Samson Dome, Northern Norway: Implications for petroleum systems in the Barents Sea. Tectonophysics, 690, 76-96. doi:10.1016/j.tecto.2016.04.043

Minescu, F., Popa, C., Grecu, D. (2010). Theoretical and Practical Aspects of Tertiary Hydrocarbon Migration. Petroleum Science and Technology, 28(6), 555-572. doi:10.1080/10916460903073318

Ngeri, A.P., Tamunobereton-ari, I., Amakiri, A.R.C. (2015). Ant-Tracker Attributes: An Effective Approach To Enhancing Fault identification And Interpretation. IOSR Journal of VLSI and Signal Processing (IOSR-JVSP), Volume 5, Issue 6, Ver. II (Nov -Dec. 2015), 67-73

NPD, Halland, E.K., Bjørnestad, A., Gjeldvik, I. T. , Bjørheim M., Magnus C., Meling I. M., Mujezinović J., Riis F., Rød R. S., Pham V. T. H., Tappel I., (Retrieved December 1st 2016 from http://www.npd.no/en/Publications/Reports/Compiled-CO2-atlas/6-The-Barents-Sea/61-Geology-of-the-Barents-Sea/). Geology of the Barents Sea.

NPD, n.d. Norwegian Petroleum Directorate, Factpages. Available at: http://npdmap1.npd.no/website/NPDGIS/viewer.htm

Nyland, B., Jensen, L., Skagen, J., Skarpnes, O., Vorren, T. (1992). Tertiary Uplift and Erosion in the Barents Sea: Magnitude, Timing and Consequences. Structural and Tectonic Modelling and Its Application to Petroleum Geology, 153-162. doi:10.1016/b978-0-444-88607-1.50015-2

Pigott, J. D., Kang, M., Han, H. (2013). First order seismic attributes for clastic seismic facies interpretation: Examples from the East China Sea. Journal of Asian Earth Sciences, 66, 34-54. doi:10.1016/j.jseaes.2012.11.043

Polteau, S., Hendriks, B. W., Planke, S., Ganerød, M., Corfu, F., Faleide, J. I., Myklebust, R. (2016). The Early Cretaceous Barents Sea Sill Complex: Distribution, 40Ar/39Ar geochronology, and implications for carbon gas formation. Palaeogeography, Palaeoclimatology, Palaeoecology, 441, 83-95. doi:10.1016/j.palaeo.2015.07.007

Ritzmann, O., Faleide, J. I. (2007). Caledonian basement of the western Barents Sea. Tectonics, 26(5). doi:10.1029/2006tc002059

Roberts, D. (2003). The Scandinavian Caledonides: Event chronology, palaeogeographic settings and likely modern analogues. Tectonophysics, 365(1-4), 283-299. doi:10.1016/s0040-1951(03)00026-x

Roberts, D., Bally, A. (2012). Regional geology and tectonics of sedimentary basins. Regional Geology and Tectonics: Phanerozoic Passive Margins, Cratonic Basins and Global Tectonic Maps, 2-17. doi:10.1016/b978-0-444-56357-6.00025-1

Sheriff, R. E., (1997). Seismic Resolution a Key Element. Explorer: Geophysical Corner

Sheriff , R.E., (2006). Encyclopedic Dictionary of Exploration Geophysics, 5th. Ed. Tulsa: Society of Exploration Geophysics.

Solheim, A., Riis, F., Elverhøi, A., Faleide, J., Jensen, L., Cloetingh, S. (1996). Impact of glaciations on basin evolution: Data and models from the Norwegian margin and adjacent areas—Introduction and summary. Global and Planetary Change, 12(1-4), 1-9. doi:10.1016/0921-8181(95)00008-9

Šráček O., Zachariáš J. (2002): Fluids in geological processes.

Tarleton State University, Dr. Phillip Murry. (2017, January 03). Sedimentology Lab 3. Retrieved May 25, 2017, from http://faculty.tarleton.edu/murry/Sedimentology/Sedimentology%20Labs/sedimentology-labs.html

Vadakkepuliyambatta, S., Bünz, S., Mienert, J., Chand, S. (2013). Distribution of subsurface fluid-flow systems in the SW Barents Sea. Marine and Petroleum Geology, 43, 208-221. doi:10.1016/j.marpetgeo.2013.02.007

Vorren, T. O., Richardsen, G., Knutsen, S., Henriksen, E. (1991). Cenozoic erosion and sedimentation in the western Barents Sea. Marine and Petroleum Geology, 8(3), 317-340. doi:10.1016/0264-8172(91)90086-g

Wang, X., Wu, S., Yuan, S., Wang, D., Ma, Y., Yao, G., Zhang, G. (2010). Geophysical signatures associated with fluid flow and gas hydrate occurrence in a tectonically quiescent sequence, Qiongdongnan Basin, South China Sea. Geofluids, 10(3), 351-368. doi:10.1111/j.1468-8123.2010.00292.x

Watson, E. B., Baxter, E. F. (2007). Diffusion in solid-Earth systems. Earth and Planetary Science Letters, 253(3-4), 307-327. doi:10.1016/j.epsl.2006.11.015

Wennberg, O. P., Casini, G., Jonoud, S., Peacock, D. C. (2016). The characteristics of open fractures in carbonate reservoirs and their impact on fluid flow: A discussion. Petroleum Geoscience, 2015-003. doi:10.1144/petgeo2015-003

Wiprut, D., Zoback, M. D. (2002). Fault reactivation, leakage potential, and hydrocarbon column heights in the northern North Sea. Norwegian Petroleum Society Special Publications

Hydrocarbon Seal Quantification, Norwegian Petroleum Society Conference, 203-219. doi:10.1016/s0928-8937(02)80016-9

Zieba, K. J., Felix, M., Knies, J. (2016). The Pleistocene contribution to the net erosion and sedimentary conditions in the outer Bear Island Trough, western Barents Sea. Arktos, 2(1). doi:10.1007/s41063-016-0022-3